MODELING OF HYDRATION KINETICS AND SHRINKAGE OF PORTLAND CEMENT PASTE

Feng Lin

Submitted in partial fulfillment of the
Requirements for the degree
of Doctor of Philosophy
in the Graduate School of Arts and Sciences

COLUMBIA UNIVERSITY

2006

MODELING OF HYDRATION KINETICS AND SHRINKAGE OF PORTLAND CEMENT PASTE

Feng Lin

Submitted in partial fulfillment of the
Requirements for the degree
of Doctor of Philosophy
in the Graduate School of Arts and Sciences

COLUMBIA UNIVERSITY

2006

ABSTRACT

MODELING OF HYDRATION KINETICS AND SHRINKAGE OF PORTLAND CEMENT PASTE

Feng Lin

A mathematical hydration kinetics model and a constitutive model for the shrinkage of Portland cement paste are developed, calibrated and validated in this dissertation.

First of all, a hydration kinetics model for Portland cement is formulated based on the thermodynamics of multiphase porous media, in which the effects of chemical composition and fineness of cement as well as water-cement ratio are taken into account. In particular, the influences of elevated curing temperature and high applied pressure are considered. An equation for the diameter of the largest water-filled capillary pore that is a function of the degree of hydration is also presented. The hydration kinetics model is calibrated against the experimental data for eight different Portland cements. Simple relations between the model parameters and the chemical composition of cement are obtained. This model is then used to predict the degree of hydration, chemical shrinkage, adiabatic temperature rise, and autogenous relative humidity of different cement pastes in various curing environments.

A multi-scale micromechanical constitutive model that can simulate the effective elastic properties of hardened and hardening Portland cement paste is then formulated based on the theories of poromechanics and mechanics of composites. The effective

elastic properties of cement paste are captured by applying the up-scale approach with the appropriate basic modeling schemes at four different scales, viz. calcium silicate hydrate (*C–S–H*), hydration products, solid phase of cement paste, and cement paste. The stress redistribution in the solid phase of hydrating cement paste is simulated by considering both stress equilibrium and deformation compatibility of the composite materials. This model is validated against available experimental data with the intrinsic elastic properties of the constituent components of cement paste obtained from the literature.

The micromechanical constitutive model is further extended to describe the nonlinear and creep behavior of cement paste. A constitutive model that describes the time-dependent properties of the *C–S–H* matrix is developed and used in the multi-scale modeling with intrinsic model parameters. This constitutive model together with the aforementioned hydration kinetics model are successfully used to simulate the autogenous shrinkage of different Portland cement pastes.

The proposed constitutive framework can be extended to simulate the volume changes of cement paste at high curing temperatures and high applied pressures, if and when pertinent experimental data become available.

TABLE OF CONTENTS

LIST OF TABLES ..... **v**

LIST OF FIGURES ..... **vi**

NOTATIONS AND SYMBOLS ..... **xi**

ACKNOLEDGEMENTS ..... **xxiii**

DEDICATION ..... **xxv**

CHAPTER 1 INTRODUCTION **1**

1.1 Introduction of Hydration and Shrinkage of Portland Cement **2**

1.1.1 Cement composition **3**

1.1.2 Fineness and particle size distribution of cement **3**

1.1.3 Hydration of Portland cement **4**

1.1.4 Shrinkage of cement paste **5**

1.2 Mathematical and Numerical Modeling of Hydration Kinetics for Portland Cement **8**

1.2.1 Micro numerical modeling of cement hydration kinetics **8**

1.2.2 Macro mathematical modeling of cement hydration kinetics **10**

1.2.3 Limitations of existing mathematical models **10**

1.3 Modeling Shrinkage of Cement Paste **11**

1.3.1 Macro or phenomenological models of shrinkage **12**

1.3.2 Micromechanical models of shrinkage **12**

1.3.3 Limitations of available micromechanical models of shrinkage **13**

1.4 Objectives, Scope and Outline of the Dissertation **13**

CHAPTER 2 FORMULATION OF HYDRATION KINETICS MODEL ····· 18

2.1 Introduction ····· 18

2.2 Stages and Mechanisms of Cement Hydration ····· 18

2.3 Influence Factors of Cement Hydration Kinetics ····· 19

2.3.1 Influences of chemical composition of cement ····· 20

2.3.2 Influence of water-cement ratio ····· 20

2.3.3 Influences of fineness of cement ····· 21

2.3.4 Influences of curing temperature ····· 22

2.3.5 Influence of applied pressure ····· 24

2.4 Concept of Thermo-Chemical Modeling of Cement Hydration ····· 25

2.5 Formulation of Hydration Kinetics Model ····· 27

2.5.1 Modeling the influence factors of cement hydration kinetics ····· 27

2.5.2 Modeling the ultimate degree of hydration for Portland cement ···· 31

2.5.3 Mathematical model of hydration kinetics ····· 33

2.6 Summary and Discussion ····· 36

CHAPTER 3 CALIBRATION AND VERIFICATION OF HYDRATION KINETICS MODEL ····· 40

3.1 Introduction ····· 40

3.2 Calibration of Hydration Kinetics Model ····· 40

3.3 Verification of Hydration Kinetics Model ····· 43

3.3.1 Model prediction of the degree of hydration ····· 43

3.3.2 Model prediction of adiabatic temperature rise ····· 44

3.3.3 Model prediction of chemical shrinkage ····· 44

3.4 Summary and Discussion ····· 45

CHAPTER 4 DRIVING FORCES OF SHRINKAGE ····· 59

4.1 Introduction ····· 59

4.2 Surface Tension, Disjoining Pressure and Capillary Stress ····· 60

4.2.1 Surface tension ····· 60

4.2.2 Disjoining pressure ····· 61

4.2.3 Capillary stress ····· 62

4.3 Diameter of the Largest Water-Filled Capillary Pore ····· 63

4.4 Calculation of Volume Changes Using Theory of Poromechanics ····· 68

4.4.1 Tangent thermoporoelastic properties of saturated porous media · 68

4.4.2 Equivalent pore pressure of unsaturated porous media ····· 72

4.5 Summary and Discussion ····· 74

CHAPTER 5 MULTI-SCALE AND MICROMECHANICAL CONSTITUTIVE MODELING OF THE EFFECTIVE ELASTIC PROPERTIES OF CEMENT PASTE ····· 78

5.1 Introduction ····· 78

5.2 Micromechanical Constitutive Model for the Effective Elastic Properties of Hardened Cement Paste ····· 79

5.2.1 Model formulation ····· 80

5.2.2 Model verification ····· 89

5.3 Micromechanial Constitutive Model for the Effective Elastic Properties of Hardening Cement Paste ····· 90

5.3.1 Model formulation ····· 90

5.3.2 Model verification ····· **95**

5.4 Summary and Discussion ····· **97**

CHAPTER 6 MODELING SHRINKAGE OF HARDENING CEMENT PASTE ····· **104**

6.1 Introduction ····· **104**

6.2 Assumptions ····· **105**

6.3 Model Formulation ····· **107**

6.3.1 Consideration of nonlinearity and stress redistribution in the micromechanical model ····· **107**

6.3.2 Time-dependent model for the *C–S–H* matrix ····· **111**

6.4 Model Calibration ····· **114**

6.5 Model Verification ····· **117**

6.6 Consideration Influences of High Temperature and High Pressure ····· **117**

6.7 Summary and Discussion ····· **119**

CHAPTER 7 SUMMARY AND SUGGESTIONS ····· **126**

7.1 Summary ····· **126**

7.2 Suggestions ····· **127**

REFERENCES ····· **129**

APPENDIX I COEFFICIENTS A_1, A_2 AND A_3 IN EQUATION (5-7) ····· **138**

LIST OF TABLES

1-1 Typical Oxide Composition of a General-Purpose Portland Cement [Mindess et al. (2002)] ····· 15

1-2 Typical Chemical Composition of Portland Cement [Mindess et al. (2002); Taylor (1997)] ····· 15

3-1 Cement Compositions and the Corresponding Material Constants ····· 47

5-1 Elastic Properties of the Constituent Components of Cement Paste ····· 98

5-2 Physical Data of Reactants and Products in Portland Cement Hydration [Tennis and Jennings (2000); Mindess et al. (2002)] ····· 98

6-1 Time-Dependent Material Constants of *C–S–H* ····· 121

LIST OF FIGURES

1-1 Simplified Schematic Diagram of the Oil Well Structure

(a)–Cement Paste Used for Zonal Isolation ····· 16

(b)–Loss of Zonal Isolation due to Shrinkage of the Cement Sheath ····· 16

1-2 Chemical Shrinkage (ο) and Autogenous Shrinkage (□) of a Cement Paste with *w*/*c*=0.30 [Hammer (2002)] ····· 16

1-3 Scanning Electron Micrograph of a C_3S Paste [Tennis et al. (1997)] ····· 17

2-1 Diffusion of Free Water Through Layers of Hydration Products [Ulm and Coussy (1995)] ····· 38

2-2 Influence Factors of Cement Hydration Kinetics and Their Related Model Parameters ····· 38

2-3 Simulated and Measured Ultimate Degree of Hydration at *T*=293K

(a)–Experimental Data from [Mills (1966)] ····· 39

(b)–Experimental Data from [Baroghel-Bouny et al. (2006)] ····· 39

3-1 Simulated and Measured Degree of Hydration for Cement #A (Type I) (Experimental Data from [Lerch and Ford (1948)]) ····· 48

3-2 Simulated and Measured Degree of Hydration for Cement #B (Type II) (Experimental Data from [Lerch and Ford (1948)]) ····· 48

3-3 Simulated and Measured Degree of Hydration for Cement #C (Type III) (Experimental Data from [Lerch and Ford (1948)]) ····· 49

3-4 Simulated and Measured Degree of Hydration for Cement #D (Type IV) (Experimental Data from [Lerch and Ford (1948)]) ····· 49

3-5 Simulated and Measured Degree of Hydration for Cement #E (Experimental Data from [Keienburg (1976)]) ····· 50

3-6 Simulated and Measured Degree of Hydration for Cement #F (Experimental Data from [Danielson (1962)]) ····· 50

3-7 Simulated and Measured Degree of Hydration for Cement #G (Experimental Data from [Escalante-Garcia (2003)]) ····· 51

3-8 Simulated and Measured Degree of Hydration for Cement #H (Experimental Data from [Taplin (1969)]) ····· 51

3-9 Comparison of the Simulation with the Regression Values

(a)–Eq. (3-2) for A_0' ····· 52

(b)–Eq. (3-3) for k ····· 52

(c)–Eq. (3-4) for n_0 ····· 52

3-10 Simulated and Measured Degree of Hydration for C_3S under Pressure (Experimental Data from [Bresson et al. (2002)]) ····· 53

3-11 Predicted and Measured Degree of Hydration for OPC under Pressure (Experimental Data from [Zhou and Beaudoin (2003)]) ····· 53

3-12 Predicted and Measured Degree of Hydration for CCRL Cement 115 under Different Curing Conditions (Experimental Data from [Bentz et al. (1997)]) ····· 54

3-13 Predicted and Measured Degree of Hydration for CCRL Cement 152 with Different Water-Cement Ratios (Experimental Data from [Bentz (2006)]) ····· 54

3-14 Predicted and Measured Degree of Hydration for OPC at Different Temperatures (Experimental Data from [Hill et al. (2003)]) ····· 55

3-15 Predicted and Measured Adiabatic Temperature Changes for CEM I 52.5 PM CP2

Cement with Different Water-Cement Ratios (Experimental Data from [Bentz et al. (1998)]) ····· 55

3-16 Predicted and Measured Chemical Shrinkage for Class H Cement at Different Temperatures and Pressures (Experimental Data from [Chenevert and Shrestha (1991)]) ····· 56

3-17 Predicted and Measured Chemical Shrinkage for Class G Cement with Different Water-Cement Ratios (Experimental Data from [Justnes et al. (1995)]) ····· 56

3-18 Predicted and Measured Chemical Shrinkage for P30k Cement with Different Water-Cement Ratios (Experimental Data from [Justnes et al. (1996)]) ····· 57

3-19 Predicted and Measured Chemical Shrinkage for HS65 Cement with Different Water-Cement Ratios (Experimental Data from [Justnes et al. (1996)]) ····· 57

3-20 Predicted and Measured Chemical Shrinkage for Type I Cement with Different Water-Cement Ratios (Experimental Data from [Baroghel-Bouny et al. (2006)]) ····· 58

4-1 Pore Size Distribution Measurements [Whiting and Kline (1977)] ····· 76

4-2 Simulated and Measured Relative Humidity for 52.5 OPC Pastes with Different Water-Cement Ratios (Experimental Data from [Jiang et al. (2005)]) ····· 76

4-3 Simulated and Measured Relative Humidity for a CEM I 52.5 R Paste (Experimental Data from [Lura et al. (2003)]) ····· 77

5-1 Micromechanical Model for Hardened Cement Paste ····· 98

5-2 Simulated and Measured Elastic Moduli as a Function of Water-Cement Ratio of Cement Pastes at an Age of 28 Days (Experimental Data from [Haecker et al. (2005)]) ····· 99

5-3 Simulated and Measured Elastic Moduli as a Function of Water-Cement Ratio of

Cement Pastes at an Age of 56 Days (Experimental Data from [Haecker et al. (2005)]) ····· 99

5-4 Simulated (Using the Capillary Porosity Predicted by CEMHYD3D) and Measured Elastic Moduli as a Function of Water-Cement Ratio of Cement Pastes at an Age of 56 Days (Experimental Data from [Haecker et al. (2005)]) ····· 100

5-5 Micromechanical Model for Hardening Cement Paste ····· 100

5-6 Illustrated Procedure of Simulating the Effective Mechanical Properties of the Solid Phase of Hardening Cement Paste at Time $t + Dt$ ····· 101

5-7 Simulation of the Young's Modulous of Cement Paste Using the Mori-Tanaka Scheme on Level III ····· 102

5-8 Simulated (Using the Capillary Porosity Predicted by CEMHYD3D and the Self-Consistent Scheme at Level III) and Measured Elastic Moduli as a Function of Water-Cement Ratio of Portland Cement Pastes at an Age of 56 Days (Experimental Data from [Haecker et al. (2005)]) ····· 102

5-9 Simulated and Measured Elastic Moduli as a Function of the Degree of Hydration of Cement Pastes (Experimental Data from [Boumiz et al. (1997)])

(a)–Young's Modulus ····· 103

(b)–Shear Modulus ····· 103

6-1 Illustration of Stress Redistribution in the Solid Phase of Cement Paste ····· 121

6-2 Relationship Between the Threshold Stress Level for the Viscous Behavior of *C–S–H* to Occur and Its Total Bulk Strain with Different Signs of b_1 ····· 122

6-3 Simulated and Measured Autogenous Shrinkage of Cement Paste (Experimental Data from [Hua et al. (1997)]) ····· 122

6-4 Simulated and Measured Autogenous Shrinkage of Cement Pastes with Different Water-Cement Ratios (Experimental Data from [Horita and Nawa (2003)]) ····· 123

6-5 Simulated and Measured Autogenous Shrinkage of Cement Paste (Experimental Data from [Lura et al. (2003)]) ····· 123

6-6 Simulated and Measured Autogenous Shrinkage of Cement Pastes (Experimental Data from [Koenders (1997)])

(a)–CEM I 32.5R Paste ····· 124

(b)–CEM I 42.5R Paste ····· 124

(c)–CEM I 52.5R Paste ····· 125

NOTATIONS AND SYMBOLS

A_0 = Initial chemical affinity of cement hydration [J/m^3]

A_0' = Normalized initial chemical affinity of cement hydration [J/m^3]

A_1, A_2, A_3 = Functions of f_{ace}, G_{ace}, G_{hp}, n_{ace} and n_{hp}

A_a = Chemical affinity of cement hydration [J/m^3]

a = Parameter of the equation for the diameter of the largest water-filled capillary pore

b = Biot's coefficient

b_1 = Parameter of the shrinkage model

b_{ij} = The ij^{th} component of Biot's tangent tensor

Blaine = Value of the Blaine fineness [m^2/kg]

C_{ijkl} = The $ijkl^{th}$ component of the tensor of skeleton tangent elastic stiffness moduli [GPa]

c = Mass of cement [g]

c_1, c_2, c_{10} = Parameters of the equation for the diameter of the largest water-filled capillary pore

E = Young's modulus [GPa]

E_a = Apparent activation energy [J/mol]

E_{LDCSH} = Young's modulus of low-density *C–S–H* [GPa]

E_{HDCSH} = Young's modulus of high-density *C–S–H* [GPa]

e_{ij} = Deviatoric components of the strain tensor

f_1 = Function of $Blaine$ and a

f_2 = Function of T and a

f_{ace} = Volume fraction of the anhydrous cement inclusions in the solid phase of cement paste

f_{ace-ih} = Volume fraction of the core formed by anhydrous cement and the inner layer of the newly formed hydration products

f_{CH} = Volume fraction of CH inclusions in the hydration products

f_{in} = Volume fraction of the original anhydrous cement core in the original volume the of solid phase of cement paste

f_{nc1-fh} = Volume fraction of the core formed by anhydrous cement, the inner layer of the newly formed hydration products and the previously formed hydration products

f_{nc2-oh} = Volume fraction of the solid phase of cement paste

f_{void} = Volume fraction of voids

G = Shear modulus [GPa]

G_{ace} = Shear modulus of the anhydrous cement clinker [GPa]

G_{ace-ih} = Effective shear modulus of the core formed by anhydrous cement and the inner layer of the newly formed hydration products [GPa]

G_{cep} = Effective shear modulus of cement paste [GPa]

G_{ces} = Effective shear modulus of the solid phase of cement paste [GPa]

G_{CH} = Shear modulus of *CH* [GPa]

G_{CSH} = Shear modulus of *C–S–H* [GPa]

G_{CSH}^{t} = Tangent shear modulus of *C–S–H* [GPa]

G_{fh} = Effective shear modulus of the previously formed hydration products [GPa]

G_{hp} = Effective shear modulus of hydration products [GPa]

G_{hp}^{t} = Tangent shear modulous of the previously formed hydration products [GPa]

G_{ih} = Effective shear modulus of the inner layer of the newly formed hydration products [GPa]

G_{m} = Shear modulus of the matrix in a composite medium [GPa]

G_{nc1-fh} = Effective shear modulus of the core formed by anhydrous cement, the inner layer of the newly formed hydration products and the previously formed hydration products [GPa]

G_{nc2-oh} = Effective shear modulus of the solid phase of cement paste [GPa]

G_{oh} = Effective shear modulus of the outer layer of the newly formed hydration products [GPa]

G_{oh}^{t} = Tangent shear modulus of the outer layer of the newly formed hydration products [GPa]

G_{s} = Modified free energy of the skeleton in a porous medium [J/m^3]

g = Function of K_{in}^{t}, K_{hp}^{t} and G_{hp}^{t}

GMW = Gram molecular weight [g/mol]

K = Bulk modulus [GPa]

K_{ace} = Bulk modulus of the anhydrous cement clinker [GPa]

K_{ace-ih} = Effective bulk modulus of the core formed by anhydrous cement and the inner layer of the newly formed hydration products [GPa]

K_{cep}^{d} = Effective drained bulk modulus of cement paste [GPa]

K_{cep}^{u} = Effective undrained bulk modulus of cement paste [GPa]

K_{ces} = Effective bulk modulus of the solid phase of cement paste [GPa]

K_{CH} = Bulk modulus of *CH* [GPa]

K_{CSH} = Bulk modulus of *C–S–H* [GPa]

K_{CSH}^{cr} = Tangent creep bulk modulus of *C–S–H* [GPa]

K_{CSH}^{t} = Tangent bulk modulus of *C–S–H* [GPa]

K_{CSH}^{u} = Undrained bulk modulus of *C–S–H* [GPa]

K_{d} = Drained tangent bulk modulus [GPa]

K_{f} = Bulk modulus of the pore fluid [GPa]

K_{fh} = Effective bulk modulus of the previously formed hydration products [GPa]

K_{hp} = Effective bulk modulus of hydration products [GPa]

K_{hp}^{t} = Tangent bulk modulus of the previously formed hydration products [GPa]

K_{ih} = Effective bulk modulus of the inner layer of the newly formed hydration products [GPa]

K_{in}^{t} = Tangent bulk modulus of the composite volume that was originally the anhydrous cement [GPa]

K_{nc1-fh} = Effective bulk modulus of the core formed by anhydrous cement, the inner layer of the newly formed hydration products and the previously formed hydration products [GPa]

K_{nc2-oh} = Effective bulk modulus of the solid phase of cement paste [GPa]

K_{oh} = Effective bulk modulus of the outer layer of the newly formed hydration products [GPa]

K_{oh}^{t} = Tangent bulk modulus of the outer layer of the newly formed hydration products [GPa]

K_{s} = Effective bulk modulus of the solid phase in a porous medium [GPa]

K_{st} = Parameter of the shrinkage model [GPa]

K_{u} = Undrained tangent bulk modulus [GPa]

K_{w} = Bulk modulus of water [GPa]

k = Parameter of the hydration kinetics model [J]

M = Function of N, f and K_f [GPa]

M_{ce} = Amount (by mass) of cement in the paste [kg/m^3]

N = Biot's tangent modulus [GPa]

n	= Function of h_a and a	[ln(J·hr)]
n_0	= Parameter of the hydration kinetics model	[ln(J·hr)]
n_1	= Parameter of the shrinkage model	
p	= Applied pressure	[MPa]
p^*	= Averaged fluid pressure	[MPa]
p_a	= Pressure of the pore air	[MPa]
p_{atm}	= Atmospheric pressure	[MPa]
p_c	= Capillary stress	[MPa]
p_{C_2S}	= Bogue mass fraction of C_2S in cement	
p_{C_3A}	= Bogue mass fraction of C_3A in cement	
p_{C_3S}	= Bogue mass fraction of C_3S in cement	
p_{C_4AF}	= Bogue mass fraction of C_4AF in cement	
p_w	= Pressure of the pore water	[MPa]
Q	= Heat of hydration	[J/kg]
Q_{max}	= Maximum heat of hydration	[J/kg]
q_{ace}	= Specific heat of the anhydrous cement	[J/(kg·K)]
q_{hce}	= Fictitious specific heat of the hydrated part of cement	[J/(kg·K)]
q_{paste}	= Specific heat of cement paste	[J/(kg·K)]
q_w	= Specific heat of water	[J/(kg·K)]
R	= Universal gas constant	[J/(mol·K)]

RH	= Relative humidity	
S	= Entropy	[J/ m^3·K]
S_s	= Entropy of the skeleton in a porous medium	[J/(m^3·K)]
S_s'	= Function of S_s, f, U and T	[J/(m^3·K)]
S_w	= Saturation ratio of pores	
s	= Function of p and a	
s_{ij}	= Deviatoric components of the stress tensor	[MPa]
T	= Absolute temperature	[K]
t	= Time	[hr]
U	= Interfacial energy	[J/m^3]
V	= Volume	[m^3]
V_{ac}	= Volume of the original anhydrous cement core	[m^3]
V_{hp}	= Volume of the previously formed hydration products	[m^3]
V_m	= Molar volume of the pore solution	[m^3/mol]
V_{others}	= Volume of the hydration products other than *C–S–H* and *CH*	[cm^3]
V_{pore}	= Cumulative capillary pore volume	[m^3]
$V_{pore-water}$	= Cumulative water-filled capillary pore volume	[m^3]
V_{ref}	= Reference pore volume	[m^3]
v	= Volume ratio between the hydration products and the reacted cement	
v_{293}	= Volume ratio between the hydration products and the reacted cement at	

$T = 293\text{K}$

v_c = Specific volume of cement [cm^3/g]

v_{chsh} = Chemical shrinkage of cement paste

v_n = Specific volume of the chemically bound water [cm^3/g]

w = Mass of water [g]

w_n = Mass of the chemically bound water [g]

a = Degree of hydration

a_1, a_2 = Functions of K_{CSH} and G_{CSH}

a_3, a_4 = Functions of K_{ces} and G_{ces}

a_{kl} = The kl^{th} component of the tensor of skeleton tangent thermal dilation coefficients [$1/^o\text{C}$]

$3a_{th}$ = Volumetric thermal dilation coefficient [$1/^o\text{C}$]

a_u = Ultimate degree of hydration

$a_{u,293}$ = Ultimate degree of hydration at $T = 293\text{K}$

$3a_f$ = Volumetric thermal dilation coefficient related to the porosity [$1/^o\text{C}$]

b_1, b_2 = Functions of *Blaine*

b_3 = Function of s_{out}, Ds_{out}, K_{oh}^t and f_{in}

b_4 = Function of Ds_{out} and G_{oh}^t

g = Surface tension of water [N/m]

De_{in} = Change in the effective volumetric strain of the inner layer of the newly

formed hydration products and the reduced anhydrous cement core during time step Dt

De_{out} = Change in the effective volumetric strain of the solid phase of cement paste during time step Dt

De'_{out} = Change in the volumetric strain of a spherical shell subject to both inner and outer pressures during time step Dt

Ds_{in} = Change in the effective stress of the inner layer of the newly formed hydration products and the reduced anhydrous cement core during time step Dt [MPa]

Ds_{out} = Change in the effective stress of the original volume of the solid phase of cement paste during time step Dt [MPa]

d_{ij} = Kronecker delta

e_{CSH} = Total bulk strain of *C–S–H*

e_{CSH}^{cr} = Creep bulk strain of *C–S–H*

e_{CSH}^{e} = Elastic bulk strain of *C–S–H*

e_{ij}, e_{kl} = The ij^{th} and the kl^{th} component of the strain tensor

e_{sv} = Volumetric deformation of the solid phase in a porous medium

e_{v} = Volumetric deformation

h = Parameter of the shrinkage model [$(\text{GPa})^{n_1}$]

h_1 = Function of G_{ace}, G_{hp}, n_{ace} and n_{hp}

h_2 = Function of G_{ace}, G_{hp} and n_{ace}

h_3 = Function of G_{ace}, G_{hp} and n_{hp}

h_a = Normalized permeability of the hydration products around the anhydrous cement core [1/(J·hr)]

n = Poisson's ratio

n_{ace} = Poisson's ratio of the anhydrous cement clinker

n_{cep}^{d} = Effective drained Poisson's ratio of cement paste

n_{hp} = Poisson's ratio of the hydration products

p = Equivalent pore pressure [MPa]

r = Density [kg/m^3]

r_{paste} = Density of cement paste [kg/m^3]

s_b = Bulk (hydrostatic) stress of the porous medium [MPa]

s_{CSH} = Bulk stress of *C–S–H* [MPa]

s_{ij} = The ij^{th} component of the stress tensor [MPa]

s_{in} = Effective bulk stress of the anhydrous cement core [MPa]

s_{out} = Effective bulk stress of the solid phase of cement paste [MPa]

s_{sb} = Bulk stress of the solid phase in a porous medium [MPa]

s_{st} = Threshold stress level for the viscous behavior of the *C–S–H* matrix to occur [MPa]

$F_{A\to B}$ = Dissipation associated with the chemical reaction $A \to B$ [J/(m^3·hr)]

f = Capillary porosity

j	= Diameter of the capillary pore diameter	[m]
j_0	= Diameter of the smallest capillary pore	[m]
$j_{pore-water}$	= Diameter of the largest water-filled capillary pore	[m]
Y	= Free energy	[J/m^3]
Y_s	= Free energy of the skeleton in a porous medium	[J/m^3]
y_s	= Free energy of the solid phase in a porous medium	[J/m^3]

ACKNOWLEDGEMENTS

For the last three and a half years, I have had the good fortune to work at Columbia University with Prof. Christian Meyer, who has been consistently offering his support, guidance and encouragement through the process of this study. His enormous help, both professional and otherwise, will always be appreciated.

I am very grateful to Professors Rene B. Testa, James S. Im, Andrew W. Smyth, and James C. Hone for their serving on the Defense Committee and for their review of this dissertation.

The support of this study was provided by Halliburton Energy Services (HES), which is cordially appreciated. The enthusiastic help from Lewis Norman, Anthony Badalamenti, David Meadows, Dennis Gray, B.R. Reddy, David Mcmechan, Kris Ravi and many other HES personnel is gratefully acknowledged.

Special thanks go to Wolfgang Deeg and his wife, Janet, for their hospitality, care and generosity during my stays in Duncan.

I would also like to thank the faculty of the Department of Civil Engineering and Engineering Mechanics and other departments for teaching and mentoring me. Gratitude also goes to the departmental staff for their great help over the years. The assistance in literature collection from the staff of the Columbia University Library is thankfully acknowledged.

Sincere thanks are also extended to Dr. Dale Bentz, Dr. H.J.H. Brouwers, Dr. Edward J. Garboczi, Prof. Ole Mejlhede Jensen, Prof. Eddy A.B. Koenders, Prof. Pietro Lura, Prof. Klaas van Breugel, Dr. Vincent Waller, and many others for their helpful

communications with me on professional issues related to this study.

Many thanks are expressed to Xiaopeng Qin, Yuhong He and others for their friendship and help during these years.

And most of all, I would like to express my utmost love and gratefulness to my family. To my sister Nan and brother-in-law Fei, thank you for your constant concern and unconditional assistance that have inspired me all the time. To Shangao, thank you for your understanding and support before and wish you a happy life in the future. To my parents, thank you for always being there for me. None of this work would have been possible without your love. Mom and Dad, this work, with heartfelt love, is dedicated to you.

To My Mom and Dad

献给我的爸爸妈妈

CHAPTER 1

INTRODUCTION

Portland cement was invented in the early 19th century. Since then, it has gained universal popularity with applications covering many different fields, primarily in civil engineering and petroleum engineering. The most important application of Portland cement is concrete, a “man-made stone” that contains mainly Portland cement paste and aggregates including gravel and sand. It is a strong and durable construction material used for most of our built infrastructures such as buildings, roads, bridges, dams and underground structures. Omitting the large-size aggregates leads to another construction material, mortar, which is used for some specific applications such as masonry construction. Portland cement paste (without any aggregate) is also used in engineering, e.g. for zonal isolation in oil wells to prevent the cross-flow of fluids such as oil, water and gas between different geological layers, where it is critical for successful oil extraction, as shown in Fig. 1-1.

In order to improve the performance of the cement-based construction materials, whether concrete, mortar or cement paste, chemical and/or mineral admixtures are usually added. However, the most important properties of the cementitious materials are associated with the hydration of Portland cement and its related phenomena. One such phenomenon is shrinkage. Cracks may develop in concrete structures if the autogenous and drying shrinkage of cement paste are constrained; zonal isolation in oil wells may be compromised due to the reduction of contact pressure between the cement sheath and the rock formation caused by the autogenous shrinkage of cement paste and the bulk

deformation induced by the externally applied hydrostatic pressure, as shown in Fig. 1-1(b).

Although the computer modeling of cement hydration, microstructure development, shrinkage, strength growth and other properties of concrete is in great need in a large variety of practical problems, concrete material technology has always been highly empirical until a modern discipline, namely computational materials science was applied to this area in the 1980's. Due to the complex random natures of concrete and mortar, such computer modeling should start with the simulation of cement hydration and the associated mechanical and chemical properties of cement paste. Although great efforts have been exerted in this field, simple, versatile, and easy-to-use mathematical models for Portland cement hydration and the associated autogenous shrinkage are still wanting.

In this chapter, the mechanisms of hydration and shrinkage of Portland cement are briefly described, followed by a review of the pertinent literature on mathematical and numerical modeling. The objective, scope and outline of the dissertation conclude this chapter.

1.1 Introduction of Hydration and Shrinkage of Portland Cement

Portland cement is produced by heating a mixture of limestone and clay, or other materials of similar bulk composition and sufficient reactivity, to a temperature of about 1450°C (2642°F), at which partial fusion occurs and nodules of clinker are formed. The clinker is then mixed with a few percent of gypsum and finely ground. A detailed description of the production process for Portland cement is given in Taylor (1997).

1.1.1 Cement composition

There exist two forms in which to describe the composition of cement, one is by the oxide composition as given in Table 1-1 [Mindess et al. (2002)], which is determined by standard methods; the other one is by the chemical composition as shown in Table 1-2 [Mindess et al. (2002); Taylor (1997)], the direct analysis of which requires special skills and equipment. Therefore, the second form is usually determined using the compound stoichiometries and the values of the first form. The *Bogue calculation* [Bogue (1947)] is considered the most classic one of such mathematical methods. For convenience, the universal shorthand notation listed in the second column of Table 1-1 and the third column of Table 1-2 are used in this dissertation.

1.1.2 Fineness and particle size distribution of cement

The mean size of ordinary Portland cement particles ranges from 10 to 15μm. The fineness of cement is generally denoted by the specific surface of the particles, which means the sum of the surface areas of all the particles per unit mass. It should be pointed out that because of the variable morphology of cement particles, different methods to measure specific surface yield different results. Thus, the value of specific surface should be accompanied by the method used to measure it. In this dissertation, the *Blaine* fineness (ASTM C 204) is used, which is determined by the air-permeability method based on the correlation between the surface area of the particles in a porous bed and the rate of air that passes through.

The particle size distribution of cement is usually expressed by the percentage by mass passing a series of sieves with different diameters. Currently used methods of measuring the particle size distribution of cement include sedimentation-based methods,

laser diffraction, air separator, optical microscopy and the Coulter Counter, all of which convert the real particle sizes being measured to the diameters of equivalent spheres [van Breugel (1991)].

1.1.3 Hydration of Portland cement

The reaction of Portland cement and water is defined as *hydration*; and the new solids formed through such hydration are called *hydration products*. The hydration of Portland cement consists of a series of exothermic reactions and is too complex to be described by simple chemical equations. The following basic reactions found in the literature are a generally accepted approximation of hydration of the constitutive clinker phases with coexisting gypsum [e.g. Mounanga et al. (2004)].

$$2C_3S + 10.6H \rightarrow C_{3.4}S_2H_8 + 2.6CH \quad (1\text{-}1)$$

$$2C_2S + 8.6H \rightarrow C_{3.4}S_2H_8 + 0.6CH \quad (1\text{-}2)$$

$$C_3A + 3C\bar{S}H_2 + 26H \rightarrow C_6A\bar{S}_3H_{32} \quad (1\text{-}3)$$

$$2C_3A + C_6A\bar{S}_3H_{32} + 4H \rightarrow 3C_4A\bar{S}H_{12} \quad (1\text{-}4)$$

$$C_3A + 6H \rightarrow C_3AH_6 \quad (1\text{-}5)$$

$$C_4AF + 3C\bar{S}H_2 + 30H \rightarrow C_6A\bar{S}_3H_{32} + CH + FH_3 \quad (1\text{-}6)$$

$$2C_4AF + C_6A\bar{S}_3H_{32} + 12H \rightarrow 3C_4A\bar{S}H_{12} + 2CH + 2FH_3 \quad (1\text{-}7)$$

$$C_4AF + 10H \rightarrow C_3AH_6 + CH + FH_3 \quad (1\text{-}8)$$

The principal hydration product is the calcium silicate hydrate, which is usually in gel form and of a composition that varies over a wide range. Therefore, the formula $C_{3.4}S_2H_8$ is only approximate, and the designation *C–S–H* is more frequently used

instead. Other major hydration products include calcium hydroxide (*CH*) and calcium sulfoaluminate hydrate that mainly consists of ettringite ($C_6A\bar{S}_3H_{32}$) and monosulfoaluminate ($C_4A\bar{S}H_{12}$), all of which are in crystal forms.

1.1.4 Shrinkage of cement paste

The volume of the hydration products is smaller than the combined volume of the reacted cement and water. This reduction in volume is called the *chemical shrinkage* of cement paste and is the main cause of the *self-desiccation shrinkage*, which is defined as the bulk shrinkage of cement paste in a closed isothermal system (i.e. without moisture exchange). The self-desiccation shrinkage constitutes the principal part of the *autogenous deformation*, which also includes the possible short-term expansion that may be attributed to the formation of ettringite at the early stage of cement hydration. Another kind of shrinkage, which is usually referred to as the *drying shrinkage*, is caused by the loss of water during hydration due to evaporation when cement paste is exposed to the open air. There also exist other kinds of deformation, such as the *thermal deformation* due to temperature change; the *carbonation shrinkage* due to the reaction between *CH* in the cement paste with water and CO_2 in the air; and the deformation due to external loads. Many investigations have been conducted on the shrinkage of cementious materials via experiments and theoretical analysis. Thorough reviews of the autogenous deformation and its measurements can be found in Justnes et al. (1994) and Jensen and Hansen (1996, 2001). A discussion of drying shrinkage is given in Hansen (1987). In this section, the causes of shrinkage, the shrinkage of cement paste under curing conditions of elevated temperature and applied pressure, and the experimental

techniques to measure chemical and autogenous shrinkage are briefly described.

Three factors have been identified that may contribute to the autogenous shrinkage, namely capillary stress, disjoining pressure and surface tension [e.g. Hua et al. (1995, 1997); Koenders and van Breugel (1997); Shimomura and Maekawa (1997)]. It is generally accepted that surface tension is the major driving force of shrinkage when the internal relative humidity (*RH*) of cement paste is low [e.g. Ferraris and Wittmann (1987)], while at higher relative humidity, capillary stress and disjoining pressure may play important roles [e.g. Jensen (1993, 1995); Beltzung and Wittmann (2005)]. However, the absolute value of disjoining pressure is very difficult to quantify, especially for hardening cement paste [e.g. Lura et al. (2003)].

In oil wells, cement paste used for zonal isolation is likely to cure and harden in the environments of high temperature and high pressure [Chenevert and Shrestha (1991)]. Under such curing conditions, the shrinkage of cement paste exhibits different characteristics than under ambient conditions. However, due to the difficulties of simulating downhole conditions in a laboratory, only very few investigations of the shrinkage of cement pastes at high curing temperatures and high pressures have been reported. The few pertinent studies found in the open literature are those by Beirute and Tragesser (1973), Chenevert and Shrestha (1987, 1991), Sabins and Sutton (1991) and Goboncan and Dillenbeck (2003). According to these studies,

— Elevated temperature and high pressure tend to reduce chemical shrinkage.

— Shrinkage occurs mainly after the initial setting.

— The bulk volume changes of cement paste under downhole conditions include the autogenous shrinkage and the load-induced bulk deformation.

— Cement expansion additives can be used to reduce the shrinkage of cement paste under downhole conditions.

However, extensive research is still required to fully understand the shrinkage of cement paste under the curing conditions of high temperature and high pressure.

Chemical shrinkage is usually measured using a gravimetric method [Mounanga et al. (2004)]. In this method, cement paste is placed in a flask, the remaining empty part of which is filled with distilled water. The flask is closed, hung from a balance and immersed in water at the required curing temperature. To measure autogenous shrinkage, there exist two different ways, viz. volumetric and linear measurement [Jensen and Hansen (2001)]. The former is carried out by sealing the cement paste in a rubber balloon immersed in water and recording the amount of water displaced by the immersed sample [Douglas and Hover (2004)]; while the latter is performed by placing the cement paste in a rigid mold with low restraint and measuring the length change by a displacement transducer at the end of the specimen. As shown in Fig. 1-2 [Hammer (2002)], autogenous shrinkage coincides with chemical shrinkage during the first few hours after mixing, in which the cement paste is considered to be in the “liquid phase”. As cement hydration progresses, cement paste becomes sufficiently stiff and the autogenous and chemical shrinkage start to diverge.

The measurement of autogenous shrinkage under high temperatures and high pressures also requires good sealing of the cement paste and special heating and pressurizing equipment [Chenevert and Shrestha (1987)]. An increase in temperature has been observed to shorten the setting time [Baroghel-Bouny et al. (2004)], while an increase in pressure yields longer setting time because high pressure impedes the

formation of the semi-rigid (self-supporting) skeleton of cement paste. Since in an oil well the rate of increase in pressure is much larger than that in temperature, the deviation of autogenous shrinkage from chemical shrinkage occurs later under downhole conditions than under ambient conditions.

1.2 Mathematical and Numerical Modeling of Hydration Kinetics for Portland Cement

The phenomena of heat liberation, strength development and shrinkage result from cement hydration, which contains a series of chemical, physical and mechanical processes. A thorough understanding of these processes is a critical prerequisite for modeling the hydration kinetics of Portland cement.

1.2.1 Micro numerical modeling of cement hydration kinetics

A branch of computational materials science has arisen over the past twenty years with the objective of the computer modeling of hydration and microstructure development of cementitious materials. Noteworthy studies include those of Jennings and Johnson (1986), Bentz and Garboczi (1989), van Breugel (1991), Navi and Pignat (1996), and Maekawa et al. (1999). Among these, the NIST model referred to as CEMHYD3D [Benz (1997)] and the Dutch HYMOSTRUC model [van Breugel (1991)] appear to be the most advanced and widely used ones.

The CEMHYD3D model constitutes a three-dimensional representation of cement using a measured particle size distribution and a set of scanning electron microscopy images. Cement particles are simulated as a collection of pixels. A set of

cellular-automata rules is applied to the initial microstructure to simulate the chemical reactions of all the major clinker phases during cement hydration. The evolution of microstructure is organized in cycles consisting of dissolution, diffusion, and reaction steps and is given in terms of elapsed cycles. The model can be used to predict the degree of hydration, heat release, chemical shrinkage, percolation, diffusivity and setting of cementitious materials, and the degree-of-hydration predictions can be further used to predict the compressive strength development.

In the HYMOSTRUCT model, spheres of different diameters are used to simulate cement particles. Hydration is assumed to occur at the particle/water interface and the hydration products grow around the diminishing particles of anhydrous cement. The hydration process is assumed to be a combination of a phase boundary-controlled reaction and a diffusion-controlled one. The model can reproduce the degree of hydration as a function of the chemical composition of cement, particle size distribution, water-cement ratio, and curing temperature. The hydration kinetics of cements at a curing temperature up to 50°C was predicted by van Breugel (1991) using this model. The HYMOSTRUCT has also been extended to model the aggregate/paste interfacial transition zone, the development of the elastic moduli, the early age creep and the autogenous shrinkage of both cement paste and concrete [Koenders (1997); Lokhorst (1998)].

These micro numerical approaches attempt to simulate cement hydration and microstructure formation on the elementary level of cement particles, which is the most rational way, as long as the chemical, physical and mechanical characteristics of cement hydration are properly taken into account. However, such models are usually

computationally demanding.

1.2.2 Macro mathematical modeling of cement hydration kinetics

For most practical applications, microscopic models are too complex, and simpler mathematical models are needed to describe and quantify hydration kinetics. In fact, numerous attempts have been undertaken with that objective and many such simplified formulations can be found in the literature, e.g. Byfors (1980), Knudsen (1982), Freiesleben Hansen and Pedersen (1985), Basma et al. (1999), Nakamura et al. (1999), Cervera et al. (2002), Schindler and Folliard (2005), and Bentz (2006).

In contrast to the microscopic models of Section 1.2.1, most of these simplified models are based on experimental observations of macroscopic phenomena, and they capture the effects of curing temperature, water-cement ratio, fineness, particle size distribution and chemical composition of cement with different degrees of accuracy. For example, in Schindler and Folliard (2005), the apparent activation energy is related to the chemical composition and fineness of cement through regression analysis of the experimental data for several different cements; and in Bentz (2006), the instantaneous rate of cement hydration is related to the local probabilities of dissolution and precipitation of clinker phases.

1.2.3 Limitations of existing mathematical models

The mathematical models for hydration kinetics of Portland cement that have been presented so far have several limitations. Their range of curing temperature is small and does not exceed 60°C, and none of them include the effect of applied pressure. However, elevated temperatures and high pressures are frequently encountered in oil

wells where they must be addressed. Also, the identification of the model parameters for most of these models is usually difficult and sometimes even arbitrary, with no simple guidelines for that purpose. Therefore, most of these models are less likely to be suitable for blind predictions of hydration kinetics of Portland cement at elevated curing temperatures and high pressures.

1.3 Modeling Shrinkage of Cement Paste

Modeling the shrinkage of cement paste is difficult because of its multiphase constituent components as well as their chemical, physical and mechanical properties and structures. Fig. 1-3 shows a scanning electron micrograph of a C_3S paste [Tennis et al. (1997)], which is made up of hydration products, anhydrous C_3S and macro-pores. For a Portland cement paste, the constituent components and structure can be much more complicated. The mathematical descriptions of the pore structure, the water or moisture diffusion, the constituent components including *C–S–H*, *CH* and anhydrous cement as well as their elastic, viscoelastic, plastic and even viscoplastic properties, and most important of all, the combined effects of these factors on the shrinkage behavior of hardened cement paste are intriguing. The aging characteristics of hardening cement paste make the mathematical modeling task even more demanding.

In spite of these difficulties, the importance of shrinkage in various fields of engineering calls for concerted research efforts in this area. Limited models with different levels of complexity and applicability can be found in the literature of the past several decades. From a material property point of view, they can be categorized in two families, viz. the macro or phenomenological models and the micromechanical ones.

1.3.1 Macro or phenomenological models of shrinkage

Some models, such as those of Paulini (1994), Hua et al. (1995), Koenders and van Breugel (1997), Shimomura and Maekawa (1997), and Lura et al. (2003), regard cement paste as one macro material and assign one single set of material properties such as elastic moduli to the shrinking cement paste. The effects of aging on the material properties of hardening cement were considered in some of these models [e.g. Koenders and van Breugel (1997)], by making the material properties functions of the degree of hydration. This approach is simple, but the material constants required for such models usually do not have clear physical meanings and are difficult to obtain.

1.3.2 Micromechanical models of shrinkage

The other group of models considers the microstructure and/or the constituent components of cement paste, such as those of Bentz et al. (1995), Neubauer et al. (1996), Hua et al. (1997), Xi and Jennings (1997), Mabrouk et al. (2004), and Eguchi and Teranishi (2005). Although more logical in model formulation, these models are usually very sophisticated and their degrees of validity depend on the clear understanding and reasonable assumptions of the microstructure and constituent components of cement paste. In Bentz et al. (1995) and Hua et al. (1997), numerical approaches such as the finite element method were utilized to represent the microstructure and constituent components of cement paste, and the shrinkage was obtained from complicated numerical analysis. Therefore, this approach is likely to be too involved to be applicable for practical problems. Haecker et al. (2005) used a similar approach to calculate the effective elastic moduli of hardening cement paste. Mabrouk et al. (2004), on the other hand, employed the solidification theory proposed

by Bažant and Prasannan (1989) to analyze the shrinkage of young concrete considering the time-dependent properties of the cement matrix. Solidification theory is relevant in modeling the constitutive properties of concrete, but for cement paste it is not adequately accurate due to the much more complex components and microstructure at the scale of cement matrix [Ulm et al. (2004)]. The models proposed by Neubauer et al. (1996), Xi and Jennings (1997), and Eguchi and Teranishi (2005) are based on the mechanics of composite materials, which could address the composite characteristics of cement paste yet remain simple enough for practical applications.

1.3.3 Limitations of available micromechanical models of shrinkage

First of all, cement paste is fundamentally a porous medium [Ulm et al. (2004)]. The available micromechanical models usually do not adequately take this fact into account. Secondly, the time-dependent properties of cement paste are not properly considered in most of these models, although the most important constituent component of cement paste, *C–S–H*, exhibits highly time-dependent characteristics. And thirdly, the identification of model parameters for most of these models is not straightforward, making them difficult to apply.

1.4 Objectives, Scope and Outline of the Dissertation

The present study focuses on the mathematical modeling of the hydration kinetics and shrinkage of cement paste. The hydration kinetics modeling aims at formulating a theoretically sound, simple-to-use and versatile mathematical model that considers the effects of a wide range of curing temperature and applied pressure. For the shrinkage modeling, a multi-scale, micromechanics-based constitutive model is developed. The

framework of this constitutive model is so general that it can be extended to describe the shrinkage of cement paste under curing conditions of high temperature and high pressure, if the necessary experimental data are made available. To simplify the driving forces of shrinkage, the shrinkage model assumes that the relative humidity is high ($RH > 70\%$). However, the mechanical framework of the constitutive model is such that it can be used to simulate shrinkage of cement paste at low relative humidity as well. The hydration kinetics model and the shrinkage model aim at describing the average properties of a representative volume and can be embedded in numerical analysis of practical problems, such as the finite element analysis.

The remainder of this dissertation consists of six chapters. A hydration kinetics model for Portland cement based on thermodynamics of multiphase porous media is formulated in Chapter 2. In Chapter 3, this hydration kinetics model is calibrated against different sets of experimental data to determine its material constants. The model is then used to predict various properties of cement paste, which are compared with additional experimental data. In Chapter 4, the driving forces of shrinkage of cement paste are identified and quantified. Then, the multi-scale and micromechanical models to simulate the effective elastic properties of hardened and hardening cement paste are developed in Chapter 5. In Chapter 6, the effects of nonlinearity and creep are considered in simulating the shrinkage of hardening cement paste. The proposed models are calibrated and validated against various available experimental data. The possible extension of the constitutive model to high temperature and high pressure environments are also discussed in Chapter 6. Finally, summary and suggestions are given in Chapter 7.

Table 1-1 Typical Oxide Composition of a General-Purpose Portland Cement [Mindess et al. (2002)]

Oxide	Shorthand Notation	Common Name	Weight Percent
CaO	C	Lime	64.67
SiO_2	S	Silica	21.03
Al_2O_3	A	Alumina	6.16
Fe_2O_3	F	Ferric oxide	2.58
MgO	M	Magnesia	2.62
K_2O	K	Alkalis	0.61
Na_2O	N		0.34
SO_3	$\overline{S}$	Sulfur trioxide	2.03
CO_2	$\overline{C}$	Carbon dioxide	–
H_2O	H	Water	–

Table 1-2 Typical Chemical Composition of Portland Cement [Mindess et al. (2002); Taylor (1997)]

Chemical Name	Chemical Formula	Shorthand Notation	Weight Percent
Tricalcium Silicate (Alite)	$3CaO \cdot SiO_2$	C_3S	50% – 70%
Dicalcium Silicate (Blite)	$2CaO \cdot SiO_2$	C_2S	15% – 30%
Tricalcium Aluminate	$3CaO \cdot Al_2O_3$	C_3A	5% – 10%
Tetracalcium Aluminoferrite	$4CaO \cdot Al_2O_3 \cdot Fe_2O_3$	C_4AF	5% – 15%
Calcium Sulfate Dehydrate (Gypsum)	$CaSO_4 \cdot 2H_2O$	$C\overline{S}H_2$	4% – 6%

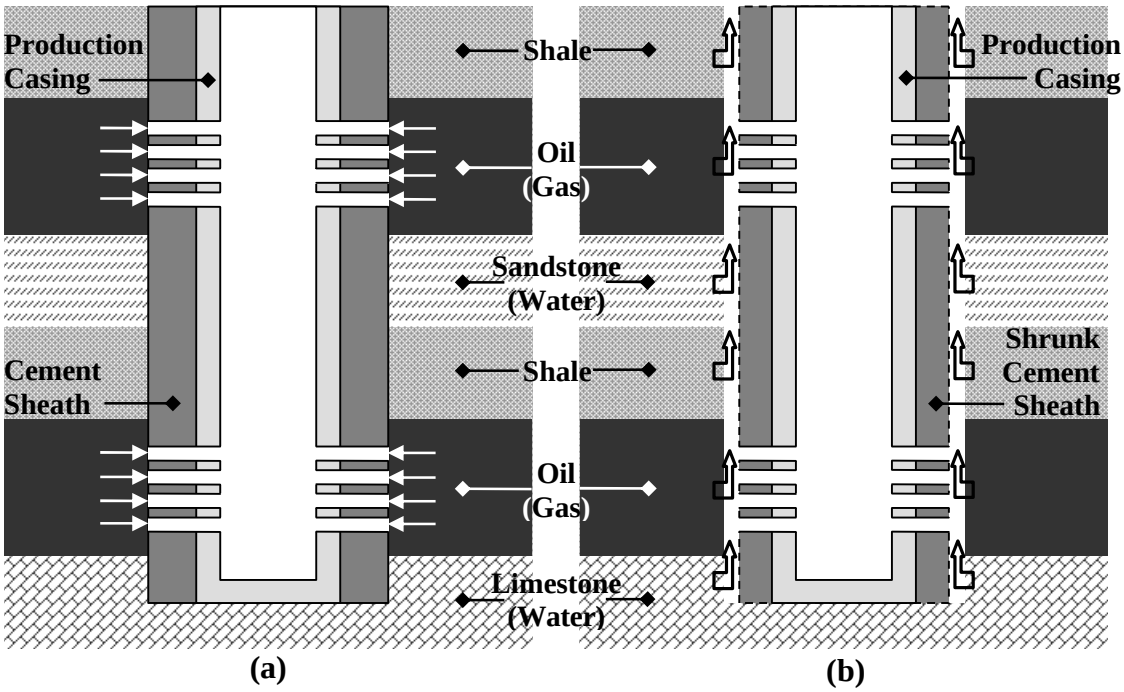

Fig. 1-1 Simplified Schematic Diagram of the Oil Well Structure
(a)–Cement Paste Used for Zonal Isolation;
(b)–Loss of Zonal Isolation due to Shrinkage of the Cement Sheath

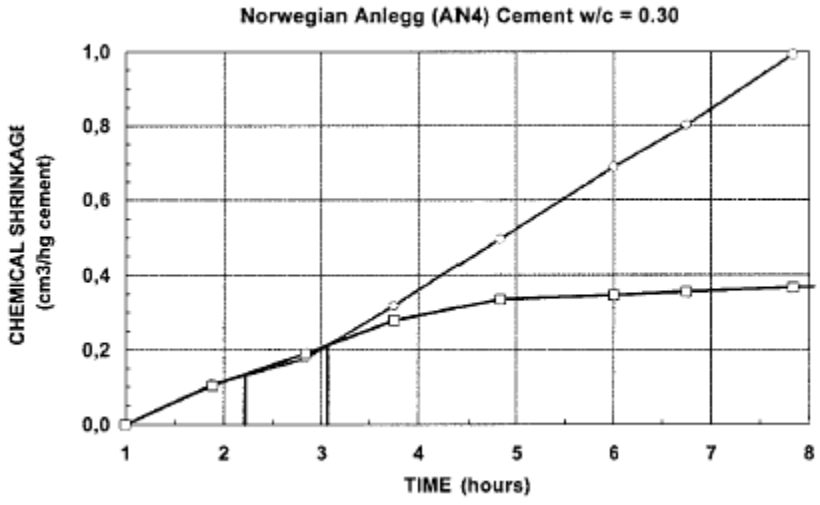

Fig. 1-2 Chemical Shrinkage (○) and Autogenous Shrinkage (□) of a Cement Paste with *w*/*c*=0.30 [Hammer (2002)]

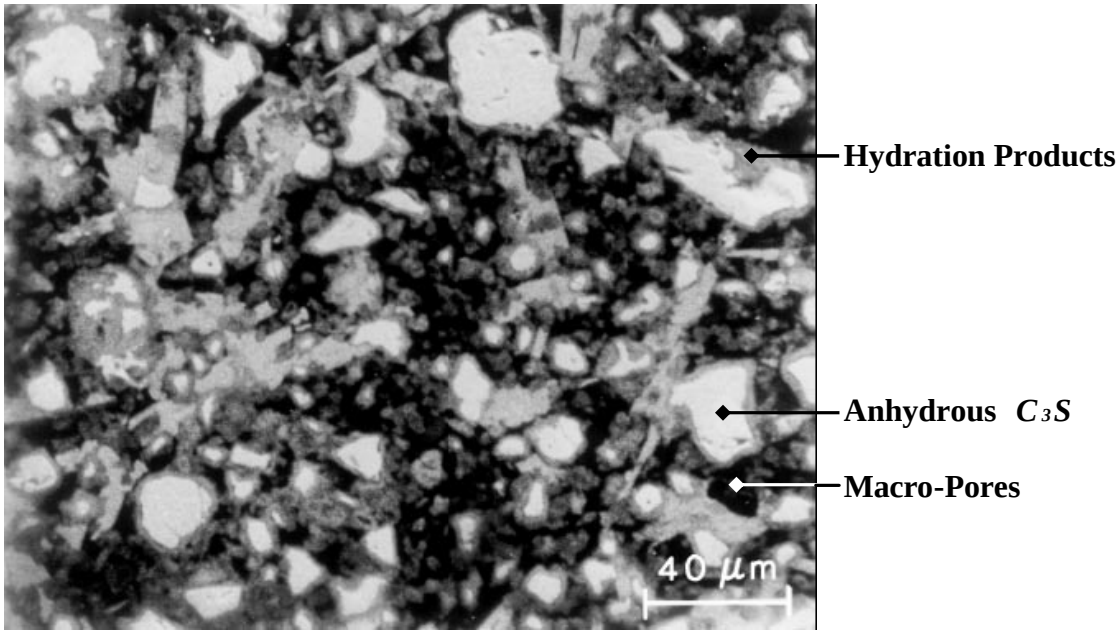

Fig. 1-3 Scanning Electron Micrograph of a C_3S Paste [Tennis et al. (1997)]

CHAPTER 2

FORMULATION OF HYDRATION KINETICS MODEL

2.1 Introduction

As mentioned in the previous chapter, in petroleum engineering, cement paste is used for zonal isolation in oil wells. The downhole conditions are quite different from the curing environments for normal cementitious materials. Due to the heat of the earth and the hydrostatic pressure, the oil well cement paste is subject to much higher curing temperatures and pressures than what normal cement-based materials may experience.

In this chapter, a hydration kinetics model is formulated based on the thermodynamics of multiphase porous media, which was first proposed by Ulm and Coussy (1995). The hardening cement paste is known to be a multiphase porous material and the thermodynamics theory of Ulm and Coussy (1995) is an ideal framework for the hydration kinetics modeling. Cervera et al. (1998, 2002) proposed an equation to describe the hydration kinetics using this theory, but it needs to be elaborated and reformulated by taking into account the experimental observations of cement hydration, especially curing temperature and applied hydrostatic pressure.

2.2 Stages and Mechanisms of Cement Hydration

Based on numerous experimental observations, the mechanism of cement hydration is now fairly clear. According to van Breugel (1991), it involves three main stages, viz. the early, middle and late periods. A short period of rapid chemical

dissolution, termed the pre-induction period, is followed by a dormant stage, which lasts for several hours. Then cement hydration enters the middle period that can last for 24 to 48 hours, in which ions transport to and from the surfaces of anhydrous cement particles through gradually growing layers of hydration products. During the late period, which is the longest and dominant one, the reaction is totally diffusion-controlled. The free water in macro-pores permeates through the hydration products formed around the anhydrous cement core, making further reactions possible. According to van Breugel (1991), cement hydration follows two different mechanisms at different stages. During the early and middle periods, the phase boundary mechanism prevails; while in the late period, the diffusion-controlled reaction dominates. However, there exist no clear boundaries between different stages, and the phase boundary mechanism can be regarded as a special case of the diffusion-controlled reaction when thickness of the layers of hydration products around the anhydrous cement cores is very thin. According to Ulm and Coussy (1995), the mechanism of cement hydration is unified as the diffusion of water through the layers of hydration products, and the thermodynamic driving force of cement hydration is the difference of chemical potentials between the free water in macro-pores and the chemically bound water in hydration products. This mechanism will be adopted in the present study.

2.3 Influence Factors of Cement Hydration Kinetics

Before a mathematical model of hydration kinetics can be developed that properly considers the various influence factors such as chemical composition of cement, water-cement ratio, fineness of cement, curing temperature and applied

pressure, the known facts of Portland cement hydration should be thoroughly surveyed. Therefore, the up-to-date findings, mostly experimental, and the effects that these factors have on Portland cement hydration will be addressed one by one in this section.

2.3.1 Influences of chemical composition of cement

The chemical composition of cement is the most important influence factor of all. Experimental results show that the four main clinker phases of cement, viz. C_3S, C_2S, C_3A, and C_4AF have different reaction rates with water and influence one another as well [e.g. Berger et al. (1979); Escalante-Garcia and Sharp (1998)]. It is well known that C_3A reacts the fastest, followed by C_3S and the other two. Due to the different reaction rates of different clinker phases and their interactions, it is generally accepted that the so-called degree of hydration of cement is just an overall and approximate measure. However, due to the difficulty of identifying and simulating the complicated interactions, the overall degree of hydration, denoted as a, is still widely used and will be employed in this study.

2.3.2 Influence of water-cement ratio

The water-cement ratio, $\frac{w}{c}$, also influences the hydration kinetics. Experimental results have shown that a higher water-cement ratio leads to a higher hydration rate after the middle period of hydration, but only has a small effect on the hydration rate in the early age [e.g. Danielson (1962); Taplin (1969)]. The water-cement ratio also determines the ultimate degree of hydration a_u. Theoretically, a water-cement ratio of about 0.4 is sufficient for the complete hydration of cement (i.e. $a_u = 1.0$). In other

words, a water-cement ratio higher than 0.4 will lead to full hydration given enough time. However, cement hydration is retarded at low internal relative humidity, and the theoretical water-cement ratio of about 0.4 is not sufficient for full hydration [Jensen (1995)]. The hydration products around the anhydrous cement particles prevent further hydration if the free water in macro-pores is insufficient. From experimental observations, the relationship between the ultimate degree of hydration a_u and the water-cement ratio can be described by a hyperbola with $a_u \leq 1.0$. Mills (1966) conducted a series of tests investigating the effect of water-cement ratio and derived an equation for a_u, which is:

$$a_u = \frac{1.031\frac{w}{c}}{0.194 + \frac{w}{c}} \leq 1.0 \qquad (2\text{-}1)$$

This equation has been frequently used in hydration kinetics modeling [e.g. Schindler and Folliard (2005)]. However, it does not consider the effects of cement fineness and curing temperature and may underestimate the ultimate degree of hydration in some cases.

2.3.3 Influences of fineness of cement

The fact that fineness of cement influences the ultimate degree of hydration a_u as well as the hydration rate has been observed in experiments and numerical simulations [Keienburg (1976); Bentz and Haecker (1999)]. The finer the cement particles, the higher a_u, and the higher the hydration rate. However, Bentz and Haecker (1999) also found that at low water-cement ratios, the influence of cement

fineness on a_u diminishes. A finer cement, or cement with a larger surface area, provides a larger contact area with water and hence a higher hydration rate. Also, at the same degree of hydration, a larger surface area corresponds to a thinner thickness of hydration products around the anhydrous cement, which increases the ultimate degree of hydration.

Besides fineness of cement particles, the particle size distribution of cement also influences the hydration rate, as proven by the experimental results of Frigione and Marra (1976). The effects of particle size distribution on hydration rate have also been investigated by other researchers such as Knudsen (1982), Pommersheim and Clifton (1979), Bezjak (1986) and van Breugel (1991). However, it is not considered in the present study, for reasons to be explained later.

2.3.4 Influences of curing temperature

The effects of curing temperature on hydration kinetics have been shown to be twofold. On the one hand, the reaction rate $\dot{a}$ of cement increases with the increase in temperature, which can be considered using the Arrhenius equation:

$$\dot{a} \propto \exp\left(-\frac{E_a}{RT}\right) \tag{2-2}$$

in which E_a is the apparent activation energy, R is the universal gas constant and T is the absolute temperature. As can be seen from various experimental results in the literature, the hydration rate at early age increases more rapidly at higher temperatures [e.g. Lerch and Ford (1948); Kjellsen and Detwiler (1992); Escalante-Garcia (2003)]. On the other hand, the density of hydration products at higher temperature is higher

[Bentur et al. (1979)], making the permeation of free water through the hydration products more difficult. Therefore, during the late period, the hydration rate is lower at elevated temperature and the ultimate degree of hydration may thus also be lower. Based on the experimental results of Bentur et al. (1979), van Breugel (1991) proposed the following equation for the volume ratio between hydration products and the reacted cement at temperature *T*:

$$v(T) = \frac{Volume\ \ of\ \ Hydration\ \ Products\ \ at\ \ T}{Volume\ \ of\ \ Reacted\ \ Cement\ \ at\ \ T} = v_{293} \exp\left[-28\times10^{-6}\left(T-293\right)^2\right] \tag{2-3}$$

Generally, according to Powers and Brownyard (1947),

$$n_{293} = \frac{Volume\ \ of\ \ Hydration\ \ Products\ \ at\ \ 293K}{Volume\ \ of\ \ Reacted\ \ Cement\ \ at\ \ 293K} \approx 2.2 \tag{2-4}$$

However, it should be pointed out that the available experimental results regarding the effects of elevated curing temperature on hydration kinetics are still very limited. Very few publications can be found on the effects of curing temperature higher than 60°C (333K). Chenevert and Shrestha (1991) and Hills et al. (2003) are the two research teams worth mentioning.

An issue related to the effects of curing temperature is the apparent activation energy E_a. Because cement is a mixture of different chemical components rather than a pure material, the activation energy describing the effects of curing temperature in Eq. (2-2) is merely phenomenological and can only be referred to as the apparent activation energy. Different and conflicting conclusions regarding the value of the apparent activation energy have been drawn based on experiments and theoretical analysis. Van Breugel (1991) argued that E_a is a function of chemical composition of cement,

curing temperature and the degree of hydration. Xiong and van Breugel (2001) proposed an equation for E_a that is a function of both curing temperature and the degree of hydration. Freiesleben Hansen and Pedersen (1977), on the other hand, suggested that E_a is only a function of curing temperature. Schindler (2004) proposed an equation for E_a that considers the chemical composition and fineness of cement. Among these studies, the work of Schindler (2004) is found to be most convincing because of its applicability and simplicity. Therefore, in the hydration kinetics model proposed here, a single value of E_a will be used for one type of cement, as characterized by its chemical composition and fineness.

2.3.5 Influence of applied pressure

The experiments to investigate the influence of applied pressure on hydration kinetics are even scarcer than those involving curing temperatures. Bresson et al. (2002) conducted hydration tests on C_3S subject to hydrostatic pressure up to 850bars (85MPa, 12.3ksi) and found that a higher pressure causes a higher hydration rate. Zhou and Beaudoin (2003) also found that applied hydrostatic pressure increases the hydration rate of Portland cement, but only has a negligible effect on the pore structure of hydration products when different cement pastes at similar degrees of hydration are compared. The finding of Zhou and Beaudoin (2003) is important since it implies that the density of the hydration products is not considerably affected by the applied hydrostatic pressure, at least not up to 6.8MPa (986psi), which is the pressure they used.

2.4 Concept of Thermo-Chemical Modeling of Cement Hydration

The fundamental concept of thermo-chemical modeling of cement hydration based on the theory of reactive porous media was originally proposed by Ulm and Coussy (1995). It was extended and developed into a hydration kinetics model for cementitious materials by Cervera et al. (1998, 2002). According to them, cement hydration can be interpreted as a chemical reaction in which the free water in macro-pores combines as a reactant phase with the anhydrous cement and becomes the chemically bound water as a product phase, and the dominant mechanism of the reaction kinetics is the diffusion of free water through layers of hydration products, as illustrated in Fig. 2-1 [Ulm and Coussy (1995)]. Using thermodynamics of reactive porous media and assuming a closed system, the thermodynamic inequality equation can be expressed as:

$$s_{ij}\dot{e}_{ij} - S\dot{T} - \dot{Y} + F_{A\to B} \geq 0 \tag{2-5}$$

in which s_{ij} is the ij^{th} component of the stress tensor; $\dot{e}_{ij}$ is the ij^{th} component of the strain rate tensor; S is the entropy; $\dot{T}$ is the variation rate of temperature; $\dot{Y}$ is the variation rate of free energy; and $F_{A\to B}$ is the dissipation associated with the chemical reaction $A \to B$. For cement hydration, according to the aforementioned mechanism, A is the free water in macro-pores and B is the chemically bound water in hydration products. The chemical dissipation $F_{A\to B}$ can be expressed as:

$$F_{A\to B} = A_a \dot{\alpha} \geq 0 \tag{2-6}$$

where A_a is the affinity of the chemical reaction $A \to B$, viz. the chemical affinity of cement hydration, and $\dot{\alpha}$ is the reaction rate, i.e. the variation rate of the degree of

hydration. Using the Arrhenius equation, the chemical affinity A_a can be written as:

$$A_a = \frac{\dot{a}}{h_a} \exp\left(\frac{E_a}{RT}\right) \tag{2-7}$$

in which h_a represents the permeability of the hydration products around the anhydrous cement. With Eq. (2-7), the hydration rate $\dot{a}$ can be written as:

$$\dot{a} = A_a h_a \exp\left(-\frac{E_a}{RT}\right) \tag{2-8}$$

In Cervera et al. (1998, 2002), the chemical affinity A_a was expressed as:

$$A_a = k\left(\frac{A_0}{k a_u} + a\right)(a_u - a) \tag{2-9}$$

And the permeability h_a (normalized) was expressed as:

$$h_a = \exp\left(-n\frac{a}{a_u}\right) \tag{2-10}$$

Then the hydration rate $\dot{a}$ becomes:

$$\dot{a} = k\left(\frac{A_0}{k a_u} + a\right)(a_u - a)\cdot \exp\left(-n\frac{a}{a_u}\right)\cdot \exp\left(-\frac{E_a}{RT}\right) \tag{2-11}$$

in which *k*, A_0 and *n* are model parameters. A_0 is actually the initial chemical affinity of cement hydration ($a = 0$).

Eq. (2-8) provides an ideal framework for the modeling of hydration kinetics of cement. What needs to be done is to identify the factors that influence the chemical affinity A_a and those affecting the permeability h_a, and then to express A_a and h_a as functions of these factors. Eq. (2-11) as proposed by Cervera et al. (1998, 2002) will be expanded and reformulated in this chapter by including the various influence factors

of hydration kinetics discussed in Section 2.3.

2.5 Formulation of Hydration Kinetics Model

A hydration kinetics model for Portland cement based on the aforementioned thermo-chemical theory is developed in this section. First of all, the various factors that influence the hydration kinetics are characterized. Then, a model of the ultimate degree of hydration is formulated based on the available experimental results and theoretical analysis. Finally, a hydration kinetics model is developed.

2.5.1 Modeling the influence factors of cement hydration kinetics

As discussed in Section 2.3.1, the chemical composition of cement plays the most important role in cement hydration. It is easy to understand that it affects both the chemical affinity A_a and the permeability h_a. Another important factor, the water-cement ratio, only influences the chemical affinity A_a, since it determines the chemical potential of free water in the multiphase system of cement paste to a certain extent. In this study, Eq. (2-9) by Cervera et al. (1998, 2002) is accepted in describing the chemical affinity of cement hydration. It implicitly considers the so-called water shortage effect as pointed out by van Breugel (1991), since the ultimate degree of hydration a_u is affected by the water-cement ratio. Using an exponential equation to represent the permeability h_a is also valid, as it can describe the gradual decrease in permeability of hydration products with the development of hydration. In fact, the exponential function has been frequently used in describing hydration kinetics [e.g. Schindler and Folliard (2005)]. However, the permeability as defined by Cervera et al.

(1998) in Eq. (2-10) needs to be reformulated. Since the water-cement ratio only influences the chemical affinity, the permeability term should not involve the ultimate degree of hydration a_u. Therefore, Eq. (2-10) is modified to read:

$$h_a = \exp(-na) \tag{2-12}$$

As discussed in Section 2.3.2, the water-cement ratio has a negligible effect on the early hydration of cement, and with Eq. (2-12), this phenomenon can be described.

When scrutinizing Eqs. (2-9) and (2-12), it can be seen that the chemical composition of cement influences the three parameters *k*, A_0 and *n*, while the water-cement ratio affects only a_u. With different values of a_u, the effects of water-cement ratio on hydration rate can be implicitly considered by Eqs. (2-8), (2-9) and (2-12).

For the sake of simplicity and application, only the fineness of cement particles but not the actual particle size distribution is taken into account in this model. Since for most general-purpose Portland cements, the shapes of their particle size distribution curves are similar, this simplification does not introduce significant errors. The fineness of cement can be represented by the *Blaine* value with units of m^2/kg (see Section 1.1.2). It influences the initial reaction rate of cement. Therefore, it should appear in the expression of the parameter A_0, which represents the initial chemical affinity of cement hydration, hence the following equation is used to express A_0:

$$A_0 = \frac{A_0' \times Blaine}{350} \tag{2-13}$$

in which A_0' is the normalized initial chemical affinity of cement hydration and is only

a function of the chemical composition of cement.

The *Blaine* fineness also affects the permeability h_a and the ultimate degree of hydration a_u. For permeability, it is noticed that the finer the cement particles, the larger the *Blaine* value, the thinner the thickness of the hydration products, hence the higher the permeability of the hydration products and the smaller the parameter *n* [Eq. (2-12)]. Therefore, it is assumed that:

$$n \propto 1 + (1 - a)^2 \ln\left(\frac{350}{Blaine}\right) \tag{2-14}$$

As can be seen in the above equation, the effect of *Blaine* fineness is not constant throughout the hydration process. With an increase in the degree of hydration a, the effect of *Blaine* fineness decreases.

The effects of curing temperature can be partly considered by involving one term of the Arrhenius equation as shown in Eq. (2-11). However, the densifying effect of elevated curing temperature on the hydration products should also be considered. Since the density of the hydration products is closely related to the permeability h_a, the parameter *n* in Eq. (2-12) should also be a function of curing temperature. And since the hydration rate of cement during the late period decreases at elevated curing temperatures, the parameter *n* should be an increasing function of the curing temperature *T*. In this study, Eq. (2-3), the volume ratio equation proposed by van Breugel (1991), is used, with the effect of curing temperature *T* on the parameter *n* represented as:

$$n \propto \left(\frac{v_{293}}{v(T)}\right)^{10a^4} \tag{2-15}$$

in which a is the degree of hydration and $n(T)$ and n_{293} are as given in Eqs. (2-3) and (2-4). Eqs. (2-12) and (2-15) imply that the effect of curing temperature on the permeability h_a is a decreasing function of the degree of hydration a, which is consistent with experimental results [e.g. Lerch and Ford (1948); Kjellsen and Detwiler (1992); Escalante-Garcia (2003)]. The curing temperature *T* also influences the ultimate degree of hydration a_u, as will be discussed in the next section.

The applied hydrostatic pressure *p* is assumed to influence only the chemical affinity A_a, as supported by the experimental results of Zhou and Beaudoin (2003). According to the tests conducted by Bresson et al. (2002), the chemical affinity A_a is set to be:

$$A_a \propto \exp\left\{0.02\left(\frac{p}{p_{atm}}-1\right)^{0.07}\left[\frac{a}{a_u}-1.5\left(\frac{a}{a_u}\right)^2+0.4\right]\right\} \qquad (2\text{-}16)$$

where p_{atm} is the atmospheric pressure. Eq. (2-16) shows that the reaction rate increases with the increase in the applied pressure *p*. It should be noted that the reference pressure is the normal, i.e. the atmospheric pressure, instead of zero.

The influence factors of cement hydration kinetics and their related model parameters are summarized in Fig. 2-2. It can be concluded now that the chemical affinity A_a is a function of the degree of hydration a, the water cement ratio $\frac{w}{c}$ (through the ultimate degree of hydration a_u), the *Blaine* fineness (through the initial chemical affinity A_0 and the ultimate degree of hydration a_u), the applied pressure *p* [through Eq. (2-16)], and the chemical composition of cement (through the parameters

A_0' and k). And the parameter n that controls the permeability of free water through the hydration products is a function of the curing temperature T [through Eq. (2-15)], the degree of hydration α, the *Blaine* fineness [through Eq. (2-14)], and the chemical composition of cement. Thus, if the ultimate degree of hydration α_u is identified, the parameters that remain in the hydration kinetics model will be related to the chemical composition of cement only.

2.5.2 Modeling the ultimate degree of hydration for Portland cement

Eq. (2-9) is used as the foundation when expressing chemical affinity A_u. Therefore, it is critical to describe the dependency of the ultimate degree of hydration α_u on the water-cement ratio and the fineness of cement. For that purpose, the available experimental and numerically simulated results for α_u as a function of the fineness of cement were collected and analyzed [Mills (1966); Taplin (1969); Bentz (1995); Ye (2001); Baroghel-Bouny et al. (2006)]. The *Blaine* fineness of the cements ranges from around 270m^2/kg to 420m^2/kg and the water-cement ratio varies from 0.157 to 0.85. For some sets of data, in which the hydration ages were not long enough, small extrapolations were thus performed to obtain the corresponding ultimate degree of hydration. From the data analysis, it was found that:

1) The ultimate degree of hydration α_u may be expressed as a hyperbolic function of water-cement ratio with $\alpha_u \leq 1.0$.

2) α_u cannot exceed the theoretical value given by:

$$a_u \le \frac{\frac{w}{c}}{0.4} \tag{2-17}$$

in which 0.4 is approximately the theoretical water-cement ratio necessary for full hydration, which is the summation of the chemically bound water ratio, about 0.25, and the gel water ratio, about 0.15 [Powers and Brownyard (1947); van Breugel (1991)].

3) a_u increases as the cement particles get finer, i.e. as the *Blaine* value increases. And according to Bentz and Haecker (1999), the effect of cement fineness on a_u becomes smaller with a decrease in water-cement ratio.

Based on these observations, an equation considering both the effects of water-cement ratio and fineness of cement is obtained via theoretical analysis and data regression against the experimental results of Mills (1966) and Baroghel-Bouny et al. (2006), as shown in Fig. 2-3:

$$a_{u,293} = \frac{b_1(Blaine)\times\frac{w}{c}}{b_2(Blaine)+\frac{w}{c}} \le 1.0 \tag{2-18}$$

in which $a_{u,293}$ is the ultimate degree of hydration at $T = 293\text{K}$; b_1 and b_2 are both functions of *Blaine* fineness and are defined as:

$$b_1(Blaine) = \frac{1.0}{9.33\left(\frac{Blaine}{100}\right)^{-2.82} + 0.38} \tag{2-19}$$

$$b_2(Blaine) = \frac{Blaine - 220}{147.78 + 1.656(Blaine - 220)} \tag{2-20}$$

Eqs. (2-19) and (2-20) are valid for $Blaine \ge 270\text{m}^2/\text{kg}$. When $Blaine < 270\text{m}^2/\text{kg}$, b_1

and b_2 are assumed to remain constant, that is,

$$b_1(\,Blaine < 270m^2/kg\,) = b_1(\,Blaine = 270m^2/kg\,) \tag{2-21}$$

$$b_2(\,Blaine < 270m^2/kg\,) = b_2(\,Blaine = 270m^2/kg\,) \tag{2-22}$$

The ultimate degree of hydration a_u is also related to the curing temperature *T*. Based on the experimental results of Kjellsen and Detwiler (1992) and Escalante-Garcia (2003) for three different Portland cements, the following equation is proposed to consider the effect of curing temperature *T*:

$$a_u = a_{u,293}\exp\left[-0.00003(T-293)^2\cdot \mathrm{SGN}(T-293)\right] \tag{2-23}$$

in which

$$\mathrm{SGN}(T-293) = \begin{cases} 1, & when \quad T \geq 293K \\ -1, & when \quad T < 293K \end{cases} \tag{2-24}$$

It should be noted that the equation for a_u must also be bounded by the theoretical value. When the water-cement ratio is low, a_u predicted by Eqs. (2-18) – (2-24) is possible to be higher than the theoretical value of Eq. (2-17). Therefore, if the calculated a_u exceeds that theoretical value, it is assumed that:

$$a_u = \frac{\frac{w}{c}}{0.4} \tag{2-25}$$

2.5.3 Mathematical model of hydration kinetics

With the above discussion and formulation, a mathematical model of hydration kinetics for Portland cement can now be developed.

The rate of hydration $\dot{a}$ is given by Eq. (2-8), but normalized, that is,

$$\dot{a} = A_a h_a \cdot \exp\left(-\frac{E_a}{RT}\right) \cdot \exp\left(\frac{E_a}{293R}\right) \tag{2-26}$$

in which E_a is the apparent activation energy. The normalization in this equation ensures that the material constants of the model can be obtained from experimental results at room temperature and will not vary considerably for different values of activation energy.

The chemical affinity A_a is expressed as:

$$A_a(a, \frac{w}{c}, Blaine, p) = k\left(\frac{A_0}{k a_u} + a\right)(a_u - a) \cdot s(a, p) \tag{2-27}$$

in which the function $s(a, p)$ represents the effect of applied hydrostatic pressure p [see also Eq. (2-16)]:

$$s(a, p) = \exp\left\{0.02\left(\frac{p}{p_{atm}} - 1\right)^{0.07}\left[\frac{a}{a_u} - 1.5\left(\frac{a}{a_u}\right)^2 + 0.4\right]\right\} \tag{2-28}$$

The initial chemical affinity A_0 is defined by Eq. (2-13), and the ultimate degree of hydration a_u is given by Eqs. (2-18) – (2-25). The remaining constants A_0' and k are functions of the chemical composition of cement.

The term h_a that represents the permeability of free water through hydration products is expressed by Eq. (2-12), in which the parameter n is written as:

$$n = n_0 f_1(Blaine, a) \cdot f_2(T, a) \tag{2-29}$$

where

$$f_1(Blaine, a) = 1 + (1 - a)^2 \cdot \ln\left(\frac{350}{Blaine}\right) \tag{2-30}$$

$$f_2(T,a) = \left(\frac{v_{293}}{v(T)} \right)^{10a^4} \tag{2-31}$$

and n_0 is a material constant that is related to the chemical composition of cement only.

The last material constant of this model is the apparent activation energy E_a. In this study, it is assumed that E_a is constant for one specific type of cement [Schindler (2004)] and related to its chemical composition and fineness.

Finally, the exothermic behavior of cement hydration can be simulated by introducing the specific heat of cement paste, q_{paste}. van Breugel (1991) proposed an equation for q_{paste}, which is a function of the degree of hydration a, curing temperature *T*, and water-cement ratio:

$$q_{paste} = \frac{M_{ce}}{r_{paste}} \cdot \left[a \cdot q_{hce} + (1-a) q_{ace} + \frac{w}{c} \cdot q_w \right] \tag{2-32}$$

where M_{ce} [kg/m^3] is the cement content by mass in the paste; r_{paste} [kg/m^3] is the density of cement paste; q_{paste}, q_{ace} and q_w are the specific heats of cement paste, anhydrous cement, and water, respectively; q_{hce} [kJ/(kg·K)] is the fictitious specific heat of the hydrated part of cement, which can be expressed as:

$$q_{hce} = 0.0084(T - 273) + 0.339 \tag{2-33}$$

The temperature rise DT can be written as:

$$DT = \frac{Da \cdot Q_{max} \cdot M_{ce}}{r_{paste} \cdot q_{paste}} = \frac{Da \cdot Q_{max}}{a \cdot q_{hce} + (1-a) q_{ace} + \frac{w}{c} \cdot q_w} \tag{2-34}$$

where Da is the increase in the degree of hydration, and Q_{max} [kJ/kg] is the maximum heat of hydration. The values of the specific heat of cement and water are known as $q_{ace} \approx 0.75$kJ/(kg·K) and $q_w \approx 4.18$kJ/(kg·K), respectively. If concrete or mortar is concerned instead of cement paste, the specific heat and mass of aggregate should also be included in Eqs. (2-32) and (2-34).

With the degree of hydration a, the chemical shrinkage of cement paste can be calculated, which according to Powers and Brownyard (1947), is approximated as:

$$v_{chsh}(a) = \frac{(1 - v_n) \times \frac{w_n}{c} \times a}{v_c + \frac{w}{c}} = \frac{0.25 \times 0.25 \times a}{0.32 + \frac{w}{c}} \tag{2-35}$$

where $v_{chsh}(a)$ is the chemical shrinkage; v_n (≈ 0.75cm^3/g) is the specific volume of the chemically bound water, which means that the chemical shrinkage equals up to 25% of the volume of the chemically bound water v_n; w_n is the mass of the chemically bound water; and v_c (≈ 0.32cm^3/g) is the specific volume of cement.

2.6 Summary and Discussion

A hydration kinetics model for Portland cement has been proposed based on the thermo-chemical concepts of Ulm and Coussy (1995). The dominant mechanism of cement hydration is assumed to be the diffusion of free water through the layers of hydration products. The effects of water-cement ratio, fineness of cement, curing temperature and applied pressure are taken into account in this model. The influence of the chemical composition of cement is incorporated in the four material constants,

which are k, A_0', n_0 and E_a. The relationships between these material constants and the chemical composition of cement are calibrated and will be given in the next chapter.

Although it was reported by several investigators that the particle size distribution of cement influences the hydration kinetics to a large extent, this influence is not considered in the proposed model because of the fact that the particle size distributions of most Portland cements are quite similar. It will be demonstrated in the next chapter that this assumption does not introduce significant errors in this model for a wide variety of Portland cements.

It is also noteworthy that different methods to determine the degree of hydration can introduce considerable discrepancies between the experimental results. The parameters commonly used to approximate the actual degree of hydration vary from the liberated heat of hydration, amount of chemically bound water, chemical shrinkage, amount of *CH*, to the specific surface, strength, or dielectric properties of cement. The differences between the methods to measure the degree of hydration should be borne in mind when modeling the hydration kinetics for Portland cement.

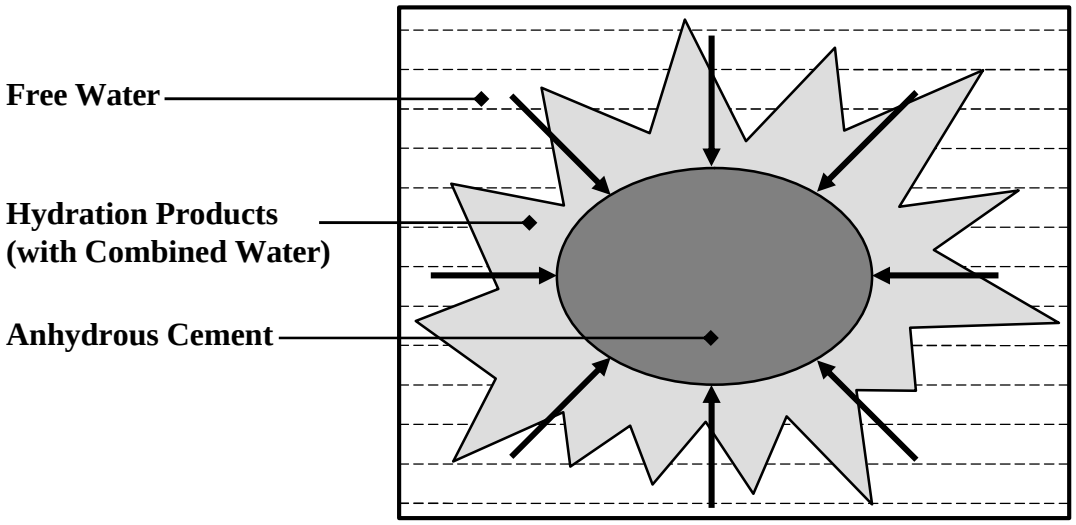

Fig. 2-1 Diffusion of Free Water Through Layers of Hydration Products [Ulm and Coussy (1995)]

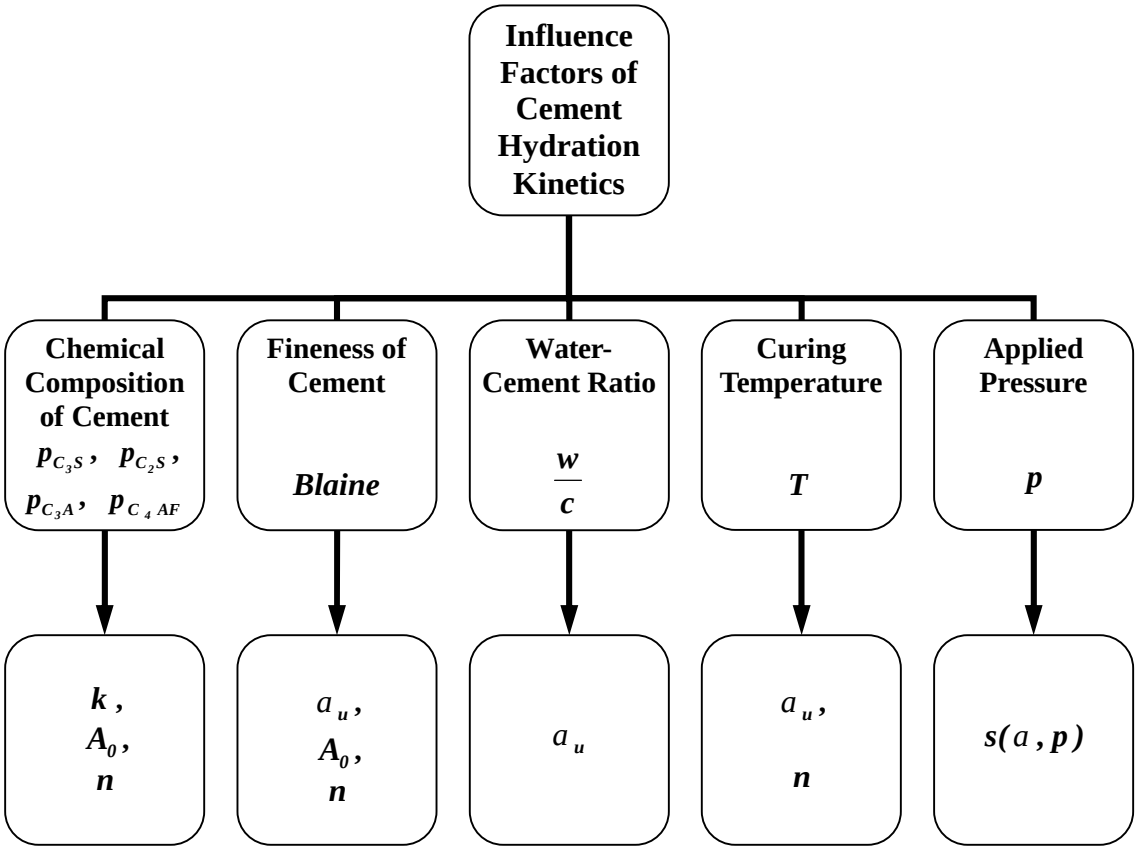

Fig. 2-2 Influence Factors of Cement Hydration Kinetics and Their Related Model Parameters

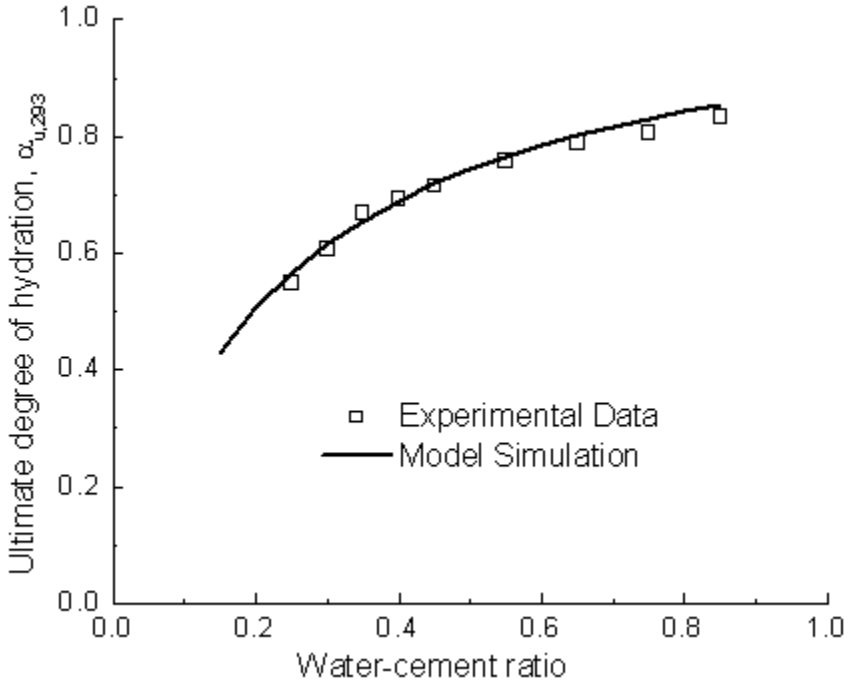

(a)

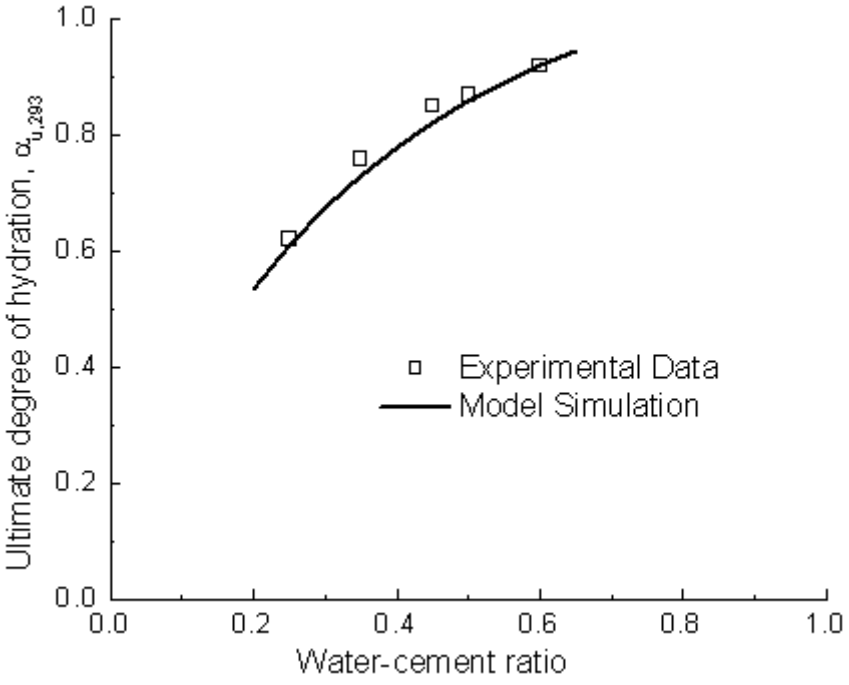

(b)

Fig. 2-3 Simulated and Measured Ultimate Degree of Hydration at *T*=293K
(a)–Experimental Data from [Mills (1966)];
(b)–Experimental Data from [Baroghel-Bouny et al. (2006)]

CHAPTER 3

CALIBRATION AND VERIFICATION OF HYDRATION KINETICS MODEL

3.1 Introduction

A hydration kinetics model for Portland cement was formulated in the previous chapter, based on thermodynamics of multiphase porous media with considering the influences of chemical composition of cement, water-cement ratio, fineness of cement, and more importantly, elevated curing temperature and high applied pressure. In this chapter, the model parameters are calibrated and related to the chemical composition of cement through simple but definite equations. The model is then verified using the experimental results of various researchers, including those on the degree of hydration, adiabatic temperature rise and chemical shrinkage.

3.2 Calibration of Hydration Kinetics Model

The proposed model contains four material constants, k, A_0', n_0 and the apparent activation energy E_a, all of which depend on the cement properties only. The first three are functions of the chemical composition of cement only, while the apparent activation energy depends also on the fineness of cement [Schindler (2004)]. To calibrate these material constants, the experimental results on the hydration kinetics for eight different Portland cements are used, namely those for Type I, Type II, Type III and Type IV cements of Lerch and Ford (1948), and those of Keienburg (1976), Danielson

(1962), Escalante-Garcia (2003), and Taplin (1969). In Table 3-1, these cements are identified as #A – #H, respectively. The experimental results used cover the effects of curing temperature, water-cement ratio, and fineness of cement on the hydration kinetics of Portland cement, with the mass fraction of C_3S in cement ranging from 0.24 to 0.717.

Schindler (2004) proposed the following equation for the apparent activation energy E_a [J/mol],

$$E_a = 22100 \times \left(p_{C_3A}\right)^{0.30} \times \left(p_{C_4AF}\right)^{0.25} \times \left(Blaine\right)^{0.35} \tag{3-1}$$

in which p_{C_3A} and p_{C_4AF} are the Bogue mass fractions (see Section 1.1.1) of C_3A and C_4AF, respectively. This equation is used in the present study to obtain the apparent activation energy if its value was not provided in the experimental data.

The Bogue compositions of the cements investigated are listed in Table 3-1. The four material constants are also shown for each cement. It can be seen from Eq. (2-26) that for experiments conducted at room temperature, E_a is not significant for the model. The other three material constants are obtained by fitting the results of the model to the experimental data. The material constants are not necessarily the ones that best fit the experimental results, as they have been adjusted after trends of their variations with the chemical compositions by conducting linear or nonlinear regression analysis with EXCEL. The comparison of the model simulations and the experimental results for the eight cements are shown in Fig. 3-1 – Fig. 3-8.

The material constants k, A_0' and n_0 of Table 3-1 can be approximately represented by certain functions of the Bogue composition of cement.

First of all, the normalized initial affinity A_0' can be expressed as a linear function of the Bogue mass fractions of C_4AF. The experimental results of Escalante-Garcia and Sharp (1998) support this relationship. It can be seen from their experimental data that the initial reaction rate of C_4AF is much smaller than that of C_3S, C_2S and C_3A, which have similar initial reaction rates. The function of A_0' is expressed as:

$$A_0' = -0.0767\, p_{C_4AF} + 0.0184 \tag{3-2}$$

with p_{C_4AF} being the Bogue mass fraction of C_4AF. The comparison of A_0' calculated by Eq. (3-2) with the values listed in Table 3-1 is shown in Fig. 3-9(a).

The constants n_0 and *k* can be represented by a linear and a nonlinear function of the Bogue mass fractions of C_3S, C_2S and C_3A, respectively:

$$k = 0.56 \times \left(p_{C_3S}\right)^{-0.206} \times \left(p_{C_2S}\right)^{-0.128} \times \left(p_{C_3A}\right)^{0.161} \tag{3-3}$$

$$n_0 = 10.945\, p_{C_3S} + 11.25\, p_{C_2S} - 4.10\, p_{C_3A} - 0.892 \tag{3-4}$$

The comparisons of *k* calculated by Eq. (3-3) and n_0 calculated by Eq. (3-4) with the values listed in Table 3-1 are shown in Fig. 3-9(b) and Fig. 3-9(c), respectively.

It can be seen in Fig. 3-9 that the three model parameters (*k*, A_0' and n_0) correlate strongly with the chemical composition of cement. Although only eight cements are used for the data regression analysis, considering the fact that the chemical compositions of these cements are very different, the trends of the functional relationships appear to be captured very well.

3.3 Verification of Hydration Kinetics Model

3.3.1 Model prediction of the degree of hydration

In order to validate the proposed model, it is used to predict the hydration kinetics for several cements.

First of all, the model capacity in predicting the degree of hydration under pressure was verified using the experimental results. As mentioned in the previous chapter, the function $s(a,p)$ in Eq. (2-28) was obtained using the experimental results for C_3S of Bresson et al. (2002). The simulated and experimental results are compared in Fig. 3-10. The model predictions of the degree of hydration for an ordinary Portland cement cured under pressure were then compared with the experimental results of Zhou and Beaudoin (2003) in Fig. 3-11. It can be seen that the model is capable of predicting the effect of applied hydrostatic pressure on cement hydration.

The hydration kinetics of three cements tested by Bentz et al. (1997), Bentz (2006) and Hill et al. (2003) are simulated using the proposed model. The experimental results of Bentz et al. (1997) exhibited the effect of curing conditions (saturated or sealed curing); those of Bentz (2006) showed the effect of water-cement ratio; and those of Hill et al. (2003) indicated the effect of curing temperature up to 90°C (363K), but the values of the degree of hydration were not provided. Such data are obtained by using the maximum heat output equation of Bogue (1947), viz.

$$a(t) \approx \frac{Q(t)}{Q_{max}} \tag{3-5}$$

The material constants used in the simulation are obtained through Eqs. (3-1) – (3-4). Since the fineness of cement was not provided either, a value of 350m^2/kg is used by

comparing the *Blaine* values of similar cements. The predictions are compared with the experimental results in Fig. 3-12 – Fig. 3-14, which show reasonably good agreement. Although the degree of hydration at the curing temperature of 90°C [Hill et al. (2003)] is over-estimated to a certain extent, in view of the difficulties of conducting tests at elevated curing temperatures, the overall prediction accuracy can be considered acceptable.

3.3.2 Model prediction of adiabatic temperature rise

The adiabatic tests for the CEM I 52.5 PM CP2 concrete by Bentz et al. (1998) are reproduced using the proposed model to verify its capacity of simulating the adiabatic behavior of cementitious materials with different water-cement ratios. The material constants, except for the apparent activation energy E_a taken directly from Bentz et al. (1998), are obtained via Eqs. (3-2) – (3-4). The results are given in Fig. 3-15. It can be seen that the model predictions agree well with the experimental results.

3.3.3 Model prediction of chemical shrinkage

The chemical shrinkage tests by Chenevert and Shrestha (1991), Justnes et al. (1995, 1996) and Baroghel-Bouny et al. (2006) are reproduced using the proposed model. It should be pointed out that the tests by Chenevert and Shrestha (1991) were conducted at high temperatures and high pressures. The material constants are again obtained via Eqs. (3-1) – (3-4). The predicted and experimental results are compared in Fig. 3-16 – Fig. 3-20, which show acceptable agreement. The *Blaine* fineness was not provided in Chenevert and Shrestha (1991), hence a value of 300m^2/kg is used for the Class H oil well cement that was used in the tests by referring to the general fineness of

this type of cement. Attention is directed to the model capacity of reproducing the behavior of oil well cements (Class G and Class H) under ambient conditions as well as downhole conditions of high temperature and high pressure. It should be noted that the cement started to hydrate before the data were recorded. Therefore, values of the original degree of hydration in the model simulation of Chenevert and Shrestha's experimental results are not zero, but set as 0.04 at 100°F (38°C) and 0.12 at 150°F (66°C), respectively.

3.4 Summary and Discussion

The hydration kinetics model formulated in the previous chapter has been calibrated using the experimental results for eight different Portland cements, and the model parameters were related to the chemical composition of cement through simple equations. The predictive capabilities of the model were demonstrated for various applications. It has been found that:

1) The proposed hydration kinetics model is theoretically sound, easy to use and capable of predicting the hydration development of various cements under different curing conditions. In particular, the effects of elevated curing temperature and high applied pressure on the hydration kinetics of cement can be reproduced.

2) The proposed model can be used for different applications, such as the prediction of hydration kinetics, adiabatic temperature changes, and chemical shrinkage of cementitious materials.

Since only eight cements were used for the data regression analysis, the relationships between the three material constants (A_0', k and n_0) and the chemical

composition of cement may not be optimal. However, the trends of the relationships appear to have been captured. According to the available experimental observations, the initial reaction rate of C_4AF is the lowest, hence the material constant A_0' should be closely related to its content. The values of *k* and n_0 determine the overall reaction rate. The larger the value of *k* and the smaller the value of n_0, the higher the reaction rate. It is well-known that C_3A and C_3S react faster, while C_2S reacts slower, hence the trends as given by Eqs. (3-3) and (3-4) are correct. The validity of using one single value of apparent activation energy E_a has been verified, but its dependence on the chemical composition and fineness of cement deserves further investigation.

The present study is focused on ordinary Portland cement without any mineral or chemical admixtures. However, it should be emphasized that this model is fundamentally capable of simulating the behavior of blended cements or cements with admixtures. Of course, in this case, the material constants would have to involve the effects of the replaced materials or the admixtures, but the model formulation would be similar.

The model's capacity of reproducing the hydration kinetics of cement under curing conditions of high temperature and high pressure was demonstrated. However, the available experimental results under such conditions are very limited, therefore, the proposed formulas still need to be verified with more reliable experimental data.

Table 3-1 Cement Compositions and the Corresponding Material Constants

Cement Identification Code	Figure Number	Bogue Composition				*Blaine* Fininess (m^2/kg)	Material Constants			
		C_3S	C_2S	C_3A	C_4AF		E_a (J/mol)	k (h^{-1})	n_0	A_0' (h)
#A [Lerch and Ford (1948)]	3-1	0.514	0.226	0.111	0.079	372	45,271 [a]	0.53	6.95	0.0123
#B [Lerch and Ford (1948)]	3-2	0.416	0.344	0.054	0.132	314	41,788 [a]	0.48	7.30	0.0080
#C [Lerch and Ford (1948)]	3-3	0.600	0.135	0.089	0.081	564	49,955 [a]	0.54	6.80	0.0120
#D [Lerch and Ford (1948)]	3-4	0.240	0.515	0.049	0.116	360	39,978 [a]	0.50	7.30	0.0100
#E [Keienburg (1976)]	3-5	0.717	0.059	0.090	0.100	350	—	0.59	7.10	0.0108
#F [Danielson (1962)]	3-6	0.567	0.172	0.067	0.079	312	—	0.51	7.00	0.0120
#G [b] [Escalante-Garcia (2003)]	3-7	0.716	0.109	0.037	0.107	376	44,166 [c]	0.47	8.10	0.0100
#H [Taplin (1969)]	3-8	0.414	0.340	0.098	0.075	312	—	0.55	7.02	0.0130

[a]: Values taken from Schindler (2004)

[b]: The chemical composition determined by quantitative X-ray diffraction analysis (QXDA) was used for this cement

[c]: Calculated value using Eq. (3-1)

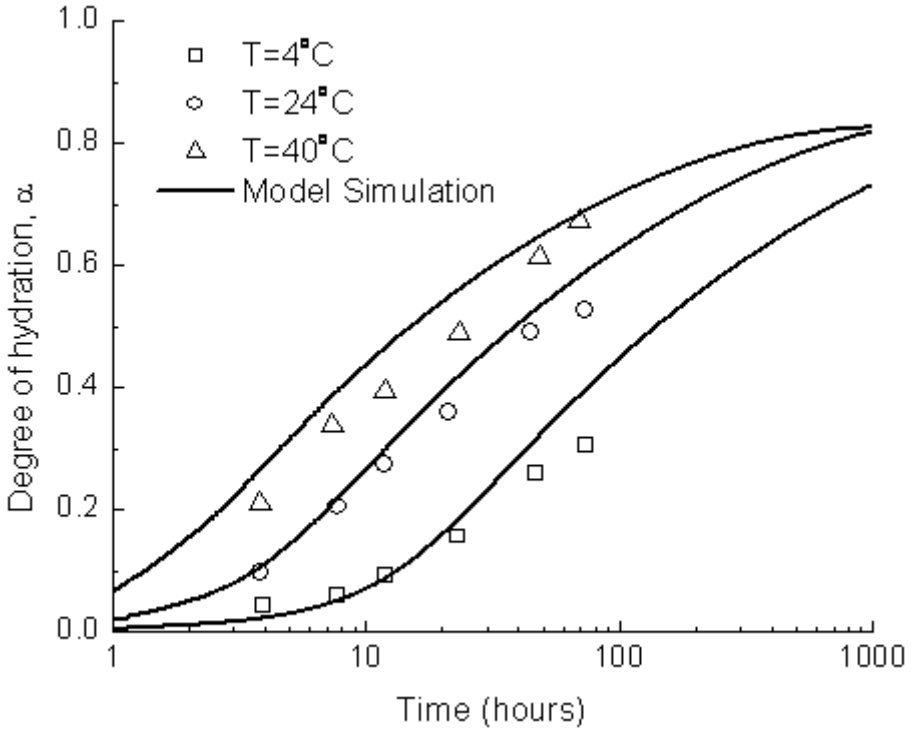

Fig. 3-1 Simulated and Measured Degree of Hydration for Cement #A (Type I) (Experimental Data from [Lerch and Ford (1948)])

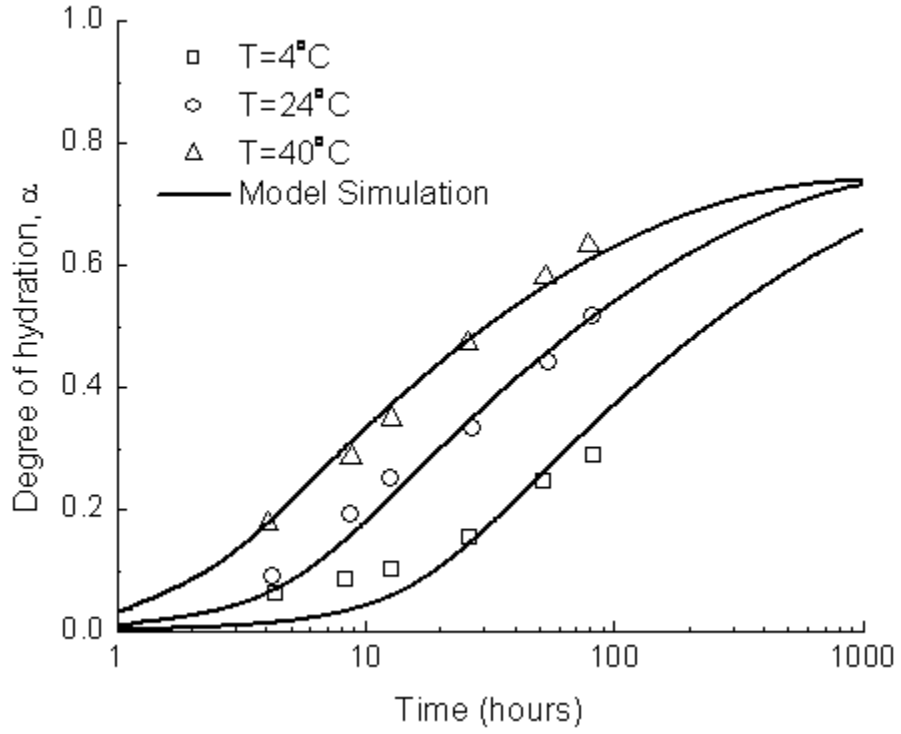

Fig. 3-2 Simulated and Measured Degree of Hydration for Cement #B (Type II) (Experimental Data from [Lerch and Ford (1948)])

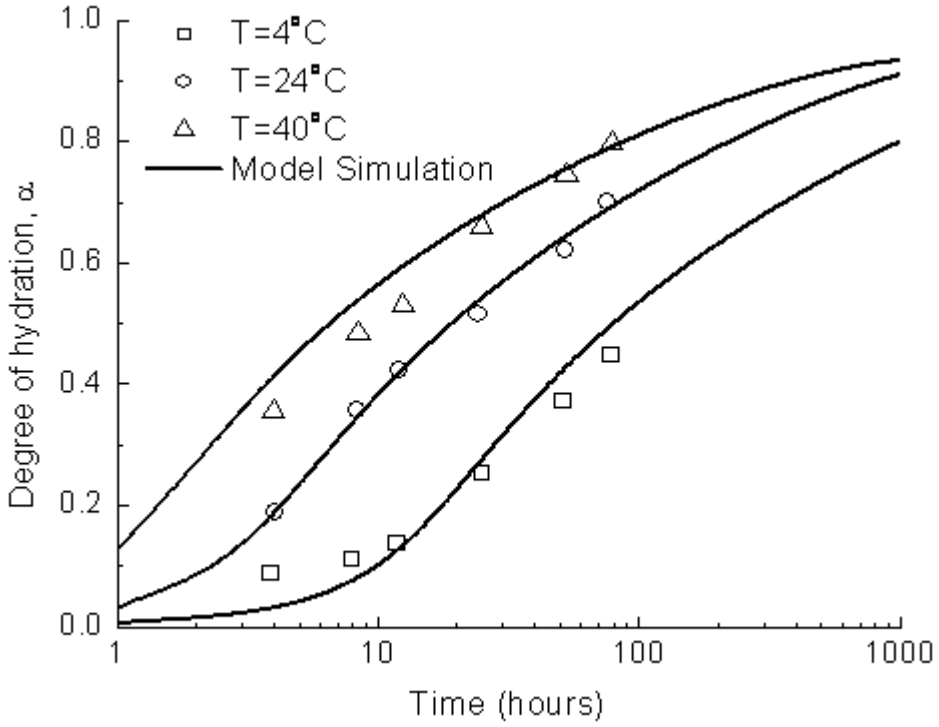

Fig. 3-3 Simulated and Measured Degree of Hydration for Cement #C (Type III) (Experimental Data from [Lerch and Ford (1948)])

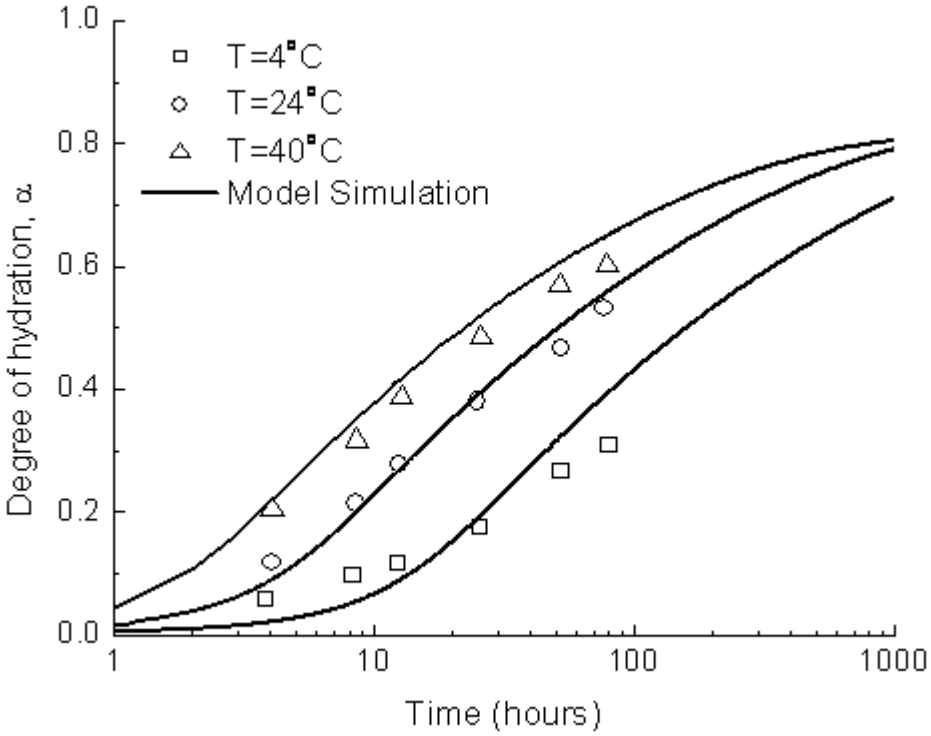

Fig. 3-4 Simulated and Measured Degree of Hydration for Cement #D (Type IV) (Experimental Data from [Lerch and Ford (1948)])

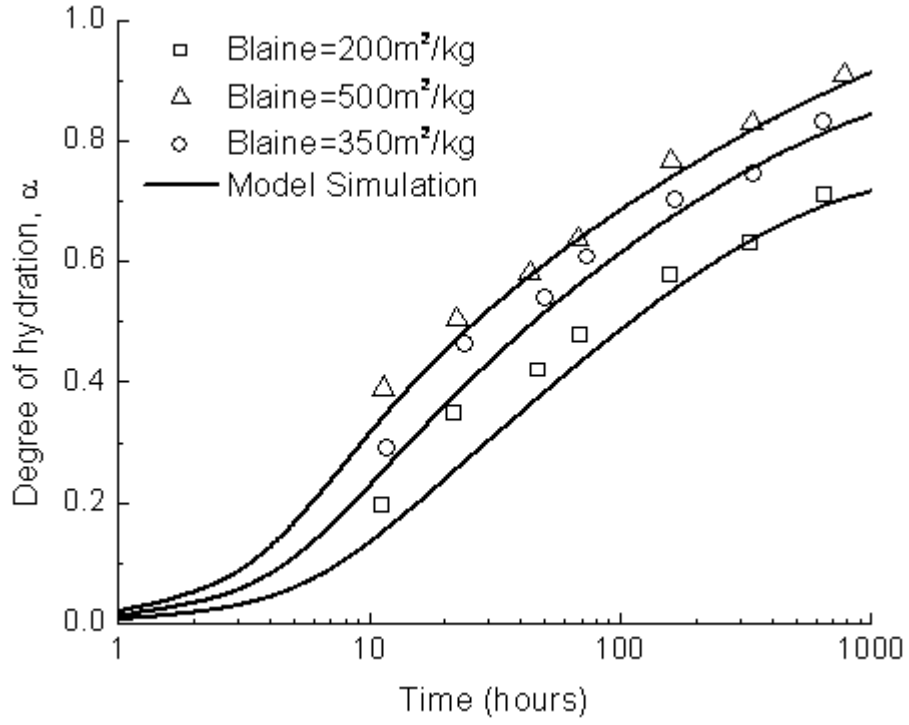

Fig. 3-5 Simulated and Measured Degree of Hydration for Cement #E (Experimental Data from [Keienburg (1976)])

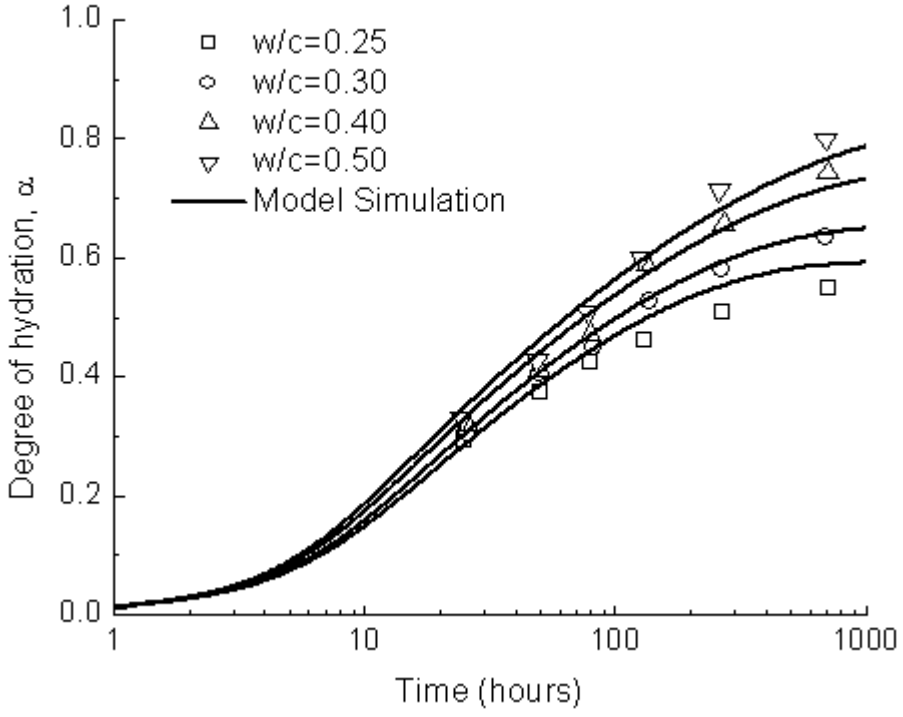

Fig. 3-6 Simulated and Measured Degree of Hydration for Cement #F (Experimental Data from [Danielson (1962)])

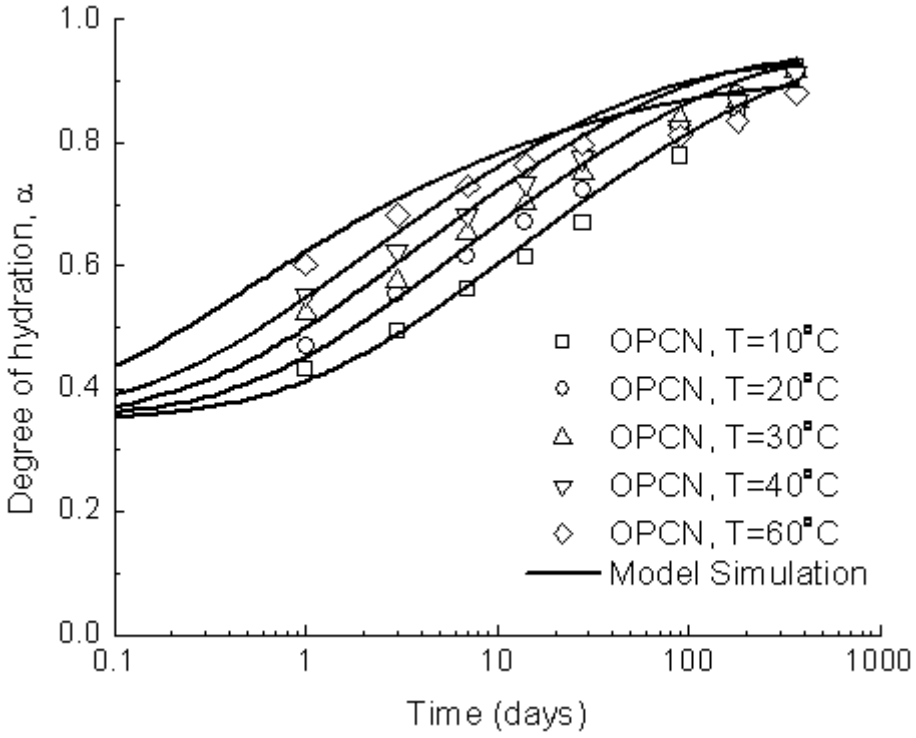

Fig. 3-7 Simulated and Measured Degree of Hydration for Cement #G (Experimental Data from [Escalante-Garcia (2003)])

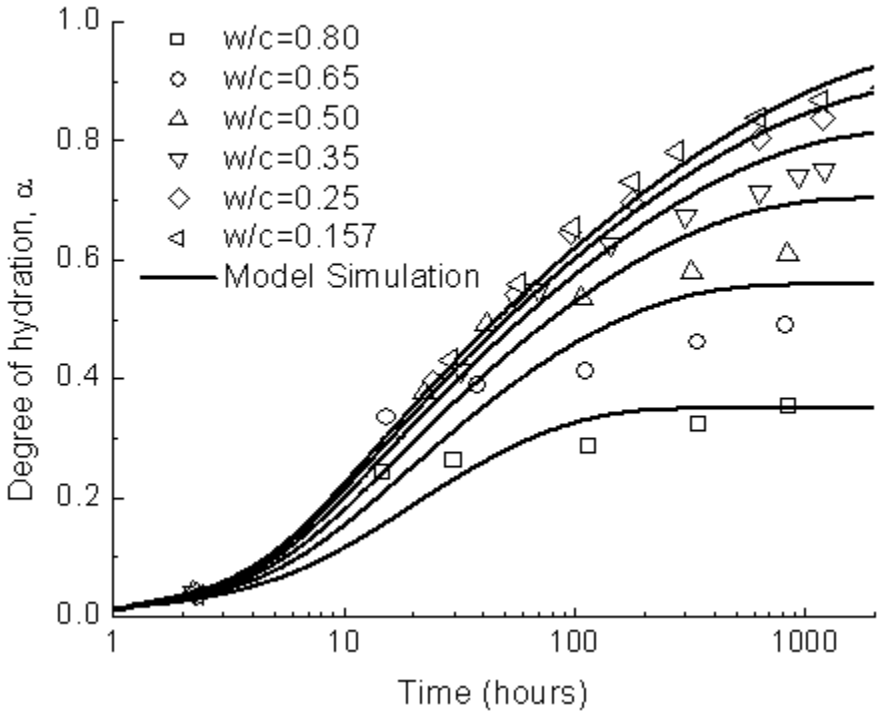

Fig. 3-8 Simulated and Measured Degree of Hydration for Cement #H (Experimental Data from [Taplin (1969)])

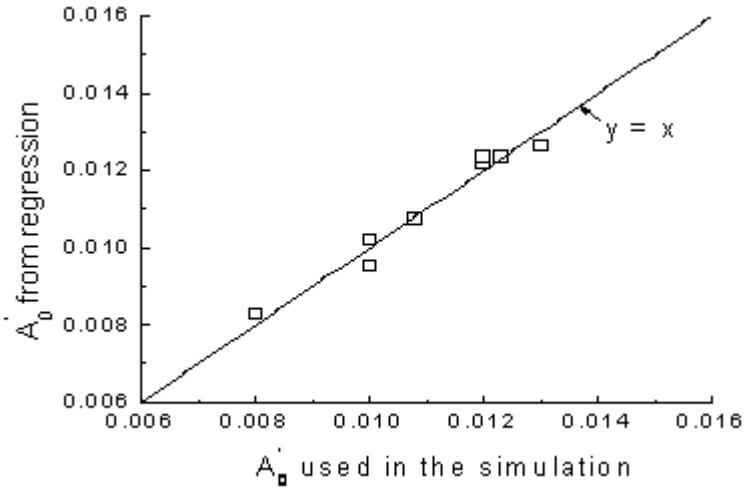

(a)

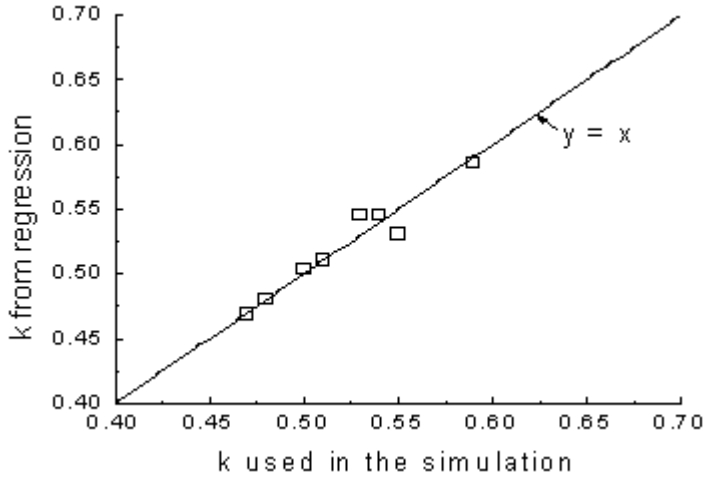

(b)

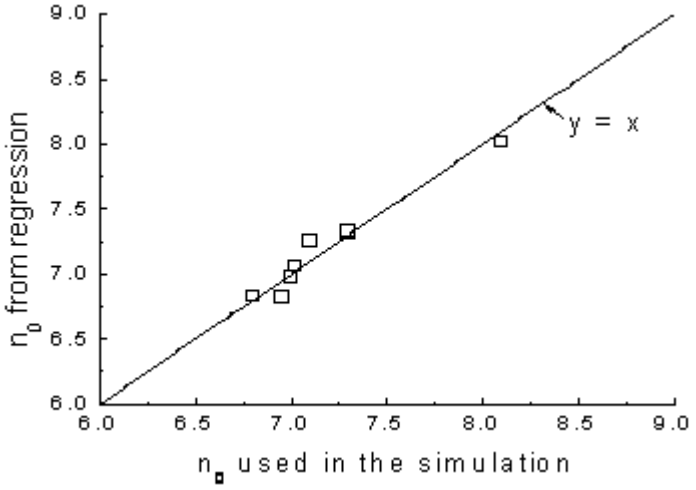

(c)

Fig. 3-9 Comparison of the Simulation with the Regression Values (a)–Eq. (3-2) for A_0°; (b)–Eq. (3-3) for k ; (c)–Eq. (3-4) for n_0

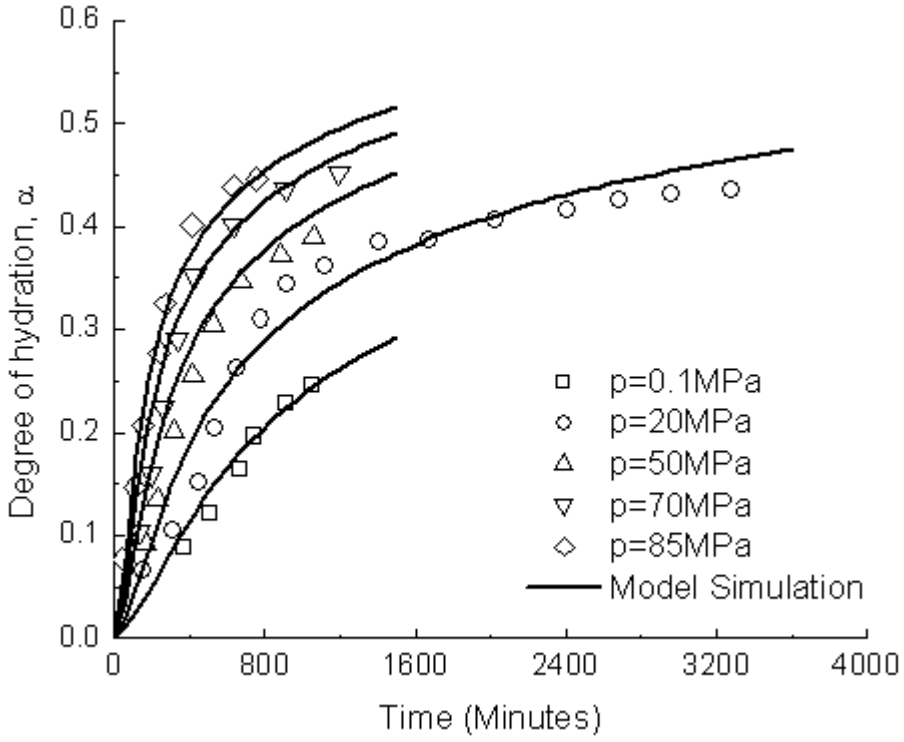

Fig. 3-10 Simulated and Measured Degree of Hydration for C_3S under Pressure (Experimental Data from [Bresson et al. (2002)])

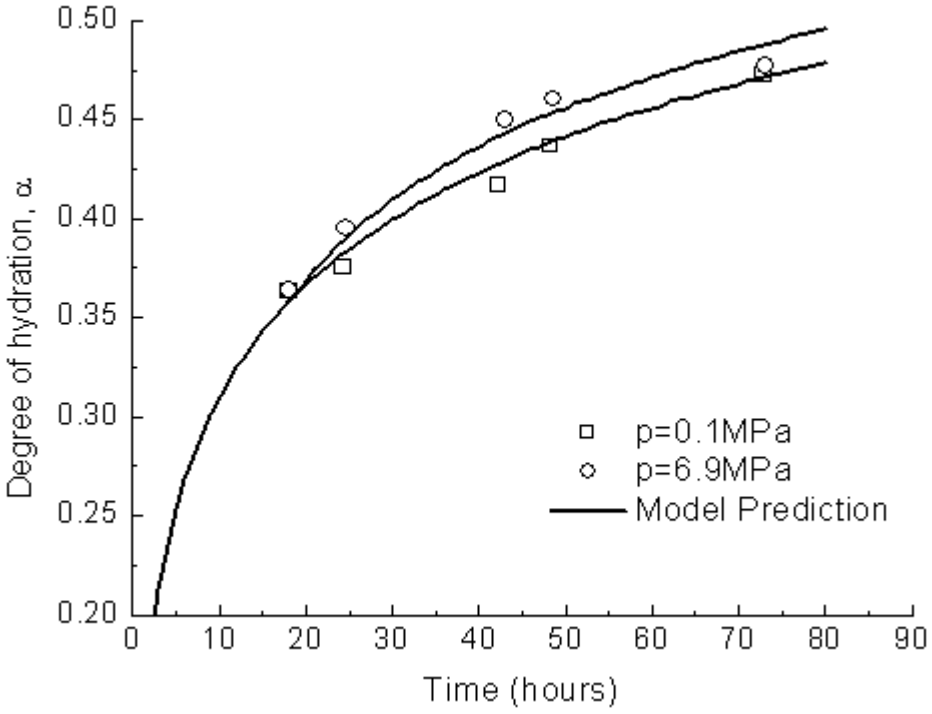

Fig. 3-11 Predicted and Measured Degree of Hydration for OPC under Pressure (Experimental Data from [Zhou and Beaudoin (2003)])

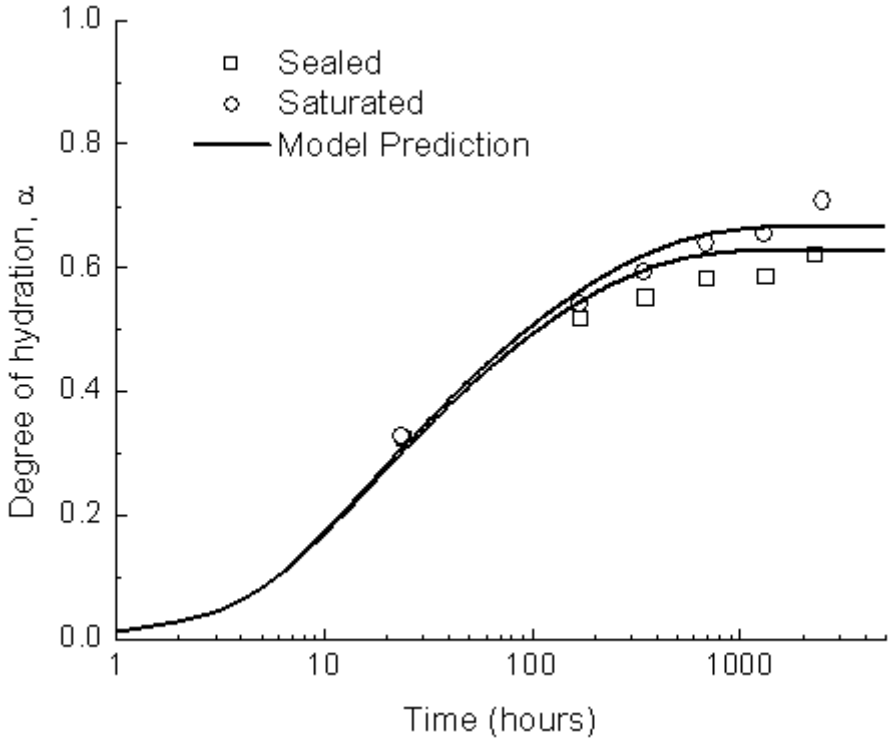

Fig. 3-12 Predicted and Measured Degree of Hydration for CCRL Cement 115 under Different Curing Conditions (Experimental Data from [Bentz et al. (1997)])

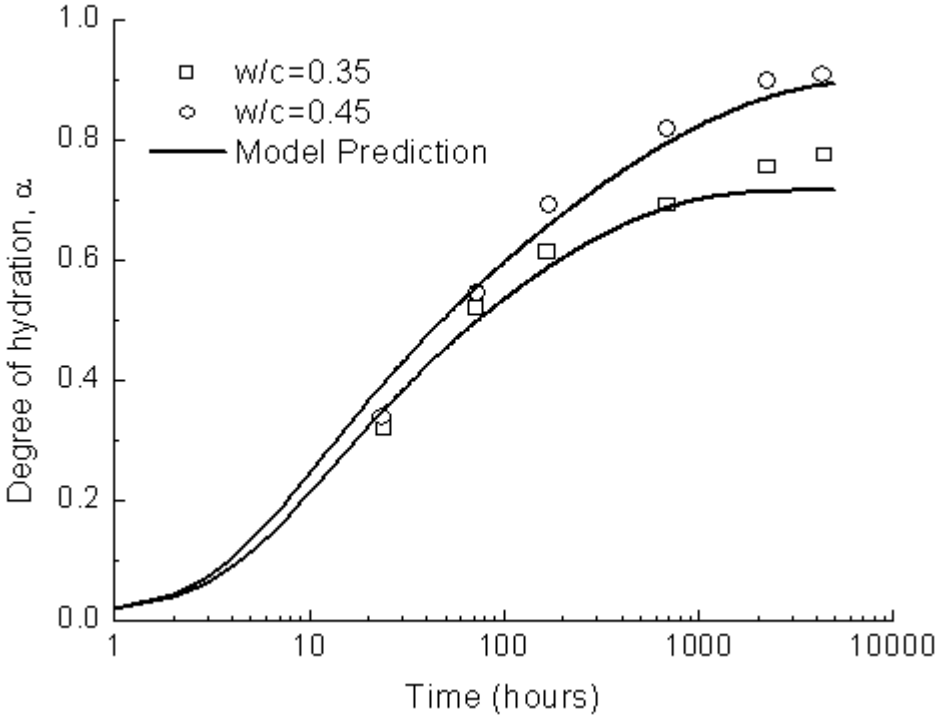

Fig. 3-13 Predicted and Measured Degree of Hydration for CCRL Cement 152 with Different Water-Cement Ratios (Experimental Data from [Bentz (2006)])

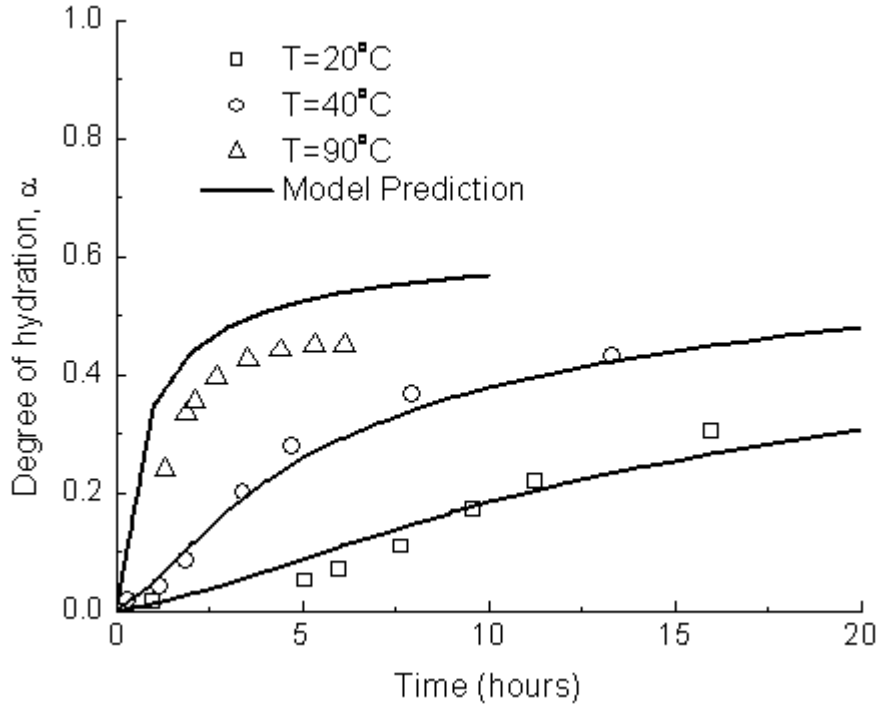

Fig. 3-14 Predicted and Measured Degree of Hydration for OPC at Different Temperatures (Experimental Data from [Hill et al. (2003)])

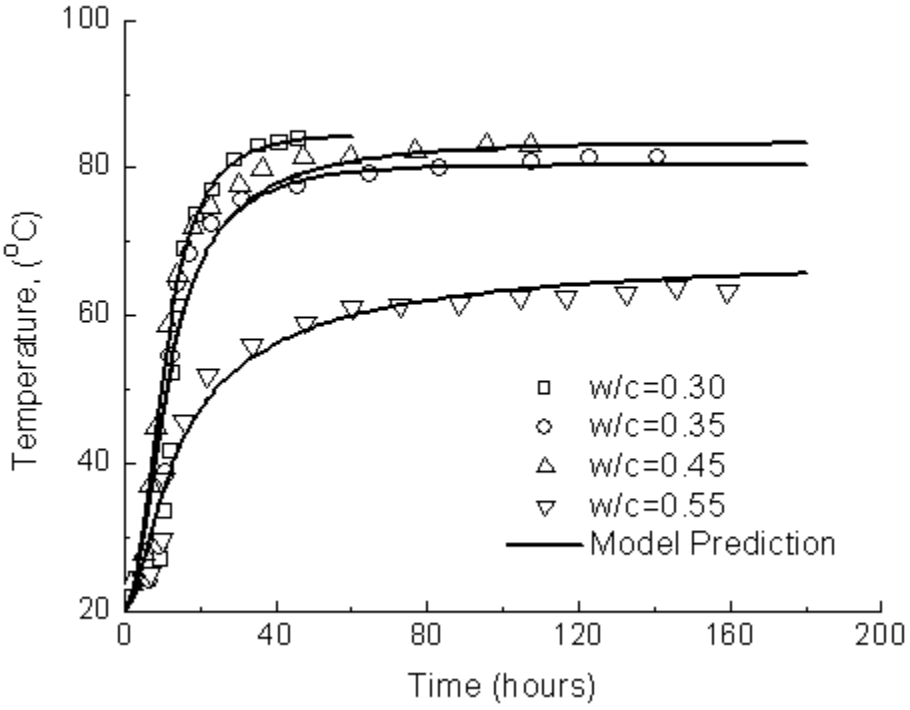

Fig. 3-15 Predicted and Measured Adiabatic Temperature Changes for CEM I 52.5 PM CP2 Cement with Different Water-Cement Ratios (Experimental Data from [Bentz et al. (1998)])

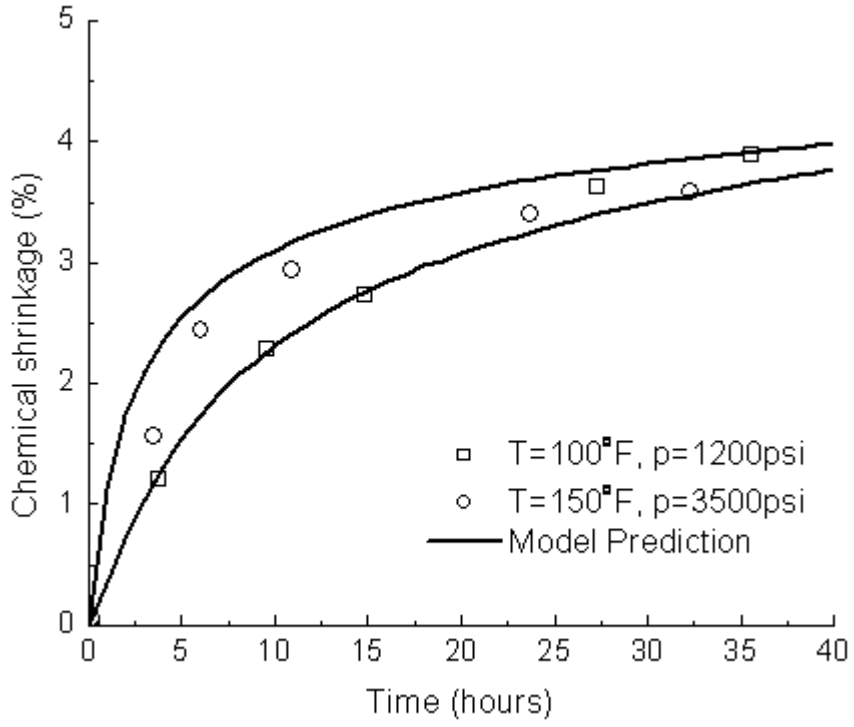

Fig. 3-16 Predicted and Measured Chemical Shrinkage for Class H Cement at Different Temperatures and Pressures (Experimental Data from [Chenevert and Shrestha (1991)])

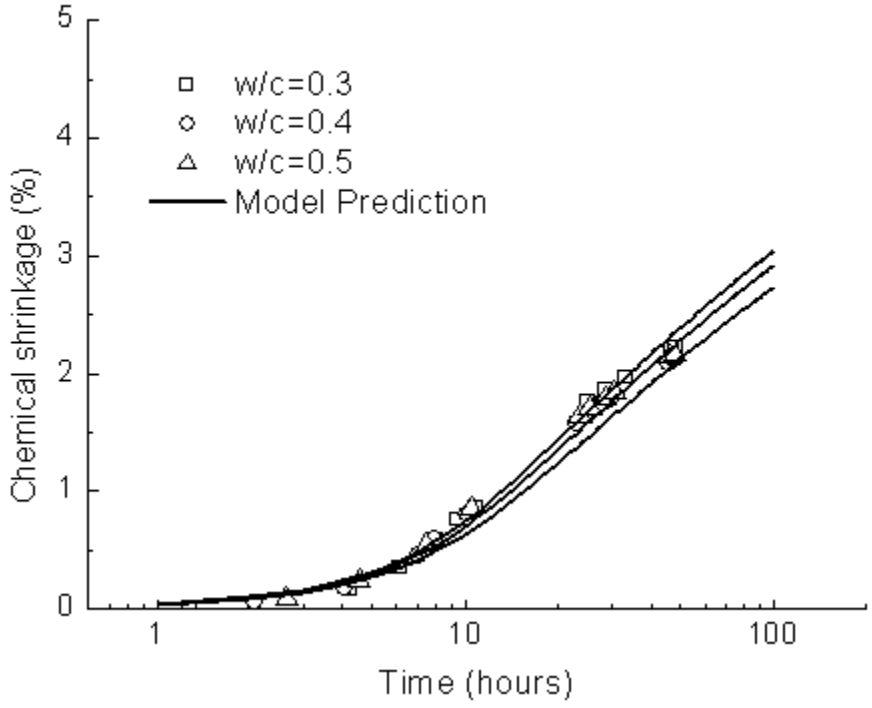

Fig. 3-17 Predicted and Measured Chemical Shrinkage for Class G Cement with Different Water-Cement Ratios (Experimental Data from [Justnes et al. (1995)])

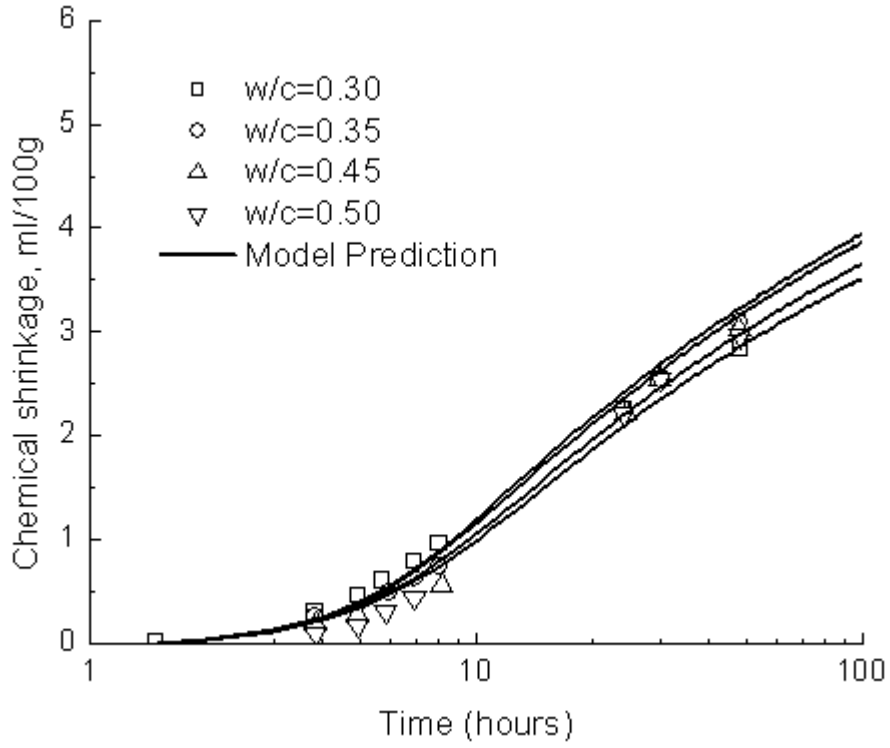

Fig. 3-18 Predicted and Measured Chemical Shrinkage for P30k Cement with Different Water-Cement Ratios (Experimental Data from [Justnes et al. (1996)])

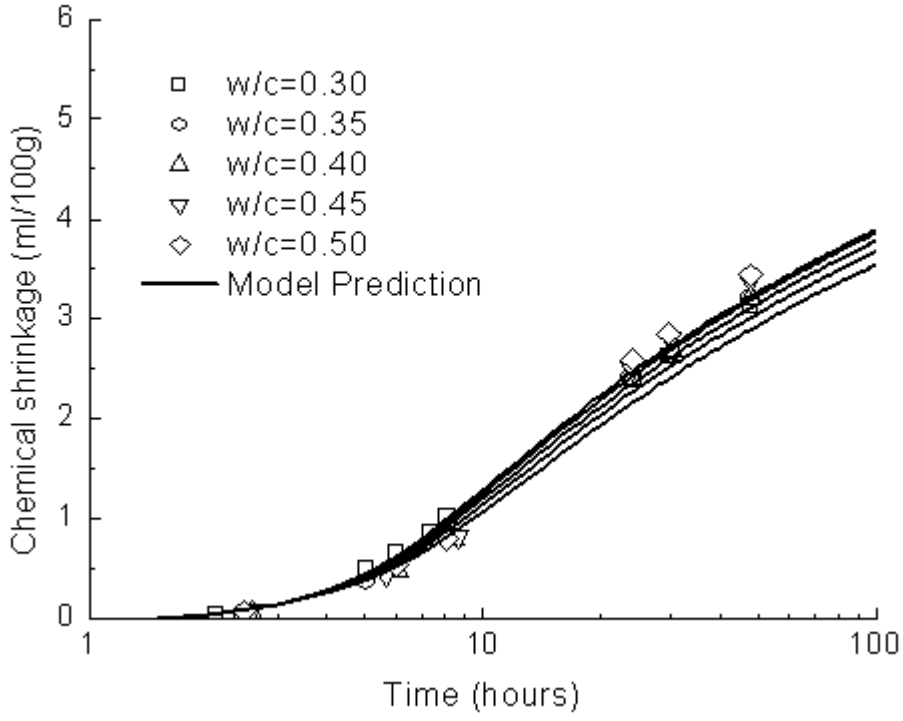

Fig. 3-19 Predicted and Measured Chemical Shrinkage for HS65 Cement with Different Water-Cement Ratios (Experimental Data from [Justnes et al. (1996)])

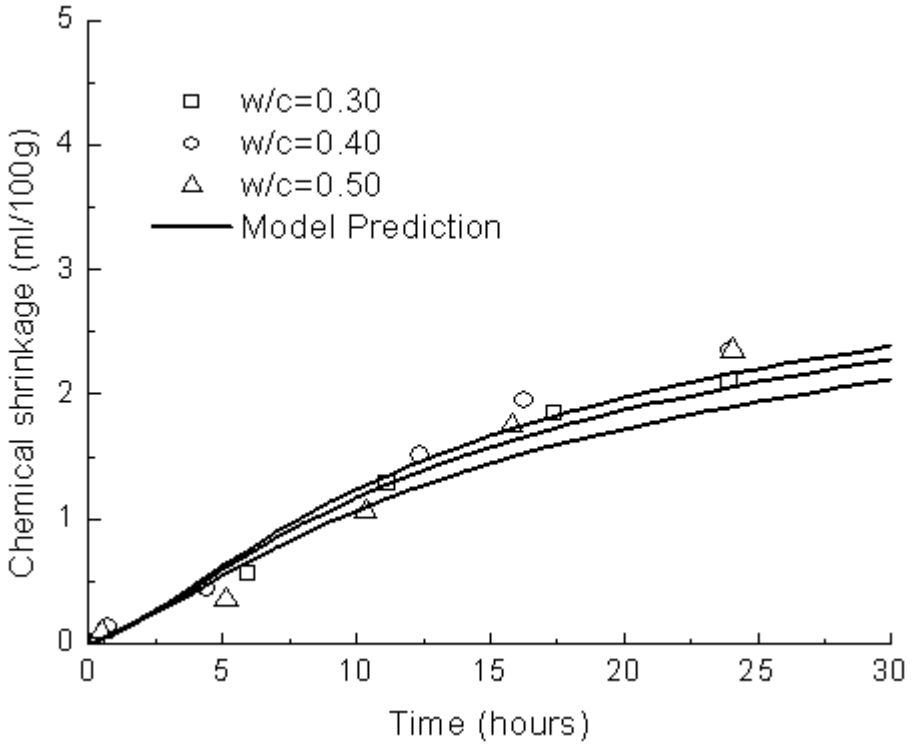

Fig. 3-20 Predicted and Measured Chemical Shrinkage for Type I Cement with Different Water-Cement Ratios
(Experimental Data from [Baroghel-Bouny et al. (2006)])

CHAPTER 4

DRIVING FORCES OF SHRINKAGE

4.1 Introduction

To determine the volume changes of cement paste, a porous medium, the driving forces need to be identified, which can be divided into two categories: one is the applied pressure, the other is the “internal load” resulting from the chemical shrinkage and/or desiccation of cement paste. The applied pressure is easy to quantify; while the internal load, which is the driving force of autogenous shrinkage and/or drying shrinkage, is much more difficult to identify. The quantification of the internal load and its consideration together with the applied pressure must be addressed on sound theoretical and experimental bases when predicting volume changes.

Surface tension, capillary stress, and empirical relations have all been used as the internal load to calculate autogenous shrinkage of cement-based materials. Koenders and van Breugel (1997) used surface tension to calculate autogenous shrinkage of hardening cement paste; while Hua et al. (1995, 1997), Shimomura and Maekawa (1997) and Lura et al. (2003) considered capillary stress to be the most important driving force of autogenous shrinkage. Different empirical relations were also used in shrinkage calculations [e.g. Xi and Jennings (1997); Mabrouk et al. (2004)].

Since the shrinkage of cement paste at high internal relative humidity is the main concern of the present study, the corresponding internal load will be identified and quantified in detail subsequently. The theory of poromechanics [Coussy (2004)], which

will be briefly introduced in this chapter, is the theoretical framework for quantifying both the internal load and the applied pressure when modeling volume changes.

4.2 Surface Tension, Disjoining Pressure and Capillary Stress

The reduction of water in the capillary pores due to chemical shrinkage and drying or desiccation of cement paste is the essential cause of shrinkage. Chemical shrinkage results from the consumption of water during cement hydration, while drying or desiccation is the result of water loss due to evaporation or moisture diffusion. Accompanying the reduction of water in capillary pores, surface tension, disjoining pressure and capillary stress may take effect, resulting in the shrinkage of cement paste as a function of the internal relative humidity in the capillary pores.

4.2.1 Surface tension

According to Powers (1968), the surface tension of a solid particle is at a maximum when it is in a vacuum, becomes smaller when it is immersed in a liquid or gas, and equals zero when it is immersed in like substance. The surface tension of the pore walls of cement paste can be one of the driving forces of shrinkage.

Solid surface tension was investigated as early as the 1930's. Bangham and Fakhoury (1930) proposed an equation that relates the bulk volume change of coal to its surface tension. To calculate the shrinkage of cement-based materials, Koenders and van Breugel (1997) proposed a model that utilizes surface tension as the driving force in the full range of relative humidity, i.e. with *RH* ranging from 0 to 100%. The dependence of surface tension on *RH* was also included in their model.

However, solid surface tension is only effective when the adsorbed water film is

very thin. The changes in surface tension of the cement gel particles due to adsorption of water molecules are significant for the first three adsorbed layers only. The outer layers are bound by weak forces and their influence on the particle surface tension is negligible [Ferraris and Wittmann, (1987); Lura et al. (2003)]. Therefore, the importance of surface tension decreases with an increase in relative humidity. It does not play a major role when $RH > 70\%$ [Jensen (1993)], which is the case for self-desiccation of cement paste. As a matter of fact, the Bangham approach [Bangham and Fakhoury (1930)] was used to calculate drying shrinkage of cement paste only for a relative humidity range of 0 ~ 40% [e.g. Bažant and Wittmann (1982); Ferraris and Wittmann (1987)].

4.2.2 Disjoining pressure

Disjoining pressure between solid particles is the combined effect of van der Waals' forces, double layer repulsion and liquid/pore-wall adsorption [Scovazzo and Todd (2001)], in which van der Waals' forces are always contractive, double layer repulsion is always repulsive, and liquid/pore-wall adsorption could be contractive or repulsive, depending on the adsorption characteristic of the liquid. Therefore, disjoining pressure is a function of the thickness of fluid between solid particles as well as of the fluid characteristics. For cement-based materials, the disjoining pressure can vary for different concentrations of Ca^{2+} [Beltzung et al. (2001)]. And since the thickness of fluid between solid particles in cement-based materials is directly dependent on the internal relative humidity, the disjoining pressure varies with the changes in relative humidity.

Disjoining pressure increases with the increasing layers of adsorbed water, viz. liquid thickness, which varies rapidly with the variation of relative humidity [Ferraris and Wittmann (1987)], hence it can be an important driving force of shrinkage at high relative humidity. However, the quantification of disjoining pressure is difficult. It can be determined for contacting solid particles with simple geometries [e.g. Scovazzo and Todd (2001)], but for cement paste, especially the hardening cement paste at early age, the complex pore structure makes it very difficult to quantify the disjoining pressure and its variation with relative humidity.

4.2.3 Capillary stress

The mechanism of capillary stress inducing shrinkage of cement paste at high relative humidity is clearly understood [e.g. Hua et al. (1995, 1997); Lura et al. (2003)]. Capillary stress is related to the water/air menisci in the partially saturated pores of cement paste. It is a function of the diameter of the largest water-filled capillary pore and the surface tension of water. According to the Young-Laplace equation, capillary stress of cement paste can be expressed as:

$$p_c = \frac{4g}{j_{pore-water}} \tag{4-1}$$

in which p_c is the pressure difference across the curved surface, i.e. the capillary stress; g is the surface tension of water, equaling 07197N/m; and $j_{pore-water}$ is the diameter of the largest water-filled capillary pore.

The effect of capillary stress should be present within the high relative humidity range [Soroka (1979)]. Capillary stress can be related to the internal relative humidity

through the Kelvin equation:

$$\ln(RH) = \frac{-4V_m g}{j_{pore-water} RT} = \frac{-p_c V_m}{RT} \tag{4-2}$$

where V_m is the molar volume of the pore solution, which in our case, equals $18\times10^{-6}m^3/mol$; R is the universal gas constant that is 8.314J/(mol·K); and T is the absolute temperature. The relationship between capillary stress and shrinkage of cement paste has also been demonstrated by experiments. It has been found in different independent investigations that the autogenous shrinkage after a certain period of hydration can be related to the relative humidity through unique functions [e.g. Jensen and Hansen (1996); Jiang et al. (2005)].

As the main concern of the present study is the shrinkage of cement paste at high relative humidity (i.e. $RH > 70\%$), surface tension is considered to be irrelevant. Disjoining pressure may play an important role, but its absolute value is difficult to quantify. Moreover, since the change in stress of the adsorbed water is analogous to that of the evaporable water, quantification of the change in disjoining pressure is strongly related to that of the capillary stress [Powers (1968)]. Therefore, capillary stress is assumed to be the main driving force of shrinkage in this model. It is noted that some investigators also used capillary stress as the main driving force when calculating shrinkage [e.g. Hua et al. (1995, 1997); Shimomura and Maekawa (1997); Lura et al. (2003)].

4.3 Diameter of the Largest Water-Filled Capillary Pore

From Eq. (4-1), it can be seen that the capillary stress can be identified as long as

the diameter of the largest water-filled capillary pore, $j_{pore-water}$, is determined, hence in order to calculate the capillary stress during cement hydration, the relationship between $j_{pore-water}$ and the properties of cement paste must be addressed.

According to the available experimental results on the pore structure of cement paste [e.g. Whiting and Kline (1977)], the relationship between the accumulated pore volume and the corresponding largest pore diameter can be expressed as:

$$\frac{V_{pore}}{V_{ref}} = a \ln\left(\frac{j}{j_0}\right) \tag{4-3}$$

in which j_0 is the diameter of the smallest capillary pore, which according to Powers and Brownyard (1947), ranges from 0.002 to 0.003μm; V_{ref} is the reference pore volume; V_{pore} is the cumulative pore volume up to some pore diameter j. The parameter *a* in the above equation can be interpreted as the *secant* ratio slope of the $\frac{V_{pore}}{V_{ref}}$ vs. $\ln\left(\frac{j}{j_0}\right)$ curve as shown in Fig. 4-1. Eq. (4-3) can be uniquely determined if *a* can be identified.

If letting V_{pore} in Eq. (4-3) equal the cumulative volume of the water-filled capillary pores, $V_{pore-water}$, the corresponding $j_{pore-water}$ turns to be:

$$j_{pore-water} = j_0 \exp\left(\frac{V_{pore-water}}{aV_{ref}}\right) \tag{4-4}$$

Since the surface tension of water g is known to be 0.07197N/m, the capillary stress p_c can be obtained by substituting the above $j_{pore-water}$ into Eq. (4-1).

Therefore, the critical task in identifying the capillary stress is to determine the

parameter *a* in Eq. (4-4). In Koenders and van Breugel (1997), *a* is taken as constant for a specific cement. However, according to the available experimental results, *a* should be a function of the fineness of cement, water-cement ratio, and the degree of hydration. The self-desiccation tests show that the internal relative humidity of cement paste cannot drop below 70%. A constant parameter *a* for a specific cement paste disregarding the effects of water-cement ratio and degree of hydration would predict a very low relative humidity at a high degree of hydration when the water-cement ratio is low.

The dependence of *a* on the fineness of cement has been recognized by Koenders and van Breugel (1997). It is well known that coarser cement results in larger pores in the paste, hence according to Eq. (4-4), for the same $V_{pore-water}$, the value of *a* is larger for finer cement, the *Blaine* value of which is larger. In this study, the relationship between *a* and the *Blaine* fineness is assumed to be linear:

$$a \propto \frac{Blaine}{350} \tag{4-5}$$

where the *Blaine* value has units of m^2/kg.

The relationship between the value of *a* and water-cement ratio as well as the degree of hydration can be obtained from the experimental results on internal relative humidity of cement paste under sealed curing conditions. It has been demonstrated by several researchers that higher internal relative humidity results from a higher water-cement ratio. As referred to by Jensen (1995), the relative humidity approaches a constant value of about 70% during the late period of hydration when the water-cement ratio is low.

In order to simulate the aforementioned properties of cement hydration and

calculate the capillary stress at various stages of hydration, the parameter *a* should be determined as a function of both the water-cement ratio and the degree of hydration. More importantly, the value of *a* must allow for a limit to the development of internal relative humidity when the water-cement ratio is low. It is thereby proposed that:

$$a \propto \frac{V_{pore-water}}{V_{ref}} \tag{4-6}$$

With Eq. (4-6), the internal relative humidity of cement paste under sealed curing conditions can level off at a certain value during the late period of hydration.

Using the limited available test results on internal relative humidity, *a* is finally expressed as:

$$a = 0.205 \times \frac{Blaine}{350}\left(\frac{w}{c}\right)^{-0.718}\left[1.0 - c_1\left(a_u - a\right)^{c_2}\right] \cdot \frac{V_{pore-water}}{V_{ref}} \tag{4-7}$$

$$c_1 = c_{10}\left(\frac{w}{c}\right)^{-0.476} \tag{4-8}$$

$$c_2 = \frac{\frac{w}{c}}{0.323 + 1.19\frac{w}{c}} \tag{4-9}$$

in which c_{10} is a material constant that depends on the chemical composition of cement and can be calibrated using the experimental data on internal relative humidity under sealed curing conditions.

Eqs. (4-4) and (4-7) – (4-9) imply that the pore diameter can be determined from water-cement ratio, *Blaine* fineness and the degree of hydration using the experimental data on relative humidity of cement paste under sealed curing conditions, without referring to the cumulative volume of free water in cement paste, that is:

$$j_{pore-water} = j_0 \exp\left(\frac{1.0}{0.205 \times \frac{Blaine}{350}\left(\frac{w}{c}\right)^{-0.718}\left[1.0 - c_1\left(a_u - a\right)^{c_2}\right]}\right) \qquad (4\text{-}10)$$

From a modeling point of view, Eq. (4-10) can introduce a limit to the development of relative humidity [see also Eq. (4-2)].

Fig. 4-2 and Fig. 4-3 show the simulated and predicted results compared with the experimental data of Jiang et al. (2005) and Lura et al. (2003), respectively. The material constant c_{10} is 0.46 for both of these two cements. As a matter of fact, the experimental results of Lura et al. (2003) are predicted using the parameters calibrated from the experimental results of Jiang et al. (2005).

It should be pointed out that Eq. (4-10) is obtained using limited experimental data on relative humidity of cement paste under sealed curing conditions. Especially, the parameters in Eq. (4-10) might vary for cements with different chemical compositions. However, the variation trends of the internal relative humidity of different cements are similar, and from Fig. 4-2 and Fig. 4-3, it can be seen that Eq. (4-10) can predict the variation trends satisfactorily. More in-depth experiments on cements with different chemical compositions are required to obtain and calibrate more definitely the parameters in Eq. (4-10), including c_{10}.

It should also be noted that because curing temperature and applied pressure influence the pore structure as well, they should be taken into account when calculating *a* using Eqs. (4-7) – (4-9). However, due to the lack of pertinent experimental data, these two factors are not included in the present equations. The effects of curing temperature and applied pressure deserve further investigation.

4.4 Calculation of Volume Changes Using Theory of Poromechanics

Although capillary stress can be obtained using Eq. (4-1), its role in volume changes of cement paste still needs to be resolved. Set cement paste in its very nature is a porous medium, the constituent components of which may include anhydrous cement particles, hydration products and capillary pores. Anhydrous cement particles are surrounded and connected by hydration products, constituting the "solid phase" of the porous medium; while capillary pores may be saturated or unsaturated with pore water, depending on the curing conditions. The solid phase, the capillary pores and the pore water and air together constitute a porous medium, the mechanical behavior of which, including volume changes, can be addressed within theoretical framework of poromechanics [Coussy (2004)] as well as the role of capillary stress in volume change of cement paste. In the present study, the porous characteristic of the *C–S–H* matrix is not considered, based on the fact that the pores (viz. gel pores and inter-layer spaces) in hydration products are much smaller than the capillary pores, and at high relative humidity, they are always filled with pore fluid. The aforementioned properties of the *C–S–H* matrix indicate that it can not be simply considered as a linear elastic solid. Its mechanical behavior should rather be taken into account using a time-dependent constitutive model, as will be discussed in the subsequent chapters.

4.4.1 Tangent thermoporoelastic properties of saturated porous media

For a nonlinear thermoporoelastic medium, the thermodynamic dissipation is zero, that is:

$$s_{ij} de_{ij} + p_w df - S_s dT - dY_s = 0 \tag{4-11}$$

in which s_{ij} is the ij^{th} component of the stress tensor of the porous medium; e_{ij} is the ij^{th} component of the strain tensor; p_w is the pressure of the pore water; f is the porosity; S_s is the entropy of the skeleton that consists of the solid phase and pores; T is the absolute temperature; and Y_s is the free energy of the skeleton.

If G_s is defined as the modified free energy of the skeleton by letting:

$$G_s = Y_s - p_w f \tag{4-12}$$

Eq. (4-11) becomes:

$$s_{ij} de_{ij} - f dp_w - S_s dT - dG_s = 0 \tag{4-13}$$

The state equations can now be obtained as:

$$s_{ij} = \frac{\partial G_s}{\partial e_{ij}} \tag{4-14}$$

$$f = -\frac{\partial G_s}{\partial p_w} \tag{4-15}$$

$$S_s = -\frac{\partial G_s}{\partial T} \tag{4-16}$$

Differentiating Eqs. (4-14) and (4-15) gives:

$$ds_{ij} = C_{ijkl} de_{kl} - b_{ij} dp_w - C_{ijkl} a_{kl} dT \tag{4-17}$$

$$df = b_{ij} de_{ij} + \frac{dp_w}{N} - 3a_f dT \tag{4-18}$$

In Eqs. (4-17) and (4-18), C_{ijkl} , b_{ij} , a_{kl} , $\frac{1}{N}$ and $3a_f$ are all the thermoporoelastic tangent properties. Among them, C_{ijkl} is the $ijkl^{th}$ component of the tensor of skeleton tangent elastic stiffness moduli; b_{ij} is the ij^{th} component of

Biot's tangent tensor; a_{kl} is the kl^{th} component of the tensor of skeleton tangent thermal dilation coefficients; $\frac{1}{N}$ is the inverse of Biot's tangent modulus linking the pressure variation dp_w and the porosity variation df; and $3a_f$ is the volumetric thermal dilation coefficient related to the porosity. The sign convention in Eqs. (4-17) and (4-18) is tension positive.

Assuming isotropy of the porous medium, the constitutive equations can now be written as:

$$ds_b = K_d de_v - bdp_w - 3a_{th} K_d dT \tag{4-19}$$

$$ds_{ij} = 2Gde_{ij} \tag{4-20}$$

$$df = bde_v + \frac{dp_w}{N} - 3a_f dT \tag{4-21}$$

in which

$$s_b = \frac{1}{3} s_{ii} \tag{4-22}$$

$$s_{ij} = s_{ij} - s_b d_{ij} \tag{4-23}$$

$$e_v = e_{ii} \tag{4-24}$$

$$e_{ij} = e_{ij} - \frac{1}{3} e_v d_{ij} \tag{4-25}$$

where s_b is the bulk stress of the porous medium; e_v is the volumetric deformation; b is the bulk Biot's coefficient, or simply Biot's coefficient; $3a_{th}$ is the volumetric thermal dilation coefficient; K_d is the "drained" tangent bulk modulus of the porous medium. The expression "drained" is used here to indicate that K_d could be obtained

by keeping the pore pressure p_w and temperature T constant, which could only be conducted in an isothermal test with the pore fluid "free to flow", or in other words, in a drained condition.

Since the main concern of the present study is shrinkage, it would be more convenient if the sign convention of compression positive is applied. Further more, if the coefficient a_f is assumed to be zero, or the dilation of the pores themselves is assumed to be negligible, Eqs. (4-19) and (4-21) can be rewritten as (note that pore pressure p_w is positive in both cases):

$$ds_b = K_d de_v + b dp_w + 3a_{th} K_d dT \tag{4-26}$$

$$df = b de_v - \frac{dp_w}{N} \tag{4-27}$$

The deviatoric stress-strain relationship remains the same, as shown in Eq. (4-20).

The responses of the solid phase in the porous medium can also be investigated. Assuming an isotropic and homogenous solid phase under isothermal conditions, i.e.

$$ds_{sb} = K_s de_{sv} \tag{4-28}$$

The following stress and strain partition equations hold:

$$ds_b = (1-f) ds_{sb} + f dp_w \tag{4-29}$$

$$de_v = (1-f) de_{sv} + df \tag{4-30}$$

where s_{sb}, e_{sv} and K_s are the bulk stress, volumetric deformation and effective bulk modulus related to the solid phase, respectively. The following relationships can be obtained using Eqs. (4-20) and (4-26) – (4-30):

$$b = 1 - \frac{K_d}{K_s} \tag{4-31}$$

$$\frac{1}{N} = \frac{b-f}{K_s} \tag{4-32}$$

Finally, for the undrained response of a porous medium, i.e. with the pore fluid not being allowed to flow, the effective bulk modulus is referred to as the undrained bulk modulus K_u, which can be derived as:

$$K_u = K_d + b^2 M \tag{4-33}$$

with

$$M = \frac{NK_f}{K_f + Nf} \tag{4-34}$$

where K_f is the bulk modulus of the pore fluid. The detailed derivation can be found in Coussy (2004), and is not undertaken herein.

4.4.2 Equivalent pore pressure of unsaturated porous media

Cement paste is usually an unsaturated porous medium due to chemical shrinkage and desiccation. For unsaturated porous media, the thermodynamic dissipation can be expressed as [Coussy (2004)]:

$$s_{ij} de_{ij} + p^* df - f p_c dS_w - S_s dT - dY_s = 0 \tag{4-35}$$

in which p_c is the capillary stress; S_w is the saturation ratio of pores; and p^* is the averaged fluid pressure defined by:

$$p^* = S_w p_w + (1 - S_w) p_a \tag{4-36}$$

where p_a is the pressure of the pore air, which is related to the capillary stress p_c through:

$$p_c = p_a - p_w \tag{4-37}$$

The free energy Y_s in Eq. (4-35) consists of the free energy of the solid phase y_s and the overall interfacial energy fU, i.e.

$$Y_s(e_{ij}, S_w, T) = y_s(e_{ij}, f, T) + fU(S_w, T) \tag{4-38}$$

The interfacial energy U is related to the capillary stress through:

$$p_c = -\frac{\partial U}{\partial S_w} \tag{4-39}$$

$$U(S_w, T) = \int_{S_w}^{1} p_c(S_w, T) dS_w \tag{4-40}$$

Now Eq. (4-35), the equation for the thermodynamic dissipation, can be rewritten as:

$$s_{ij} de_{ij} + \left(p^* - U\right) df - \left(S_s + f\frac{\partial U}{\partial T}\right) dT - dy_s = 0 \tag{4-41}$$

Defining an equivalent pore pressure p as:

$$p = p^* - U \tag{4-42}$$

and a new entropy S_s' as:

$$S_s' = S_s + f\frac{\partial U}{\partial T} \tag{4-43}$$

Eq. (4-41) becomes:

$$s_{ij} de_{ij} + p df - S_s' dT - dy_s = 0 \tag{4-44}$$

Comparing Eq. (4-44) with Eq. (4-11), it can be seen that they have a similar format. It follows that the derivation of the constitutive equations in Section 4.4.1 can be directly used to derive those for the unsaturated porous media. Therefore,

$$ds_b = K_d de_v + b dp + 3a_{th} K_d dT \tag{4-45}$$

$$df = b de_v - \frac{dp}{N} \tag{4-46}$$

The deviatoric stress-strain relationship remains the same as in Eq. (4-20).

From Eqs. (4-36), (4-37), (4-40) and (4-42),

$$dp = -S_w dp_c + dp_a \tag{4-47}$$

If the air pressure in the pores is assumed to be constant, the differential definition of the equivalent pore pressure p becomes:

$$dp = -S_w dp_c \tag{4-48}$$

Finally, the differential volumetric strain of cement paste can be calculated through:

$$de_v = \frac{ds_b + bS_w dp_c}{K_d} - 3a_{th} dT \tag{4-49}$$

Provided that the differential bulk stress, or in this case, the differential applied pressure ds_b is known, the remaining issues that need to be identified are the tangent properties K_d and b, and for a problem with a temperature variation, the thermal dilation coefficient a_{th}.

4.5 Summary and Discussion

The possible driving forces of shrinkage of cement paste have been discussed. Surface tension is relevant for shrinkage of cement paste at low relative humidity (i.e. $RH < 40\%$), while disjoining pressure and capillary stress play major roles at higher relative humidity, which is the main concern of the present study. However, the quantification of disjoining pressure is difficult, and its mechanism of inducing shrinkage of cement paste is not clearly understood. Capillary stress, on the other hand, can be conveniently determined with relative humidity, and its mechanism is very clear.

Therefore, capillary stress is assumed to be the main driving force of shrinkage. In order to quantify capillary stress using the Young-Laplace equation, an equation for the diameter of the largest water-filled capillary pore was proposed based on the limited experimental results of relative humidity in cement pastes during self-desiccation, in which the effects of degree of hydration, water-cement ratio, chemical composition and fineness of cement are considered. Although the constants in the equation still need to be calibrated against more experimental data, the equation can be used to simulate the development of relative humidity during cement hydration and to calculate capillary stress.

The role of capillary stress in shrinkage of cement paste can be addressed by the theory of poromechanics, based on the fact that set cement paste in its very nature can be considered a porous medium. The theories of saturated and unsaturated nonlinear thermoporoelasticity were briefly introduced. The concept of equivalent pore pressure proposed in Coussy (2004), which is directly related to the capillary stress, was discussed and will be used to calculate the volume change of cement paste.

The definite role of disjoining pressure in shrinkage of cement paste deserves further investigation.

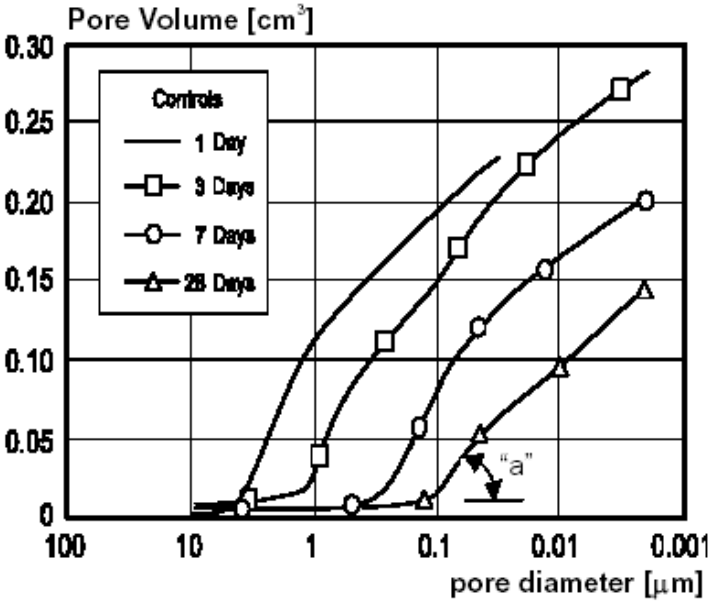

Fig. 4-1 Pore Size Distribution Measurements [Whiting and Kline (1977)]

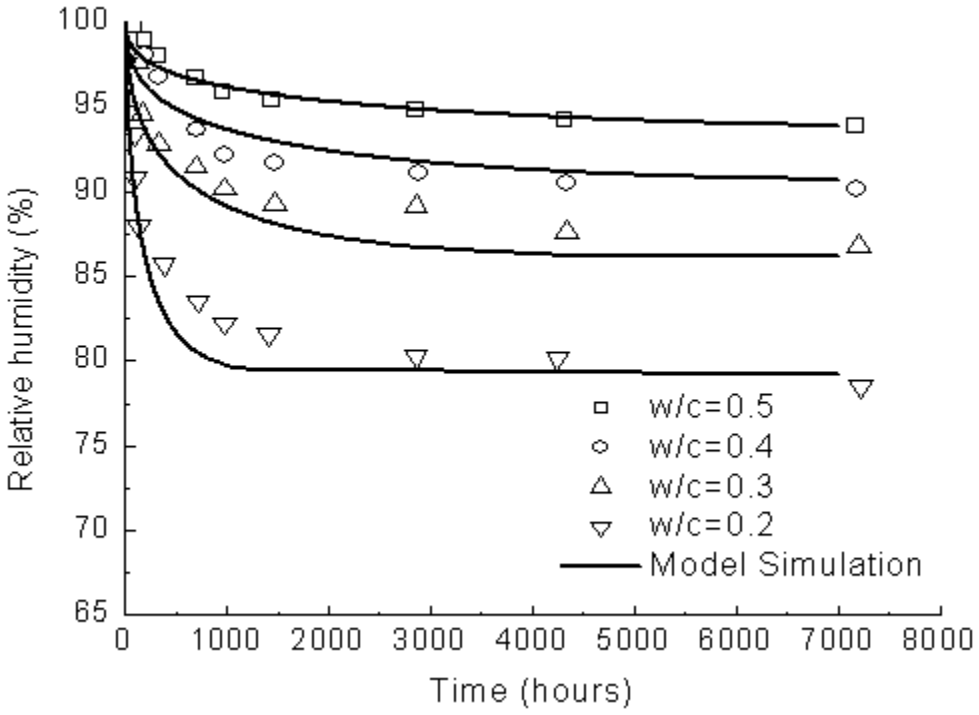

Fig. 4-2 Simulated and Measured Relative Humidity for 52.5 OPC Pastes with Different Water-Cement Ratios (Experimental Data from [Jiang et al. (2005)])

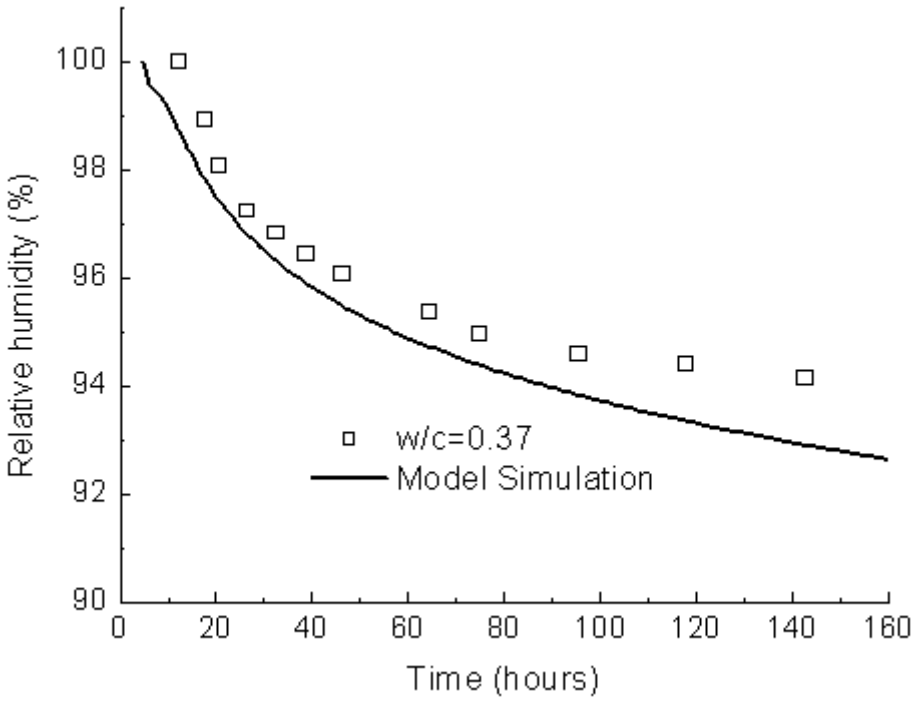

Fig. 4-3 Simulated and Measured Relative Humidity for a CEM I 52.5 R Paste (Experimental Data from [Lura et al. (2003)])

CHAPTER 5

MULTI-SCALE AND MICROMECHANICAL CONSTITUTIVE MODELING OF THE EFFECTIVE ELASTIC PROPERTIES OF CEMENT PASTE

5.1 Introduction

A rational constitutive model of autogenous shrinkage of hardening cement paste must take into account the thermo-chemo-mechanical reactions, relations and properties of its constituent components, including pores of different sizes, anhydrous cement particles, various hydration products such as *C–S–H* and *CH*, and pore water in different forms. At the same time, the model must be relatively simple, so that it can be applied to analyze practical problems. In particular, the material constants of the model should have clear physical meaning and be easy to calibrate. For its constituent components, hardened or hardening cement paste can be regarded as a composite medium, hence mechanics of composite materials can serve as a theoretical basis for the constitutive model. In addition, cement paste is fundamentally a porous medium [Ulm et al. (2004)], so the mechanics theory for porous media proposed by Coussy (2004) will also be relevant in formulating the constitutive model. Bernard et al. (2003) and Ulm et al. (2004) used both the theory of mechanics of composites and that of poromechanics to model the elastic moduli of hardened cement paste. They demonstrated that the combination of the two theories was able to capture its salient elastic properties. However, there is still a long way to go before their theory can be used to develop a

rational autogenous shrinkage model for hardening cement paste. First of all, anhydrous cement, which can be an important constituent of also hardened cement paste, was not considered in their models; secondly, the time-dependent material properties were not accounted for; and thirdly, the poromechanics issue of Biot's coefficient for the early-aged cement paste was not resolved in their models.

In this chapter, a model is developed to simulate the elastic properties of hardened cement paste first. It is then extended to consider the aging effects on hardening cement paste using a concept that is similar to the solidification theory of Bažant and Prasannan (1989). The proposed models are validated against the available experimental results. Based on the elastic model for hardening cement paste, a shrinkage model for cement paste will be presented in the next chapter that considers the time-dependent properties of *C–S–H*.

5.2 Micromechanical Constitutive Model for the Effective Elastic Properties of Hardened Cement Paste

Depending on the availability of water (water-cement ratio) during its hardening process, the constitute components of hardened cement paste may include hydration products (mainly *C–S–H* and *CH*), pores of different sizes, pore water, and anhydrous cement. For cement pastes with high water-cement ratios and after sufficiently long periods of hydration, anhydrous cement may not exist. However, the ultimate degree of hydration of a cement paste with a low water cement ratio is smaller than 1.0, in which case the anhydrous cement remains one of the important constituent components. Therefore, a general constitutive model that simulates the effective elastic properties of

hardened cement paste should consider this possibility. In the model to be proposed, anhydrous cement is considered to exist, and to be consistent with the proposed hydration kinetics model and based on the available experimental observations, the anhydrous cement is assumed to be surrounded by the hydration products, i.e. the anhydrous cement forms the *core* of the solid phase of cement paste and the hydration products form the *shell* around it. A similar structure was also assumed in Hua et al. (1997).

5.2.1 Model formulation

Depending on the chemical composition of anhydrous cement, hydration products may include *C–S–H*, *CH*, calcium sulfoaluminate hydrate (mainly ettringite $C_6A\bar{S}_3H_{32}$ and/or monosulfoaluminate $C_4A\bar{S}H_{12}$), and others. However, for most cements, *C–S–H* and *CH* are the major hydration products, and according to Haecker et al. (2005), the elastic moduli of calcium sulfoaluminate hydrate, which may be an important component of some cement pastes, are close to those of *C–S–H*. Therefore, in this model, *C–S–H* and *CH* are considered to be the only hydration products and the others are assumed to exhibit the same mechanical properties as *C–S–H*.

The elastic properties of the four major clinker phases (viz. C_3S, C_2S, C_3A and C_4AF) of anhydrous cement have been investigated extensively [e.g. Boumiz et al. (1997); Acker (2001); Velez et al. (2001a)]. Different values of the elastic moduli of the four major clinker phases were obtained by nanoindentation; however, the differences between them are small. In this study, the average values measured by Acker et al. (2001) and Velez et al. (2001a) are used as the mean effective moduli of anhydrous

cement, as shown in Table 5-1.

Other investigators have also determined the elastic moduli of *C–S–H* using nanoindentation [e.g. Helmuth and Turk (1966); Tennis and Jennings (2000); Velez et al. (2001b); Constantinides and Ulm (2004)]. According to Constantinides and Ulm (2004), two types of *C–S–H* (viz. the low-density *C–S–H* and the high-density *C–S–H*) with different elastic moduli exist in hydration products. The ratio between them depends on the water-cement ratio as well as the degree of hydration and is difficult to calculate. However, the difference in the elastic moduli between these two types of *C–S–H* are not very large [$E_{LDCSH} = 21.7\text{GPa}$ and $E_{HDCSH} = 29.4\text{GPa}$ according to Constantinides and Ulm (2004)]. Therefore, single values of elastic moduli are assigned to *C–S–H* in this study. The values calculated by Constantinides and Ulm (2004) for a cement paste with a water-cement ratio of 0.5 are adopted, as shown in Table 5-1. It should be noted that the elastic moduli measured by nanoindentation are the so-called “drained” ones [Ulm et al. (2004)], since fundamentally, the *C–S–H* matrix contains gel pores and hence is also a porous medium. The undrained elastic moduli were calculated by Ulm et al. (2004) for the aforementioned cement paste and are adopted here, as shown in Table 5-1. Haecker et al. (2005) also used a single set of elastic moduli of *C–S–H*.

For the elastic moduli of *CH*, the values measured by Monteiro and Chang (1995) are used (Table 5-1). These moduli were also used in Haecker et al. (2005). To calculate the effective undrained elastic moduli, the bulk stiffness of pore water is also needed. A value of 2.2GPa is used according to Lide (1997).

Although different investigations may determine different specific values of the aforementioned elastic moduli, the values shown in Table 5-1 are considered to be the

intrinsic properties of the constituent components of cement paste, independent of the cement type, water-cement ratio, and curing conditions.

Cement paste can be fundamentally considered as a composite medium, and the composite characteristics of the different constituent components and the pores are complex and must be investigated at different length scales. The scales proposed in Ulm et al. (2004) are applied here. However, since anhydrous cement is also considered to be one important constituent component, one more scale is introduced.

Using different length scales, four levels of composite media can be identified for cement paste. Starting from the largest scale, these four levels are cement paste (Level III), solid phase of cement paste (Level II), hydration products (Level I) and *C–S–H* matrix (Level 0). In this model, the *C–S–H* matrix is treated similarly as *CH* and the anhydrous cement, but with drained or undrained elastic moduli. Therefore, only three levels of composite media are considered. The effective elastic moduli of a lower level are used as the input for the next level, treating the lower level composite as one effective medium, which is denoted as the up-scale approach.

The three levels of composites are now discussed in some detail, starting from Level I.

Hydration products (Level I) are assumed to consist of the *C–S–H* matrix and the *CH* inclusions. The volume ratios of *C–S–H* and *CH* in hydration products are determined by the chemical composition of cement and can be calculated [Taylor (1997); Ulm et al. (2004)]. The volume fraction of *CH* is generally much smaller than that of *C–S–H*. Therefore, *CH* can be treated as randomly distributed inclusions with a small volume fraction embedding in the *C–S–H* matrix. The effective medium theory of

Mori and Tanaka (1973) is ideal for such a composite. The shape of the *CH* inclusions and the way they are distributed in the *C–S–H* matrix are difficult to define, but since their volume fraction is small, it is further assumed that the *CH* inclusions are spherical and dispersed isotropically within the *C–S–H* matrix. With these assumptions, the effective elastic moduli of hydration products can be obtained [Aboudi (1991)]:

$$K_{hp} = K_{CSH} + \frac{f_{CH}\left(K_{CH} - K_{CSH}\right)K_{CSH}}{\left(1 - f_{CH}\right)\left(K_{CH} - K_{CSH}\right)a_1 + K_{CSH}} \tag{5-1}$$

$$G_{hp} = G_{CSH} + \frac{f_{CH}\left(G_{CH} - G_{CSH}\right)G_{CSH}}{\left(1 - f_{CH}\right)\left(G_{CH} - G_{CSH}\right)a_2 + G_{CSH}} \tag{5-2}$$

in which

$$a_1 = \frac{3K_{CSH}}{3K_{CSH} + 4G_{CSH}} \tag{5-3}$$

$$a_2 = \frac{6\left(K_{CSH} + 2G_{CSH}\right)}{5\left(3K_{CSH} + 4G_{CSH}\right)} \tag{5-4}$$

and f_{CH} is the volume fraction of *CH* inclusions in the hydration products.

If the degree of hydration is less than 1.0, anhydrous cement will also exist in the cement paste. The anhydrous cement particle is assumed to be surrounded by the hydration products and they together form another effective composite medium, the solid phase of cement paste (Level II). The anhydrous cement particle is assumed to be spherical in shape and the hydration products are assumed to form a shell around the anhydrous cement, as shown in Fig. 5-1. The volume ratio between them depends on the degree of hydration a. According to Powers and Brownyard (1947), the volume fraction of the anhydrous cement inclusions in the solid phase of cement paste is:

$$f_{ace} = \frac{0.32(1-a)}{0.32(1-a)+2.2\times 0.32a} = \frac{1-a}{1+1.2a} \tag{5-5}$$

It should be noted that it is not the actual volume of the composite sphere but the volume ratio as determined by Eq. (5-5) that is important. The composite sphere can now be considered as being surrounded by some isotropic effective medium, as shown in Fig. 5-1, which contains macro pores, pore water, and the solid phases similar to the composite sphere. The model illustrated in Fig. 5-1 is identical to the three-phase model (or the generalized self-consistent scheme model) discussed in Christensen (1979, 1990), if the hydration products are considered to be one effective medium.

The effective elastic moduli of the solid phase of cement paste (Level II) can now be obtained. According to Christensen (1990), the effective bulk modulus is expressed as:

$$K_{ces} = K_{hp} + \frac{f_{ace}\left(K_{ace}-K_{hp}\right)\left(3K_{hp}+4G_{hp}\right)}{3K_{ace}+4G_{hp}-3f_{ace}\left(K_{ace}-K_{hp}\right)} \tag{5-6}$$

in which K_{ace} is the bulk modulus of the anhydrous cement clinker given in Table 5-1. The effective shear modulus can be obtained by solving the following quadratic equation:

$$A_1\left(\frac{G_{ces}}{G_{hp}}\right)^2 + 2A_2\left(\frac{G_{ces}}{G_{hp}}\right) + A_3 = 0 \tag{5-7}$$

The three coefficients A_1, A_2 and A_3 in Eq. (5-7) are functions of the elastic properties of the hydration products and the anhydrous cement as well as the volume fraction of the anhydrous cement. These coefficients are given in Appendix I according to Christensen (1990).

The solution of Eq. (5-7) usually yields two values of G_{ces}. However, a correct value of G_{ces} can be obtained by observing the following properties of the solid phase of cement paste: first, the effective shear modulus cannot be negative; second, it is usually smaller than the effective bulk modulus. The second condition assumes that the Poisson's ratio of the solid phase is larger than $\frac{1}{8}$, the validity of which still needs to be verified by experiments.

Finally, the effective drained elastic moduli of hardened cement paste (Level III) are obtained using the Mori-Tanaka scheme again. The capillary porosity of hardened cement paste with small or modest water-cement ratios is usually not large. For such capillary porosity, the voids (capillary pores) can be assumed to be randomly dispersed within the solid phase with a small volume fraction. The effective elastic properties may then be described using the Mori-Tanaka model by considering the voids as inclusions. The assumptions used for the hydration products are also used on this level. The voids are assumed to be spherical inclusions evenly dispersed in the solid phase. The drained effective moduli can now be calculated using equations similar to Eqs. (5-1) and (5-2). The pore pressure in a porous medium does not influence its drained elastic properties [Coussy (2004)], which means that when calculating the effective drained elastic moduli of hardened cement paste, the elastic moduli of the void inclusions are equal to zero. Therefore,

$$K_{cep}^{d} = K_{ces} - \frac{f K_{ces}^{2}}{-a_{3}(1-f)K_{ces} + K_{ces}} \tag{5-8}$$

$$G_{cep} = G_{ces} - \frac{f G_{ces}^{2}}{-a_{4}(1-f)G_{ces} + G_{ces}} \tag{5-9}$$

where

$$a_3 = \frac{3K_{ces}}{3K_{ces} + 4G_{ces}} \tag{5-10}$$

$$a_4 = \frac{6\left(K_{ces} + 2G_{ces}\right)}{5\left(3K_{ces} + 4G_{ces}\right)} \tag{5-11}$$

and f is the capillary porosity, which can be calculated using Powers' theory and the volume of external shrinkage during cement hydration. If the external shrinkage can be neglected, e.g. for a cement paste cured under a saturated condition, according to Powers and Brownyard (1947), the capillary porosity can be expressed as:

$$f = \frac{0.0625a}{0.32 + \frac{w}{c}} + \frac{1.0}{0.32 + \frac{w}{c}}\left(\frac{w}{c} - 0.4a\right) = \frac{\frac{w}{c} - 0.3375a}{0.32 + \frac{w}{c}} \tag{5-12}$$

Gel pores are not considered on this level. They are assumed to be integral components of the *C–S–H* matrix. The effective elastic moduli of *C–S–H* given in Table 5-1 already account for the effects of gel pores.

The Mori-Tanaka scheme is not suitable for composites with a large volume fraction of inclusions [Aboudi (1991)]. Therefore, for the cement paste with large capillary porosity, Eqs. (5-8) – (5-11) are not relevant. Some other scheme needs to be used, which will be discussed subsequently in this chapter.

The theory of poromechanics [Coussy (2004)] can now be employed to obtain other elastic properties of cement paste. According to Eqs. (4-31) and (4-32), the Biot's coefficient *b* can be expressed as:

$$b = 1.0 - \frac{K_{cep}^{d}}{K_{ces}} \tag{5-13}$$

The inverse of Biot's modulus $\frac{1}{N}$ can be written as:

$$\frac{1}{N} = \frac{b-f}{K_{ces}} \tag{5-14}$$

And according to Eqs. (4-33) and (4-34), if assuming the pore fluid to be water, the effective undrained bulk modulus of cement paste can be obtained as:

$$K_{cep}^{u} = K_{cep}^{d} + b^2 M \tag{5-15}$$

with

$$M = \frac{NK_w}{K_w + Nf} \tag{5-16}$$

where $K_w = 2.2\text{GPa}$ is the bulk modulus of water.

The Young's modulus E and Poisson's ratio n can be calculated using the theory of isotropic elasticity,

$$E = \frac{9KG}{3K+G} \tag{5-17}$$

$$n = \frac{3K-2G}{2(3K+G)} \tag{5-18}$$

It is noted that some investigators have proposed empirical expressions for the Biot's coefficient b for hardened cement paste using experimental results for certain cements [e.g. Hansen (1965); Kendal et al. (1983)]. With such expressions and the effective elastic moduli of the solid phase, the effective elastic properties of cement paste can be obtained via Eq. (5-13). However, these expressions usually do not consider the influence of the mechanical properties of the solid phase of cement paste, which is conceptually not as rational as the proposed approach.

The input parameters for the proposed model include the elastic moduli of the constituent components of Table 5-1, the degree of hydration a, the capillary porosity, and the volume fraction of *CH* in the hydration products. Among these, the elastic material constants of Table 5-1 are assumed to be intrinsic and not to change for different cements. The capillary porosity may be obtained by applying Powers' theory and using the data of shrinkage of cement paste during its hydration.

The last input parameter is the volume fraction of *CH* in hydration products. Based on the stoichiometry of Eqs. (1-1) and (1-2) which are the hydration reactions of the two calcium silicates, C_3S and C_2S, given the gram molecular weight (*GMW*) and density r of each reactant and product as shown in Table 5-2 [Tennis and Jennings (2000); Mindess et al. (2002)], the volume fraction of *CH* in the hydration products, f_{CH}, can be estimated as:

$$f_{CH} \approx \frac{0.19\, p_{C_3S} + 0.06\, p_{C_2S}}{0.69\, p_{C_3S} + 0.72\, p_{C_2S} + V_{others}} \tag{5-19}$$

in which p_{C_3S} and p_{C_2S} are the Bogue mass fractions of C_3S and C_2S, respectively; V_{others} is the volume of the hydration products other than *C–S–H* and *CH*, such as $C_6A\bar{S}_3H_{32}$, $C_4A\bar{S}H_{12}$, C_3AH_6, FH_3, etc.

It should be pointed out that only *C–S–H* and *CH*, the main hydration products of C_3S and C_2S, are considered explicitly in Eq. (5-19). This simplification is based on the fact that the modeling object is Portland cement, more than 72% (by mass) of which consists of these two calcium silicates. As pointed out in Section 1.1.3, Eqs. (1-1) – (1-8) are only approximate, especially for the hydration reactions of C_3A and C_4AF. *CH*,

as a hydration product of C_4AF in Eqs. (1-6) – (1-8), may also act as a reactant in the hydration reactions of C_3A and C_4AF, according to Tennis and Jennings (2000). Moreover, as shown in Eqs. (1-4) and (1-7), ettringite ($C_6A\bar{S}_3H_{32}$) may partially or fully transform into monosulfoaluminate ($C_4A\bar{S}H_{12}$) if gypsum ($C\bar{S}H_2$) is depleted before C_3A and C_4AF have completely hydrated. Such uncertainty of hydration reactions of C_3A and C_4AF makes it difficult to give an explicit expression for V_{others}. However, comparing with the sum of the other two terms in the denominator of Eq. (5-19), V_{others} is small. For Type I to Type V Portland cement, if $C_6A\bar{S}_3H_{32}$ fully transforms into $C_4A\bar{S}H_{12}$, V_{others} in Eq. (5-19) takes up approximately 10% – 25% of the total volume of hydration products based on the stoichiometry of Eqs. (1-1) – (1-8).

It should also be noted that the composition of *C–S–H* varies over quite a wide range [Mindess et al. (2002)]. Values of its gram molecular weight (*GMW*) and density r depend on the water content of *C–S–H*, which is related to how much "gel porosity" is included in the structure. For example, as provided in Ulm et al. (2004), the density of the saturated low-density *C–S–H* is 1.93g/cm^3, while the density of the saturated high-density *C–S–H* is 2.13g/cm^3. Therefore, either the formula $C_{3.4}S_2H_8$ in Eqs. (1-1) and (1-2) or the values of *GMW* and r of *C–S–H* in Table 5-2 are only approximate.

5.2.2 Model verification

The proposed model is evaluated using the experimental results for the D cement paste of Haecker et al. (2005). The elastic moduli of Table 5-1 are assumed to be intrinsic properties of the constituent components and were used as input for the

different cement pastes.

The elastic moduli given by Haecker et al. (2005) were measured using elastic resonance tests. The *C–S–H* matrix in such tests should be considered undrained [Ulm et al. (2004)], the undrained bulk modulus for *C–S–H* matrix shown in Table 5-1 is hence used in Eqs. (5-1) and (5-2) to calculate the effective elastic moduli of hydration products. The measured elastic moduli should also be interpreted as the undrained ones.

The measured degree of hydration is used as an input for the D cement pastes of Haecker et al. (2005). The volume fraction of *CH* provided in that reference is also used. The capillary porosity calculated by Eq. (5-12) is used to calculate the effective drained elastic moduli in Eqs. (5-8) and (5-9). Comparisons of the model predictions with the measured results for the cement pastes at an age of 28 days and an age of 56 days are shown in Fig. 5-2 and Fig. 5-3, respectively. It can be seen that the model predictions agree well with the experimental results for large water-cement ratios. For small water-cement ratios, the model underestimates the effective elastic moduli, but the differences are small. One obvious explanation is the fact that Eq. (5-12) was used to calculate the capillary porosity, disregarding the bulk shrinkage of cement paste during its hydration. If the capillary porosity predicted by CEMHYD3D [Bentz (1997)] is used instead, the model predictions are much better, as shown in Fig. 5-4.

5.3 Micromechanical Constitutive Model for the Effective Elastic Properties of Hardening Cement Paste

5.3.1 Model formulation

The proposed micromechanics concepts of the previous section can be extended

to consider the aging effects of hydrating cement paste. Two issues need to be addressed to model the mechanical behavior of hardening cement paste in addition to the concepts and methods of the previous section. First of all, the increase in the volume fraction of hydration products during cement hydration must be considered at Level II. Secondly, the large capillary porosity of cement paste at early age should be properly taken into account at Level III, since according to Aboudi (1991), the Mori-Tanaka scheme is not suitable for the cement paste with large capillary porosity.

If the constituent components of cement paste can all be considered to be elastic under any kind of loading condition, the aging effect at Level II is trivial, since in Eq. (5-5), the degree of hydration a is used to calculate the volume fraction of anhydrous cement. However, hydration products exhibit considerable inelastic behavior under large and/or sustained loading, and the mechanical properties, especially those time-dependent ones are likely to change with age. Therefore, some approach that is more logical than Eqs. (5-5) – (5-7) should be undertaken to model the mechanical properties of hardening cement paste.

Here, an approach that is similar to the solidification theory of Bažant and Prasannan (1989) is employed considering the following case: at time *t*, the degree of hydration is a ; after a certain time interval Dt, the degree of hydration becomes $a + Da$. The volume of the anhydrous cement consumed during this period is DV . If the time interval Dt is sufficiently small, the newly formed hydration products can be assumed to exhibit the same mechanical properties as the previously formed ones. Using the model for Level II as discussed in the previous section, the newly formed hydration products may exist on either inside or outside of the previously formed

hydration products, or both. Conceptually, using the three-phase model of Fig. 5-1, since the volume of the newly formed hydration products is about 2.2 times larger than the consumed anhydrous cement, i.e. $2.2\,DV$, they should exist on both inside and outside of the previously formed hydration products. Therefore, it is assumed that DV of the newly formed hydration products locate inside the previously formed hydration products, while the other $1.2\,DV$ locate outside, as shown in Fig. 5-5. Hua et al. (1997) had a similar assumption in their shrinkage model.

The effective mechanical properties of the solid phase at time $t+Dt$ can now be obtained via the following three steps, as shown in Fig. 5-6: the effective mechanical properties of the anhydrous cement core and the inner layer of the newly formed hydration products are firstly calculated using the three-phase model; in the second step, the previously formed hydration products serve as the matrix medium in the three-phase model, and the effective mechanical properties obtained from the previous step are then used as those of a new core that consists of the anhydrous cement and the inner layer of the newly formed hydration products; finally, the three-phase model is used once more to obtain the effective mechanical properties of the solid phase at time $t+Dt$, treating the outer layer of the newly formed hydration products as the matrix medium and the effective medium enclosed by it as the inclusion. For example, the bulk modulus of the solid phase at time $t+Dt$ can be obtained via the following expressions:

$$K_{ace-ih} = K_{ih} + \frac{f_{ace-ih}\left(K_{ace} - K_{ih}\right)\left(3K_{ih} + 4G_{ih}\right)}{3K_{ace} + 4G_{ih} - 3f_{ace-ih}\left(K_{ace} - K_{ih}\right)} \tag{5-20}$$

$$K_{nc1-fh} = K_{fh} + \frac{f_{nc1-fh}\left(K_{ace-ih} - K_{fh}\right)\left(3K_{fh} + 4G_{fh}\right)}{3K_{ace-ih} + 4G_{fh} - 3f_{nc1-fh}\left(K_{ace-ih} - K_{fh}\right)} \tag{5-21}$$

$$K_{nc2-oh} = K_{oh} + \frac{f_{nc2-oh}\left(K_{nc1-fh} - K_{oh}\right)\left(3K_{oh} + 4G_{oh}\right)}{3K_{nc1-fh} + 4G_{oh} - 3f_{nc2-oh}\left(K_{nc1-fh} - K_{oh}\right)} \tag{5-22}$$

The meanings of the symbols are as follows:

K_{ih} and G_{ih} – effective elastic moduli of the inner layer of the newly formed hydration products;

K_{fh} and G_{fh} – effective elastic moduli of the previously formed hydration products;

K_{oh} and G_{oh} – effective elastic moduli of the outer layer of the newly formed hydration products;

K_{ace-ih} and G_{ace-ih} – effective elastic moduli of the core formed by anhydrous cement and the inner layer of the newly formed hydration products;

K_{nc1-fh} and G_{nc1-fh} – effective elastic moduli of the core formed by anhydrous cement, the inner layer of the newly formed hydration products and the previously formed hydration products;

K_{nc2-oh} and G_{nc2-oh} – effective elastic moduli of the solid phase;

f_{ace-ih}, f_{nc1-fh} and f_{nc2-oh} – the corresponding volume fractions.

The aforementioned procedure can be repeated when more layers of hydration products are formed, which is easy to realize with computer programming. Using this approach, the aging effects on the mechanical properties of hydration products can be considered. And the linear elastic properties as predicted by this procedure are the same as those calculated using the model of Section 5.2.

For cement paste with large capillary porosity, some scheme other than the

Mori-Tanaka model has to be used at Level III to calculate the effective mechanical properties. As discussed in Aboudi (1991), the Mori-Tanaka scheme is not suitable for composites with large volume fractions of inclusions. When the capillary porosity is large, the Mori-Tanaka model overestimates the effective elastic moduli of cement paste. Fig. 5-7 shows estimates of the Mori-Tanaka model for a cement paste with a water-cement ratio of 0.3. As can be seen, the simulated effective Young's modulus decreases with time, which makes no sense.

The self-consistent scheme [Christensen (1979); Aboudi (1991)] is more appropriate for cement paste with relatively large capillary porosity. It is related to the percolation theory [Bernard et al. (2003)] and is more suitable to describe the effective behavior of cement paste at early age than the Mori-Tanaka scheme. It is also noted that when capillary porosity is small, the predictions of the Mori-Tanaka scheme and the self-consistent scheme are similar. However, the increase in the elastic moduli of cement paste with an increase in the degree of hydration can only be simulated using the self-consistent scheme. The effective drained elastic moduli of cement paste can be calculated by solving the following nonlinear equations [Aboudi (1991)]:

$$K_{cep}^{d} = K_{ces} - fK_{ces}\frac{3K_{cep}^{d} + 4G_{cep}}{4G_{cep}} \tag{5-23}$$

$$G_{cep} = G_{ces} - fG_{ces}\frac{15\left(1-n_{cep}^{d}\right)}{7-5n_{cep}^{d}} \tag{5-24}$$

in which f is the capillary porosity and n_{cep}^{d} is the effective drained Poisson's ratio of cement paste, which can be related to the effective bulk and shear moduli via the following equation:

$$n_{cep}^{d} = \frac{9K_{cep}^{d}}{2\left(G_{cep} + 3K_{cep}^{d}\right)} - 1.0 \tag{5-25}$$

However, the self-consistent scheme also has problems when the capillary porosity is very large, in which case the effective shear modulus of a composite medium with void inclusions and incompressible matrix can be obtained directly as [Christensen (1979)]:

$$G = \frac{3\left(1 - 2f_{void}\right)}{3 - f_{void}} G_m \tag{5-26}$$

with f_{void} being the volume fraction of voids. From Eq. (5-26), it can be seen that when $f_{void} \geq 0.5$, the self-consistent scheme predicts a zero or even negative shear modulus. This problem also exists for an effective medium with a compressible matrix, such as the cement paste. With a sufficiently large void ratio, the self-consistent scheme can predict a zero or even negative effective shear modulus for the early-aged cement paste. This is reasonable, because stiffness of cement paste can only develop at a certain degree of hydration at which the originally separated cement particles form a solid skeleton of hydration products [e.g. Hua et al. (1997)]. This process is known as percolation and the degree of hydration at which the cement paste is percolated (set) depends on the water-cement ratio, or the void ratio of the cement paste [Bentz and Garboczi (1991); Bentz (1997)]. This phenomenon is simulated using the self-consistent scheme. Therefore, the time when the stiffness simulated via the self-consistent scheme is larger than zero is assumed to be the time of setting.

5.3.2 Model verification

Fig. 5-8 shows the model predictions using the self-consistent scheme for the D

cement pastes of Haecker et al. (2005) at an age of 56 days. For the cement pastes with small water-cement ratios, in which cases the void ratios are small, the simulations are as close to the experimental results as those using the Mori-Tanaka scheme (see Fig. 5-4). The model slightly underestimates the experimental results for the cement pastes with large water-cement ratios, but the overall predictions are satisfactory.

The proposed model is used to simulate the elastic moduli of two hardening cement pastes [Boumiz et al. (1997)]. Fig. 5-9 shows the comparisons of the model predictions with the experimental data. The model prediction for the cement paste with $\frac{w}{c} = 0.4$ is good; while for the one with $\frac{w}{c} = 0.35$, the model overestimates the elastic moduli at very early age to some extent, but the results are still acceptable.

The discrepancy may partially attribute to the difficulties in experimental measurements at very early age of hydration [e.g. Haecker et al. (2005)], or to the parameters used for the prediction. In the proposed model, a single set of elastic properties was assigned to the four different clinker phases (i.e. C_3S, C_2S, C_3A and C_4AF); while according to the available experimental results, the specific values of the elastic properties of anhydrous cement may vary with different chemical compositions. This may explain the fact that the model overestimates the experimental results of Boumiz et al. (1997) but slightly underestimates those of Haecker et al. (2005). The simulation results shown in Fig. 5-9 demonstrate that the proposed model can be used to predict the elastic properties of hardening cement paste. It should be pointed out that for the model predictions in Fig. 5-9, no external shrinkage was considered, which may explain the slightly underestimates of the model predictions at late period.

5.4 Summary and Discussion

The elastic properties of hardened and hardening cement paste have been modeled within the frameworks of poromechanics and mechanics of composites. The up-scale approach was adopted in the constitutive modeling, starting from the layers of hydration products, to the solid phase of cement paste that consists of anhydrous cement and hydration products, and finally to the cement paste. The layers of hydration products are assumed to be composed of *C–S–H* matrix and *CH* inclusions only. The mechanical properties of other products such as the calcium sulfoaluminate hydrate are assumed to be the same as those of *C–S–H*, and the porous nature of *C–S–H* is omitted. To determine the properties of the composite materials, the Mori-Tanaka scheme was used at the scale of hydration products; the three-phase model was applied at the scale of the solid phase of cement paste; and the self-consistent scheme was employed at the scale of cement paste. The proposed models have been validated against the available experimental results, using the intrinsic elastic properties of the main constituent components of cement paste, which are anhydrous cement, *C–S–H* and *CH* reported in various references.

The proposed modeling scheme for the elastic properties of hardening cement paste can be extended to include the time-dependent properties of *C–S–H* to simulate the shrinkage behavior of cement paste, as will be discussed in the next chapter.

Table 5-1 Elastic Properties of the Constituent Components of Cement Paste

Elastic Moduli	Clinker	*C–S–H*		*CH*	Pore Water
		Drained	Undrained		
Bulk modulus *K* (GPa)	113.0	15.2	18.3	40.0	2.2
Shear modulus *G* (GPa)	53.6	9.6		16.0	—

Table 5-2 Physical Data of Reactants and Products in Portland Cement Hydration [Tennis and Jennings (2000); Mindess et al. (2002)]

Compound	Gram Molecular Weight (*GMW*) (g/mol)	Density (r) (g/cm^3)
Water	18.02	0.998
C_3S	228.32	3.15
C_2S	172.24	3.28
C_3A	270.20	3.03
C_4AF	485.97	3.73
$C\bar{S}H_2$	172.18	2.32
C–S–H	454.99 [a]	~2.0 [b]
CH	74.09	2.24
$C_6A\bar{S}_3H_{32}$	1255.26	1.75
$C_4A\bar{S}H_{12}$	622.58	1.99
C_3AH_6	378.32	2.52

[a]: Value given for $C_{3.4}S_2H_8$.

[b]: Value depends on the water content of *C–S–H*, which is related to how much "gel porosity" is included in the structure.

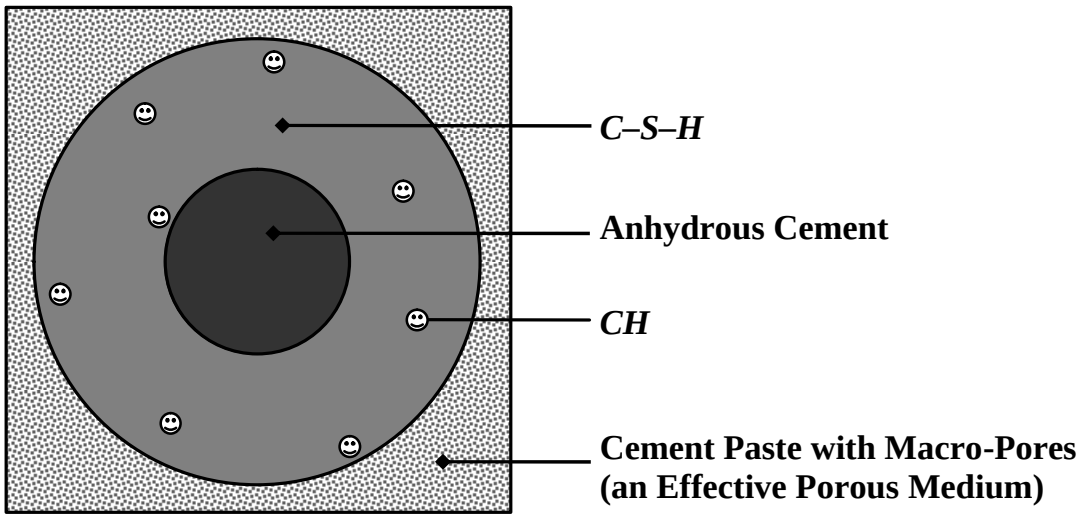

Fig. 5-1 Micromechanical Model for Hardened Cement Paste

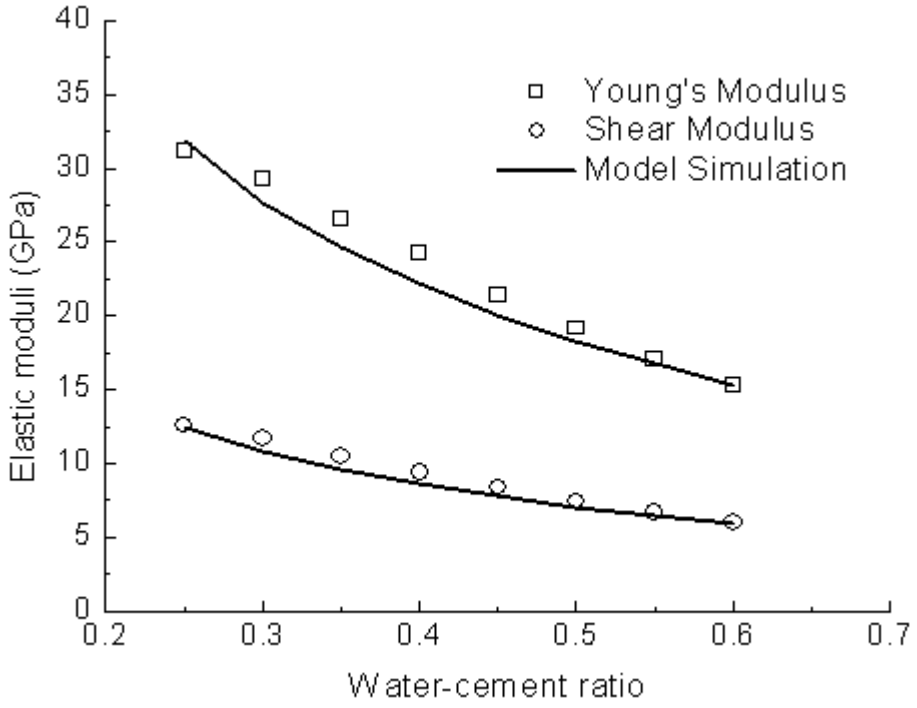

Fig. 5-2 Simulated and Measured Elastic Moduli as a Function of Water-Cement Ratio of Cement Pastes at an Age of 28 Days (Experimental Data from [Haecker et al. (2005)])

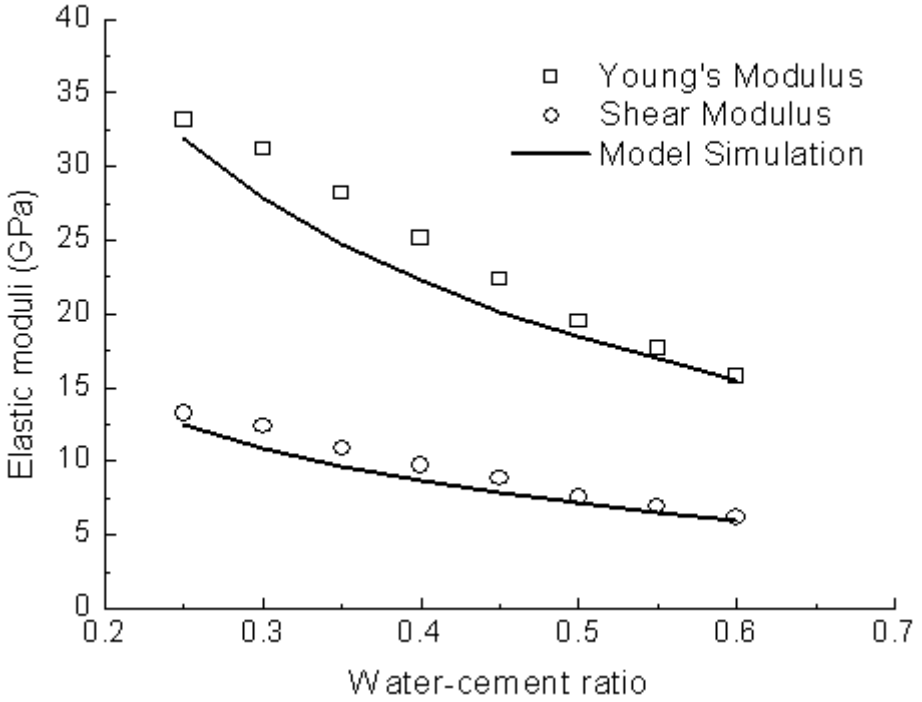

Fig. 5-3 Simulated and Measured Elastic Moduli as a Function of Water-Cement Ratio of Cement Pastes at an Age of 56 Days (Experimental Data from [Haecker et al. (2005)])

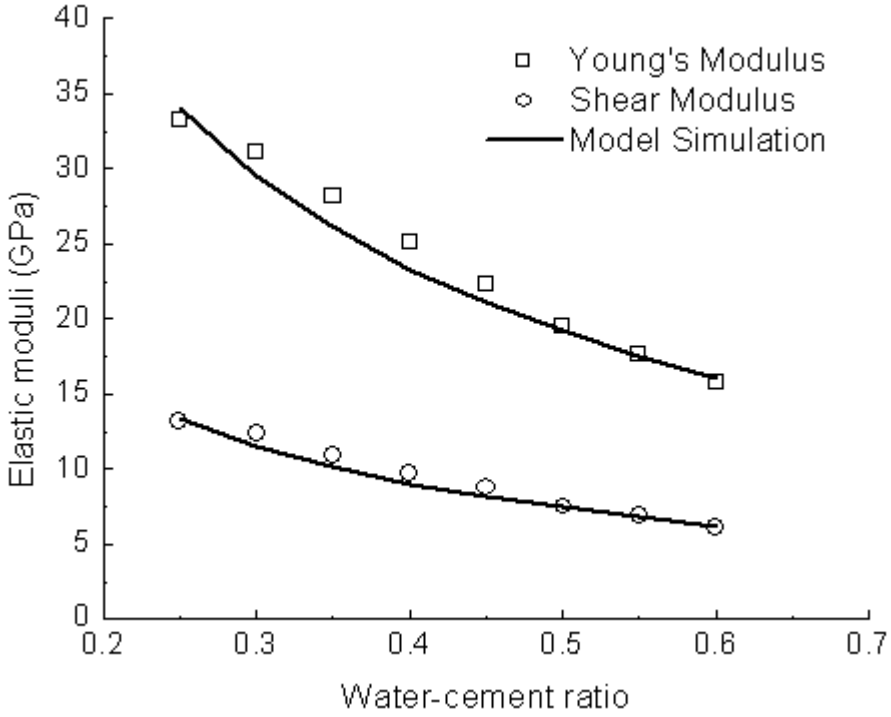

Fig. 5-4 Simulated (Using the Capillary Porosity Predicted by CEMHYD3D) and Measured Elastic Moduli as a Function of Water-Cement Ratio of Cement Pastes at an Age of 56 Days (Experimental Data from [Haecker et al. (2005)])

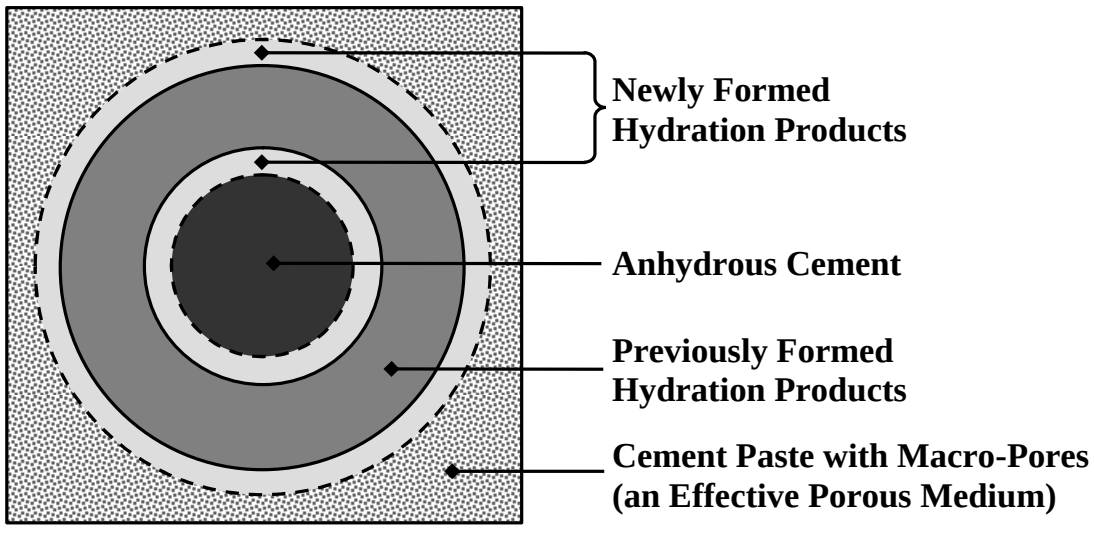

Fig. 5-5 Micromechanical Model for Hardening Cement Paste

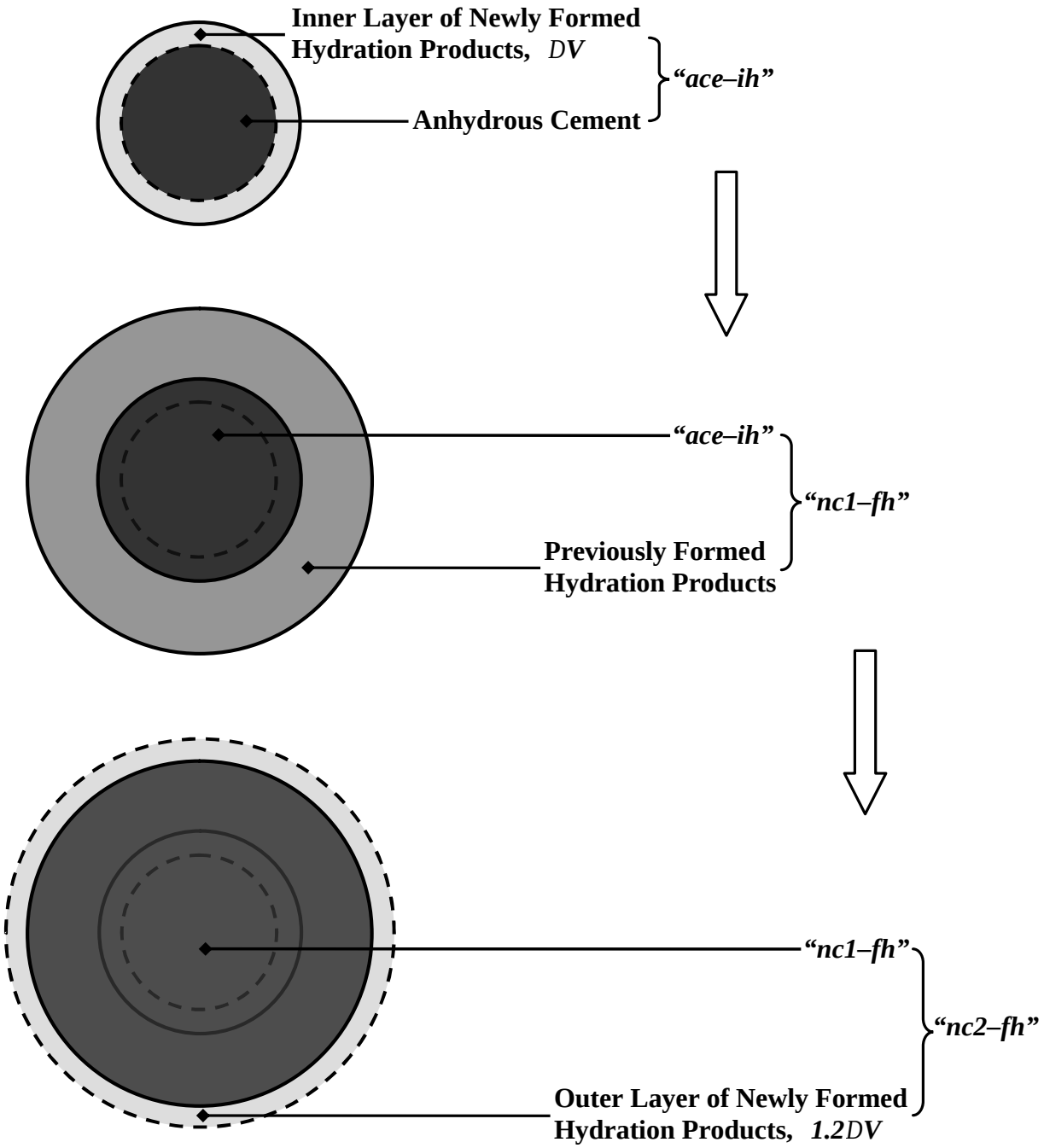

Fig. 5-6 Illustrated Procedure of Simulating the Effective Mechanical Properties of the Solid Phase of Hardening Cement Paste at Time $t + Dt$

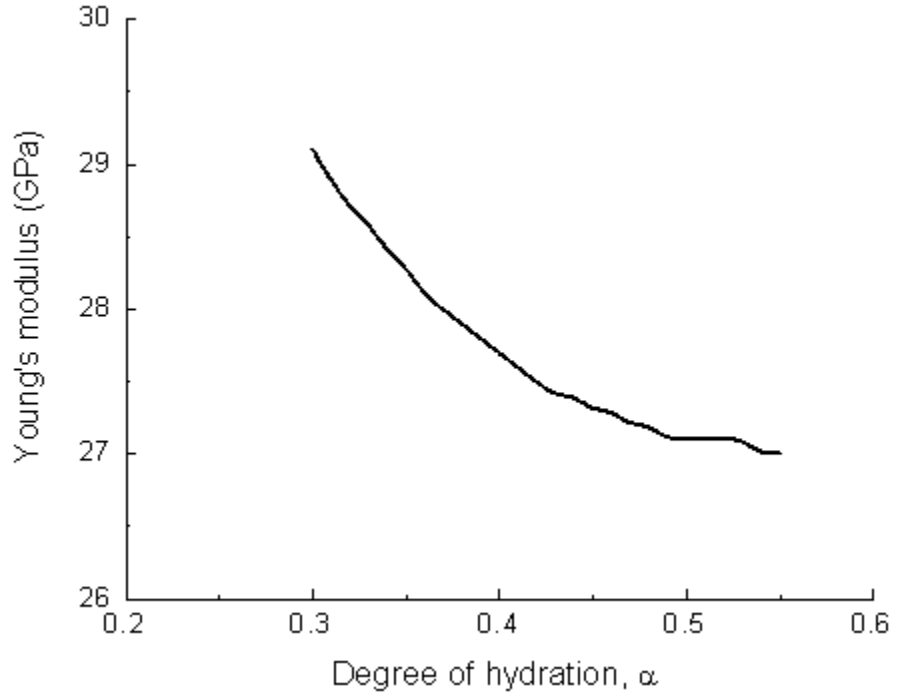

Fig. 5-7 Simulation of the Young's Modulous of Cement Paste Using the Mori-Tanaka Scheme on Level III

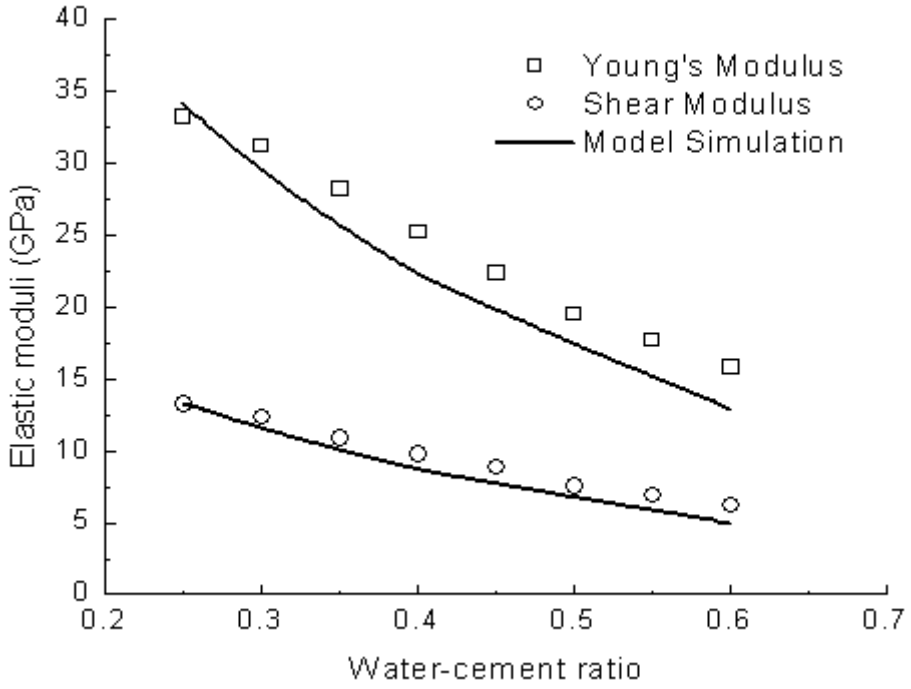

Fig. 5-8 Simulated (Using the Capillary Porosity Predicted by CEMHYD3D and the Self-Consistent Scheme at Level III) and Measured Elastic Moduli as a Function of Water-Cement Ratio of Portland Cement Pastes at an Age of 56 Days (Experimental Data from [Haecker et al. (2005)])

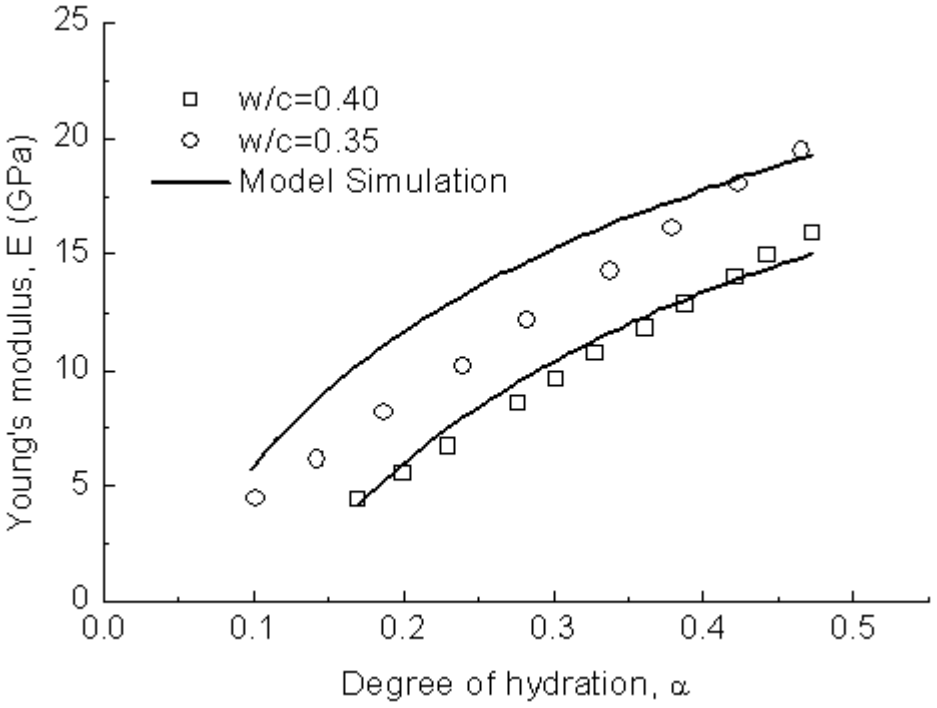

(a)

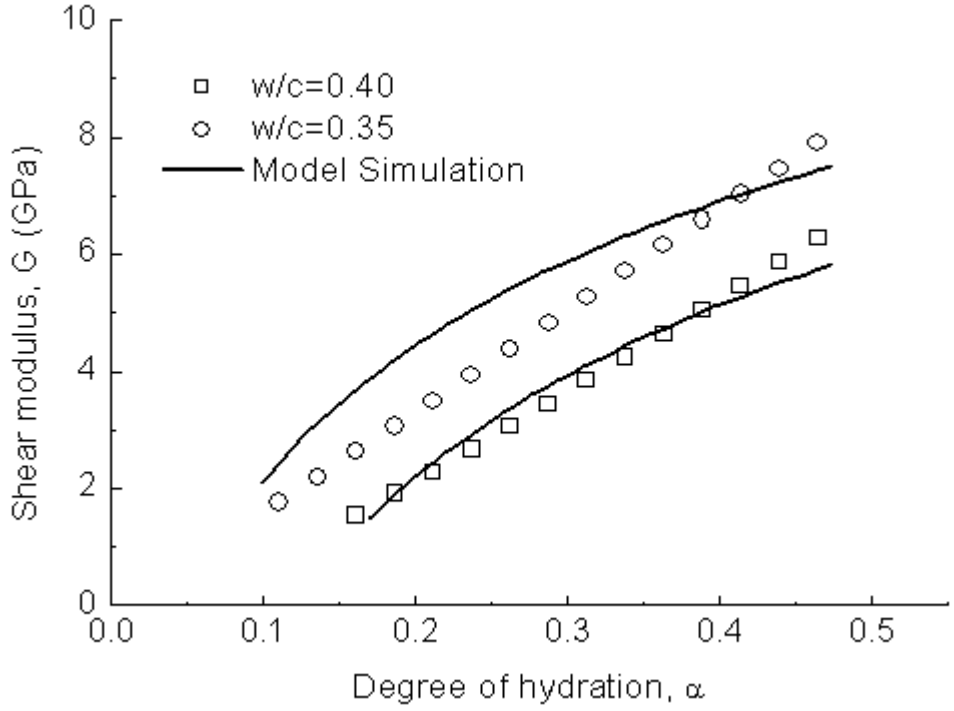

(b)

Fig. 5-9 Simulated and Measured Elastic Moduli as a Function of the Degree of Hydration of Cement Pastes (Experimental Data from [Boumiz et al. (1997)]) (a)–Young's Modulus; (b)–Shear Modulus

CHAPTER 6

MODELING SHRINKAGE OF HARDENING CEMENT PASTE

6.1 Introduction

In this chapter, a constitutive model that simulates the shrinkage of hardening cement paste is developed based on the theories of mechanics of composites and poromechanics. Since the main concern of the present study is the shrinkage of cement paste at high relative humidity, capillary stress is considered the driving force of autogenous shrinkage. The applied pressure can be another driving force of shrinkage for some applications. The model is formulated based on the previously validated multi-scale and micromechanical model for the elastic properties of hardening cement paste. The time-dependent properties of *C–S–H*, which are of great importance for the shrinkage of cement paste, are considered in the model. The material constants of the model are calibrated against the experimental results for autogenous shrinkage of cement paste. To finally testify the validity of the shrinkage model, it is used to predict the autogenous shrinkage of different cement pastes. Except for the calibrated material constants, the degree of hydration and the capillary stress required in the shrinkage model are simulated using the hydration kinetics model of Chapter 2 and Chapter 3, and the equation for the diameter of the largest water-filled capillary pore of Chapter 4, respectively. The model predictions are compared with the experimental results. The possible extension of the proposed model to simulate shrinkage of cement paste under

downhole conditions of oil wells is also discussed.

6.2 Assumptions

In addition to the assumptions made in Chapter 5 for modeling the elastic properties of cement paste, it is further assumed that:

1) Of the three solid constituents of cement paste, only *C–S–H* is considered to have time-dependent properties. While the properties of anhydrous cement and *CH* may be assumed to be time-independent, *C–S–H* must be time-dependent, since the water in its gel pores and micro pores may transport and diffuse under sustained loading [Bažant and Prasannan (1989); Hua et al. (1997); Mabrouk et al. (2004)]. Another source of time-dependent behavior may arise from the migration of pore water or moisture in the capillary pores [Bažant and Prasannan (1989)]. However, the quantification of such time-dependent behavior depends on the size of the test specimen. If the specimen is adequately small, the creep strain due to the migration of pore water or moisture is minimal and can be neglected. For a large volume of cement paste, that mechanism should be included when calculating the volume changes using numerical schemes, such as the finite element method.

2) *C–S–H* is assumed to be time-dependent, but its constitutive behavior can be described using its tangent bulk modulus and tangent shear modulus, the ratio between which is assumed to remain constant throughout the deformation of *C–S–H*, indicating a constant Poisson's ratio. This assumption is justified since the main concern of the present study is the shrinkage of cement paste. For the simple stress path of *C–S–H* associated with the deformation of cement paste, the complicated viscoelastic and

viscoplastic properties of *C–S–H* could be described using its tangent bulk and shear moduli, both of which are assumed to be time-dependent.

3) The multi-scale and micromechanical framework used to simulate the effective elastic properties of cement paste is still valid when nonlinearity and creep are taken into account. The elastic moduli of *C–S–H* are replaced with the tangent ones, but the equations for the elastic properties of Chapter 5 still apply. Eq. (4-49), the equation for the differential volumetric strain of nonlinear elastic porous media, can be used to calculate the volume change of cement paste.

4) The effects of curing temperature and applied pressure on the time-dependent properties of *C–S–H* are not considered at this step because of the lack of relevant experimental data. Since the creep deformation of *C–S–H* arises mainly from transport and diffusion of the water in gel pores and micro pores of *C–S–H* under sustained loading, curing temperature and applied pressure may both influence the time-dependent properties of *C–S–H*. Such dependency can be considered when calibrating the model parameters, provided relevant experimental data are available. According to this assumption, the volumetric deformation of cement paste in an isothermal test can be obtained via:

$$de_v = \frac{ds_b + bS_w dp_c}{K_d} \tag{6-1}$$

The meaning of symbols in which is referred to as in Section 4.4.

The above assumptions indicate that the multi-scale and micromechanical framework can be kept when determining shrinkage of cement paste. The remaining tasks are the identification of the tangent bulk modulus of *C–S–H*, and more importantly,

the consideration of stress redistribution in the different constituent components of cement paste during cement hardening and creep deformation.

6.3 Model Formulation

The rate-dependent behavior of hydrating cement paste is very complex, considering the complicated states and variations of stresses of its constituent components. First of all, different layers of the constituent components experience stress redistribution at different ages of the hydrating cement paste, with an increase in the volume of hydration products and a decrease in the corresponding volume of anhydrous cement. The variation in the applied loads, including the variation in the capillary stress, then leads to further changes in stress states of the constituent components. Even under constant external loads, such as the applied pressure in the downhole conditions, the stress state of a specific layer of hydration products of the same age thereby changes continuously. Considering these facts, a constitutive model describing the behavior of hydrating cement paste must be formulated in a differential form, so that the strain increment de during time interval dt can be obtained provided the applied stress increment ds is known, or vice versa. The variation in the capillary stress dp_c during dt should also be included.

6.3.1 Consideration of nonlinearity and stress redistribution in the micromechanical model

The micromechanical model developed in the previous chapter can be readily extended to describe the nonlinear behavior of cement paste. Herve and Zaoui (1990)

used the three-phase model to describe the nonlinearity of matrix-inclusion composites by replacing the constant elastic moduli of the constituent components with the tangent moduli. In the present study, this approach is applied to other modeling schemes of composite materials, i.e. the Mori-Tanaka and the self-consistent schemes, by replacing the constant moduli in Eqs. (5-1), (5-2) and (5-20) – (5-24) with the corresponding tangent moduli. Here, only the *C–S–H* matrix is considered to be nonlinear, while the anhydrous cement and *CH* are still assumed to behave linear elastically, which means that their tangent moduli are constant. The tangent moduli of the *C–S–H* matrix depend on the stress level, deformation history and loading rate, which will be discussed subsequently.

The difficulty lies in simulating the stress redistribution in the solid phase of hardening cement paste. Since the stress level of the *C–S–H* matrix at different ages certainly influences its nonlinear and creep behavior, the stress redistribution during cement hydration must be determined. Even if the externally applied loads on the solid phase are constant during time step Dt, the stresses in different layers of hydration products (and hence in different layers of the *C–S–H* matrices) and the anhydrous cement core do vary during this time period due to cement hydration.

This stress redistribution can be determined by considering both stress equilibrium and deformation compatibility for the composite material. According to the model of Fig. 5-5, two layers of the newly formed hydration products are formed during Dt, i.e. an inner and an outer layer. Due to cement hydration, the applied stress on the original volume of the anhydrous cement core, which is now the effective stress of the inner layer of the newly formed hydration products and the reduced anhydrous cement

core will change. This variation induces a change in stress and hence a change in strain of the previously formed hydration products. The change in the total effective volume of the previously formed hydration products, the inner layer of the newly formed hydration products and the reduced anhydrous cement core must remain compatible with the deformation of the outer layer of the newly formed hydration products. The stress redistribution in different layers of hydration products can then be calculated.

Since we are mainly concerned with the shrinkage of cement paste, only the bulk deformation is considered herein. Considering the solid phase of cement paste in Fig. 5-5, at time *t*, the effective bulk stresses of the solid phase and the anhydrous cement core are denoted as s_{out} and s_{in}, respectively. As shown in Fig. 6-1, at time $t + Dt$, the applied stress on the solid phase is assumed to be the same as that at time *t*, and the effective stress of the original volume of the solid phase becomes $s_{out} + Ds_{out}$ due to stress redistribution. The effective stress of the inner layer of the newly formed hydration products and the reduced anhydrous cement core (compared with the original anhydrous cement core) becomes $s_{in} + Ds_{in}$. The change in the effective bulk strain of the inner layer of the newly formed hydration products and the reduced anhydrous cement core, De_{in}, causes the variation in strain of the solid phase, which can be calculated using the three-phase model [Aboudi (1991)]:

$$De_{out} = \frac{De_{in}\left[f_{in}(g-1)+1\right]}{g} \tag{6-2}$$

$$g = \frac{3K_{hp}^{t} + 4G_{hp}^{t}}{3K_{in}^{t} + 4G_{hp}^{t}} \tag{6-3}$$

in which K_{hp}^{t} and G_{hp}^{t} are the tangent bulk and shear moduli of the previously

formed hydration products, respectively. K_{in}^{t}, the tangent bulk modulus of the composite volume that was originally the anhydrous cement, can be obtained as:

$$K_{in}^{t} = \frac{\Delta s_{in}}{\Delta e_{in}} \tag{6-4}$$

and

$$f_{in} = \frac{V_{ac}}{V_{ac} + V_{hp}} \tag{6-5}$$

where V_{ac} is the volume of the original anhydrous cement core, and V_{hp} is the volume of the previously formed hydration products. The change in strain, De_{in}, can be obtained using the stress $s_{in} + Ds_{in}$ and the effective bulk modulus of the composite shown in Fig. 6-1(c) as well as the original stress s_{in} and the bulk modulus of the anhydrous cement. With De_{in} and Ds_{in} known, K_{in}^{t} is readily obtained from Eq. (6-4). Since the previously formed hydration products contain layers of different ages, the above procedure usually has to be completed using iteration, which is easy to accomplish with computer.

At the same time, the effective volume change should be compatible with the deformation of the outer layer of the newly formed hydration products, which can be assumed as a spherical shell subject to both an inner pressure $s_{out} + Ds_{out}$ and an outer pressure s_{out}. The volume change of such a spherical shell, according to solid mechanics, can be calculated via:

$$De'_{out} = 1.0 - \left[1.0 - \frac{(b_3 + b_4)}{f_{in} - 1.0}\right]^3 \tag{6-6}$$

with

$$b_3 = \frac{\left(s_{out} + Ds_{out}\right) f_{in} - s_{out}}{3K_{oh}^t} \tag{6-7}$$

$$b_4 = \frac{Ds_{out}}{4G_{oh}^t} \tag{6-8}$$

where K_{oh}^t and G_{oh}^t are the tangent bulk and shear moduli of the outer layer of the newly formed hydration products.

Since Ds_{in} is unknown in advance, the above calculation procedure should be accomplished iteratively, with the convergence criterion being:

$$\left| \frac{De'_{out} - De_{out}}{De_{out}} \right| \le Tol. \tag{6-9}$$

After the stress variations of different constituent components due to stress redistribution are obtained, they can be combined with the stress variation due to any change in the external loads during the time step Dt to calculate the corresponding effective strain variations of cement paste during Dt. It should be noted that the strain calculated using the above procedure must be the same as that calculated using the micromechanical model of the previous chapter if the mechanical properties of all the constituent components of cement paste are linear elastic. The procedure is verified against the experimental data used in Chapter 5 [Haecker et al. (2005)].

6.3.2 Time-dependent model for the *C–S–H* matrix

A constitutive model that describes the time-dependent behavior of *C–S–H* matrix will now be developed. It is assumed that the bulk strain rate of the *C–S–H* matrix can be expressed as:

$$\dot{e}_{CSH} = \dot{e}^{e}_{CSH} + \dot{e}^{cr}_{CSH} \tag{6-10}$$

where $\dot{e}^{cr}_{CSH}$ is the creep bulk strain rate, and $\dot{e}^{e}_{CSH}$ is the instant elastic bulk strain rate that can be calculated by:

$$\dot{e}^{e}_{CSH} = \frac{ds_{CSH}}{K^{u}_{CSH} dt} \tag{6-11}$$

in which ds_{CSH} is the bulk stress increment in the *C–S–H* matrix during time interval dt, which may result from stress redistribution as well as any change in the external loads, and can be calculated via the previously discussed procedure. The undrained bulk modulus of *C–S–H* matrix, K^{u}_{CSH}, should be used to calculate the instant strain increment since the corresponding response of the saturated porous *C–S–H* matrix is conceptually undrained.

As mentioned above, the time-dependent properties of the *C–S–H* matrix depend on the stress level, the deformation history and the loading rate. Since the stress of a certain layer of the *C–S–H* matrix varies continuously throughout the entire service life of cement paste, the frequently used empirical creep equations are not suitable here because they usually require storing the whole stress history. In this model, the over-stress visco-plasticity theory proposed by Perzyna (1966) is applied. It has the advantage that only the present stress and strain levels are required, which considerably simplifies the model formulation.

Using the over-stress theory, the creep strain rate can be defined as:

$$\dot{e}^{cr}_{CSH} = \frac{1}{h}\left(s_{CSH} - s_{st}\right)^{n_1} \tag{6-12}$$

in which h and n_1 are the viscous model parameters, and s_{st} denotes a threshold

stress level for the viscous behavior of *C–S–H* matrix to occur. As can be seen in Eq. (6-12), when the stress s_{CSH} approaches s_{st}, the creep strain rate $\dot{e}_{CSH}^{cr}$ tends to vanish; and for $s_{CSH} < s_{st}$, $\dot{e}_{CSH}^{cr} = 0$. s_{st} is assumed to be a function of strain, which is expressed as:

$$s_{st} = \begin{cases} \dfrac{K_{st}}{b_1}\exp(b_1 e_{CSH}) - \dfrac{K_{st}}{b_1}, & b_1 \neq 0 \\ K_{st} e_{CSH}, & b_1 = 0 \end{cases} \tag{6-13}$$

where K_{st} and b_1 are both model parameters. The slope of the curve relating s_{st} and e_{CSH} defined by Eq. (6-13) increases or decreases, depending on the sign of parameter b_1, as shown in Fig. 6-2.

For time step *dt*, the strain increment in the *C–S–H* matrix can be expressed as:

$$de_{CSH} = \left(\dot{e}_{CSH}^{e} + \dot{e}_{CSH}^{cr}\right)dt \tag{6-14}$$

and the tangent bulk modulus of *C–S–H* at time *t* as:

$$K_{CSH}^{t} = \frac{K_{CSH}^{u} K_{CSH}^{cr}}{K_{CSH}^{u} + K_{CSH}^{cr}} \tag{6-15}$$

in which K_{CSH}^{cr} is the tangent creep bulk modulus of *C–S–H* at time *t* that reads:

$$K_{CSH}^{cr} = \frac{ds_{CSH}}{\dot{e}_{CSH}^{cr} dt} \tag{6-16}$$

The tangent shear modulus can be obtained by assuming constant Poisson's ratio for the *C–S–H* matrix, which means that:

$$G_{CSH}^{t} = \frac{G_{CSH}}{K_{CSH}^{u}} K_{CSH}^{t} \tag{6-17}$$

Conceptually, the four parameters, i.e. h, n_1, K_{st} and b_1, should be intrinsic

properties of the *C–S–H* matrix that do not vary for different cements. Since it is difficult to determine these properties experimentally, they are back-calibrated in the present study using the creep behavior of cement paste.

6.4 Model Calibration

Besides the elastic material constants of the various constituent components of cement paste of Table 5-1 and the volume fraction of *CH* in the hydration products discussed in Chapter 5, the four time-dependent parameters (h, n_1, K_{st} and b_1) of *C–S–H* are required for the proposed model. Since only the time-dependent properties of *C–S–H* are considered, the creep deformation of cement paste is assumed to arise from the time-dependent deformation of *C–S–H* only, which makes it possible to calibrate the time-dependent parameters of *C–S–H* against the experimental data on the volume change of cement paste.

However, there exist very limited experimental results that can be used for such a calibration purpose. Simulation of the shrinkage of cement paste using the proposed model requires not only the mechanical parameters of the constituent components, but also the developments of hydration kinetics and capillary stress. To make the obtained material parameters represent the intrinsic properties of *C–S–H* as well as possible, details of the hydration kinetics and capillary stress developments must also be provided for a specific cement paste tested. Very few available experimental data provide such comprehensive information.

Three useful sets of experimental data are identified and used to calibrate the parameters [Hua et al. (1997); Horita and Nawa (2003); Lura et al. (2003)]. In Hua et al.

(1997), the autogenous shrinkage of a Portland cement paste, the hydration kinetics and the capillary stress were provided; in Horita and Nawa (2003), the autogenous shrinkage of Portland cement pastes with different water-cement ratios, the development of relative humidity and the ratios of combined water were reported; and in the tests by Lura et al. (2003), the autogenous shrinkage of a Portland cement paste, the corresponding changes in the hydration kinetics and relative humidity were measured. All the cement pastes were cured at room temperature and under atmospheric pressure. The changes in relative humidity reported in Horita and Nawa (2003) and Lura et al. (2003) can be converted to capillary stresses via the Kelvin Equation [Eq. (4-2)]. However, due to salt solution in the pore liquid, the measured humidity is lower than that representing the meniscus radius in cement paste, as explained by Lura et al. (2003). Therefore, the reported changes in relative humidity are corrected using the method proposed by Lura et al. (2003). The drop of *RH* is corrected to start at an *RH* of 100%. The difference between the measured *RH* at the moment of *RH* dropping and 100% is assumed to result from salt solution and to be constant throughout the *RH* development. The hydration kinetics of the experiments of Horita and Nawa (2003) is obtained in the light of the reported ratios of combined water and Powers' theory [Powers and Brownyard (1947)].

At the beginning of hydration, cement paste may exhibit expansion due to the formation of ettringite and other mechanisms [Baroghel-Bouny et al. (2004)]. Such expansion is not considered in the present study. The volume change before the setting time is not taken into account either, since such behavior cannot be described within the framework of solid mechanics. As a matter of fact, any chemical shrinkage or expansion

during that period would appear as external volume change and require no constitutive model for quantification. Therefore, any measured autogenous shrinkage is set to zero at the time of volume shrinkage, or the setting time, or the time of *RH* dropping, any of which is the latest. The comparisons between the simulated and the measured shrinkage also start from that moment. The prediction of shrinkage in the next section follow this principle as well. It is noted that several other investigations followed a similar procedure [e.g. Koenders and van Breugel (1997); Hua et al. (1997); Lura et al. (2003)].

Comparisons of the simulated autogenous shrinkage with the experimental data are shown in Fig. 6-3 – Fig. 6-5 for the three sets of tests. The single set of time-dependent material constants of *C–S–H* given in Table 6-1 is used for all these cement pastes. The volume ratios of *CH* in the hydration products obtained by referring to Eq. (5-19) and the provided chemical composition of cements, are all about 0.2 for the three cements. It should be noted that the shrinkage presented here refers to the volumetric shrinkage instead of the linear shrinkage reported in some references. They are related by a factor of 3. Also, for autogenous shrinkage, capillary stress is the only driving force according to Eq. (6-1), with the applied stress s_b being 0.

Fig. 6-3 – Fig. 6-5 show that calibration of the time-dependent model parameters for *C–S–H* leads to satisfactory agreements between the simulated and measured autogenous shrinkage of cement pastes. The time-dependent parameters given in Table 6-1 can be considered to represent the intrinsic properties of *C–S–H* that can serve for the prediction of shrinkage of cement paste at ambient conditions. However, it should be pointed out that these parameters are obtained from rather limited experimental data and need to be further verified against more test results.

6.5 Model Verification

The experimental results for autogenous shrinkage of cement pastes reported by Koenders (1997) are used to validate the prediction capacity of the proposed model. The degrees of hydration of the three cement pastes are simulated using the hydration kinetics model proposed in Chapter 2 and Chapter 3, the parameters of which are obtained using the chemical composition of cements as well as Eqs. (3-1) – (3-4). The capillary stresses are calculated using the equation for the largest water-filled capillary pore [Eqs. (4-8) – (4-10)] and the Young-Laplace equation [Eq. (4-1)] of Chapter 4. The parameter c_{10} in Eq. (4-8) is taken to be around 0.5 for the three cement pastes. The obtained degrees of hydration and capillary stresses are then used to calculate the autogenous shrinkage of the three cement pastes. The results are compared with the experimental data, as shown in Fig. 6-6. It can be seen that the proposed shrinkage model, together with the hydration kinetics model and the equation for the largest water-filled capillary pore, can successfully predict the autogenous shrinkage of Portland cement paste under ambient conditions.

6.6 Consideration Influences of High Temperature and High Pressure

A multi-scale and micromechanical constitutive model for the prediction of autogenous shrinkage of cement paste has been formulated. The influences of curing temperature and applied pressure are not taken into account explicitly at present due to the lack of experimental data, but can readily be incorporated in the framework of the proposed model.

To begin with, the consideration of the applied pressure alone is straightforward,

if such a pressure is not large enough to influence the mechanical properties of the constituent components, especially those of *C–S–H*. Eq. (6-1) can be directly used to calculate the volume change of cement paste, with the material parameters provided in Table 5-1 and Table 6-1. In this case, the applied pressure appears in Eq. (6-1) as s_b.

For the downhole conditions of oil wells, in which the curing temperatures and applied pressures can be very high but the pressure variations are comparably small, the proposed framework can also be used to predict volume changes, provided that the driving forces are quantified and sufficient experimental data are available to calibrate the model parameters. Under downhole conditions with very high temperatures, pore fluid in the macro-pores of cement paste may evaporate, hence capillary stress may no more act as a major driving force of the autogenous shrinkage. If this is so, the other two driving forces, viz. disjoining pressure and surface tension, will take over, but the quantification for them is difficult and requires extensive experimental work. Another driving force, the applied pressure, on the other hand, is easy to identify, and even if its variation is small, the induced creep deformation is likely to be significant.

The material parameters of the constituent components may also be different at high temperatures and high pressures, compared to those under ambient conditions. If the anhydrous cement and *CH* are regarded as purely elastic solids, even at high temperatures and high pressures, their mechanical parameters provided in Table 5-1 can still be used. However, the mechanical properties of *C–S–H* including the instant elastic moduli and the time-dependent parameters are known to be different at high temperatures and high pressures. The time-dependent properties of *C–S–H* arise mainly from the transport and diffusion of the fluid phase in its gel pores, which would be

different at high temperature. High pressure could also influence the transport and diffusion of the gel pore fluid, which can be explained within the framework of poromechanics. Even the instant elastic moduli of *C–S–H* of Table 5-1 could be different at high pressures, since *C–S–H* is a porous medium, the instant elastic response of which would be affected by the applied pressure. Nevertheless, the model parameters can be calibrated for some specific high temperature and high pressure conditions, provided that sufficient relevant experimental data are available.

The thermal dilation and contraction due to temperature change is also an issue. Its consideration requires one more material constant, the thermal dilation coefficient a_{th} in Eq. (4-49), which needs to be determined experimentally as well.

In summary, the proposed framework for predicting volume changes of cement paste can be extended for cement pastes cured under downhole conditions. However, extensive experimental and analytical work is still needed before this can be accomplished.

6.7 Summary and Discussion

A multi-scale and micromechanical constitutive model for predicting the volume changes of hardening Portland cement paste has been formulated and validated in this chapter. The micromechanical framework based on the theories of poromechanics and mechanics of composites proposed in Chapter 5 to determine the elastic properties of hardening Portland cement paste was extended to take into account the effects of nonlinearity and creep. This was accomplished by considering both stress equilibrium and deformation compatibility at the scale of the solid phase of cement paste. A

time-dependent constitutive model for *C–S–H* that describes the volume changes of *C–S–H* based on the over-stress visco-plasticity theory [Perzyna (1966)] was proposed and incorporated in the micromechanical framework. The time-dependent model parameters were back-calibrated using three sets of experimental data on the autogenous shrinkage of Portland cement pastes. Finally, this shrinkage model and the calibrated model parameters, together with the hydration kinetics model proposed in Chapters 2 and Chapter 3, and the equation for the largest water-filled capillary pore of Chapter 4, were used to predict the autogenous shrinkage of three cement pastes, the results of which agree well with the experimental data. The possibility of extending the proposed model for cement pastes cured at high temperatures and high pressures was also discussed.

This constitutive model is formulated for a representative volume of cement paste, the exact size of which can be determined through experiments on the strain variation with size of a specimen. As the specimen gets sufficiently small, its strain ceases to depend on the change in size because the creep strain due to the migration of pore water or moisture approaches the minimum and can be neglected. The maximum volume of the specimen to meet such requirements can be regarded as the representative volume.

Table 6-1 Time-Dependent Material Constants of *C–S–H*

Material Constant	n_1	h [$(\text{GPa})^{n_1}$]	K_{st} [GPa]	b_1
Value	1.05	7×10^5	2800	1700

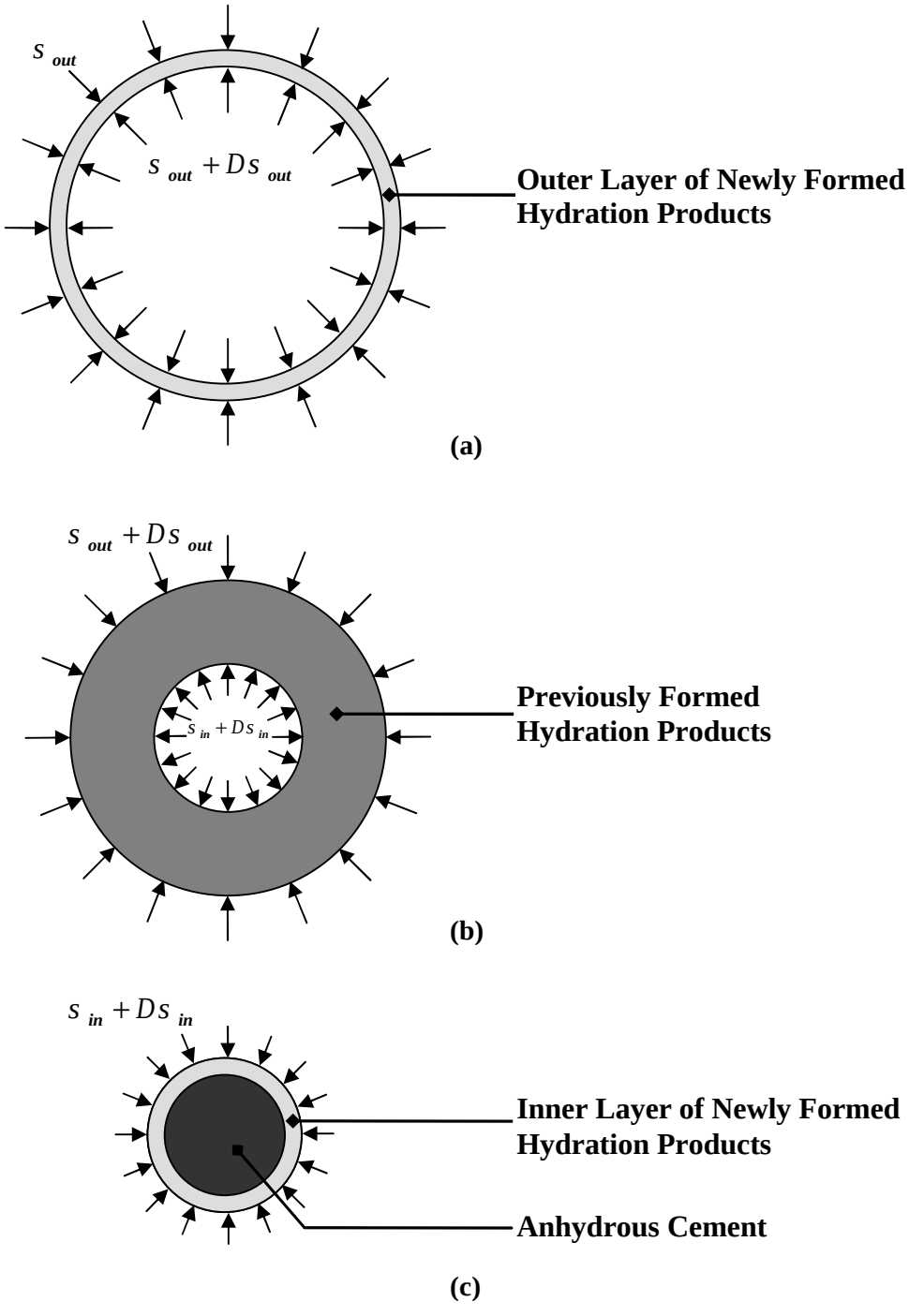

Fig. 6-1 Illustration of Stress Redistribution in the Solid Phase of Cement Paste

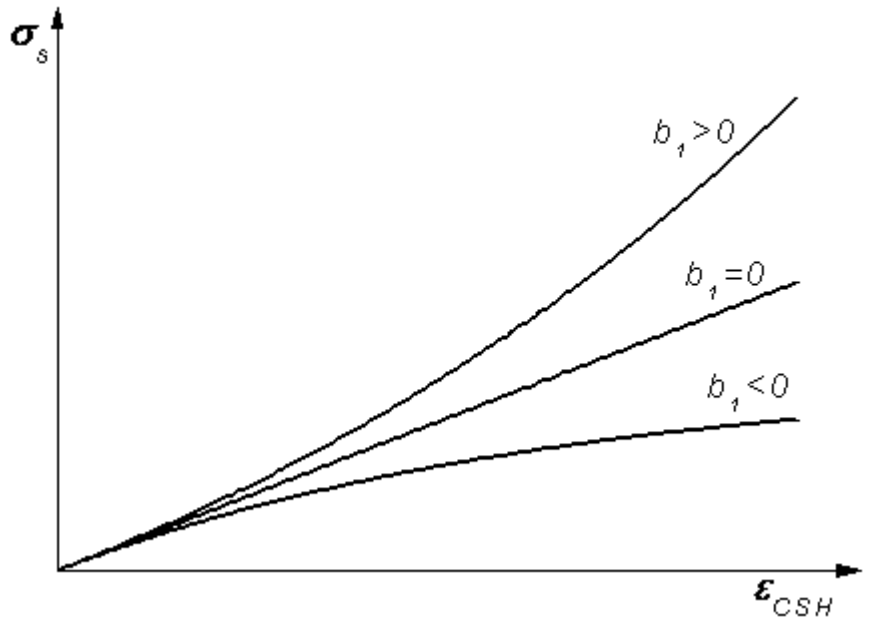

Fig. 6-2 Relationship Between the Threshold Stress Level for the Viscous Behavior of *C–S–H* to Occur and Its Total Bulk Strain with Different Signs of b_1

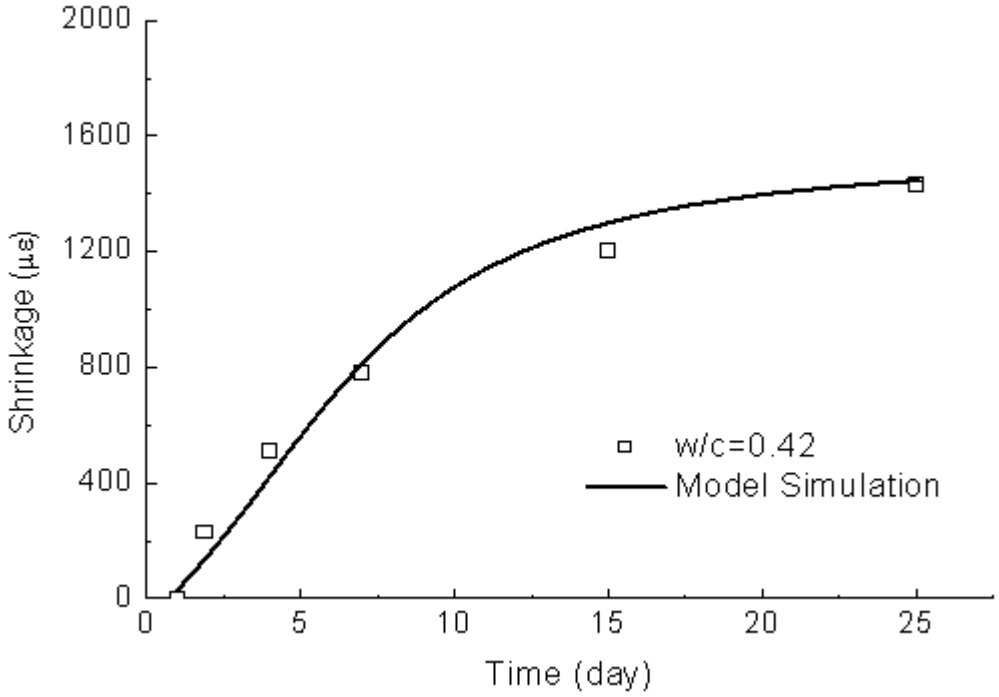

Fig. 6-3 Simulated and Measured Autogenous Shrinkage of Cement Paste (Experimental Data from [Hua et al. (1997)])

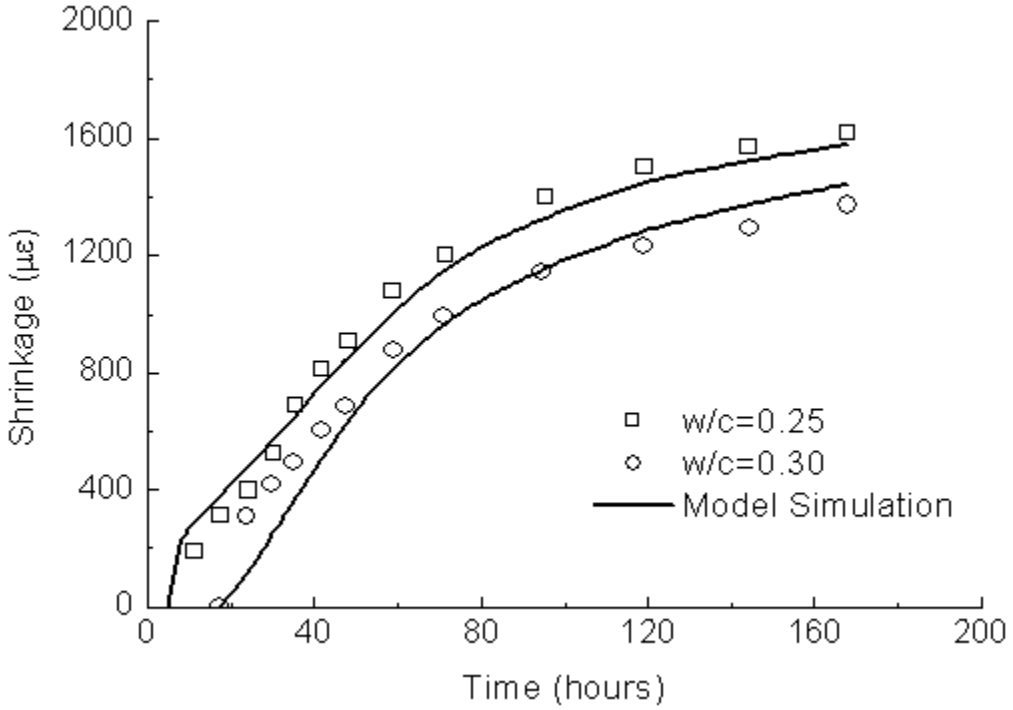

Fig. 6-4 Simulated and Measured Autogenous Shrinkage of Cement Pastes with Different Water-Cement Ratios (Experimental Data from [Horita and Nawa (2003)])

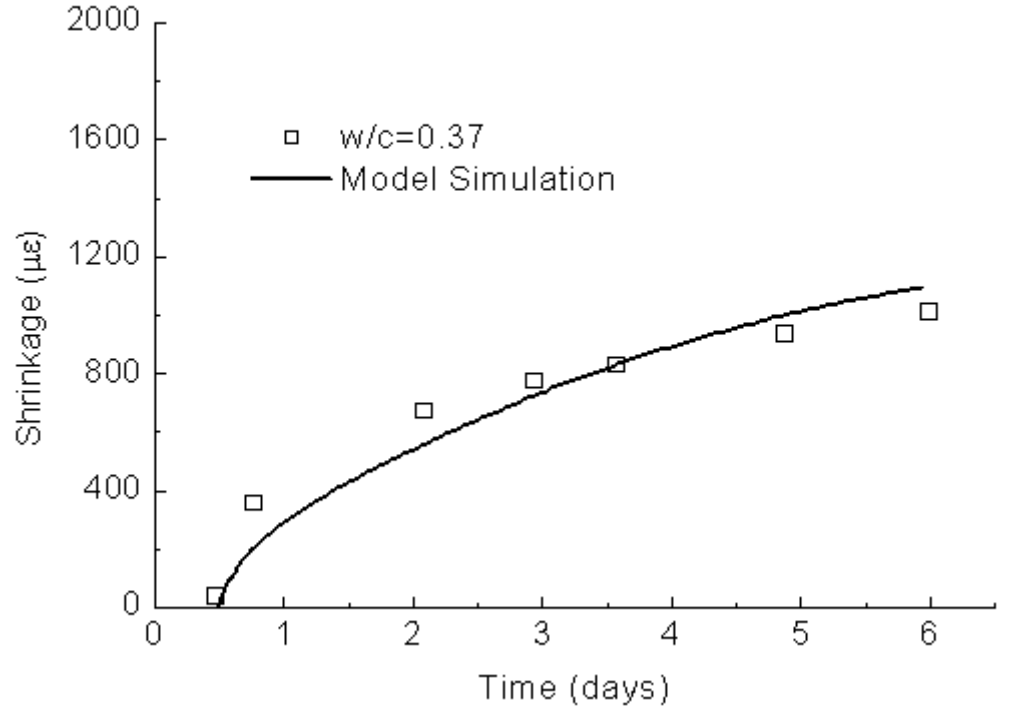

Fig. 6-5 Simulated and Measured Autogenous Shrinkage of Cement Paste (Experimental Data from [Lura et al. (2003)])

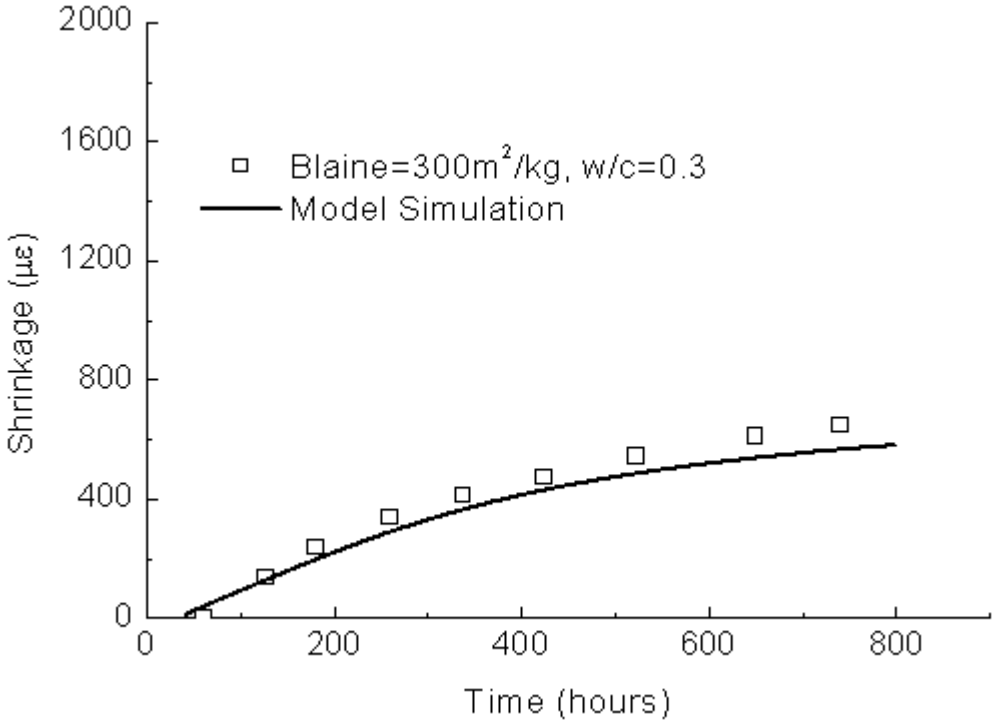
2000
1600
1200
800
400
0
Shrinkage (με)
0
200
400
600
800
Time (hours)
Blaine=300m²/kg, w/c=0.3
Model Simulation

(a)

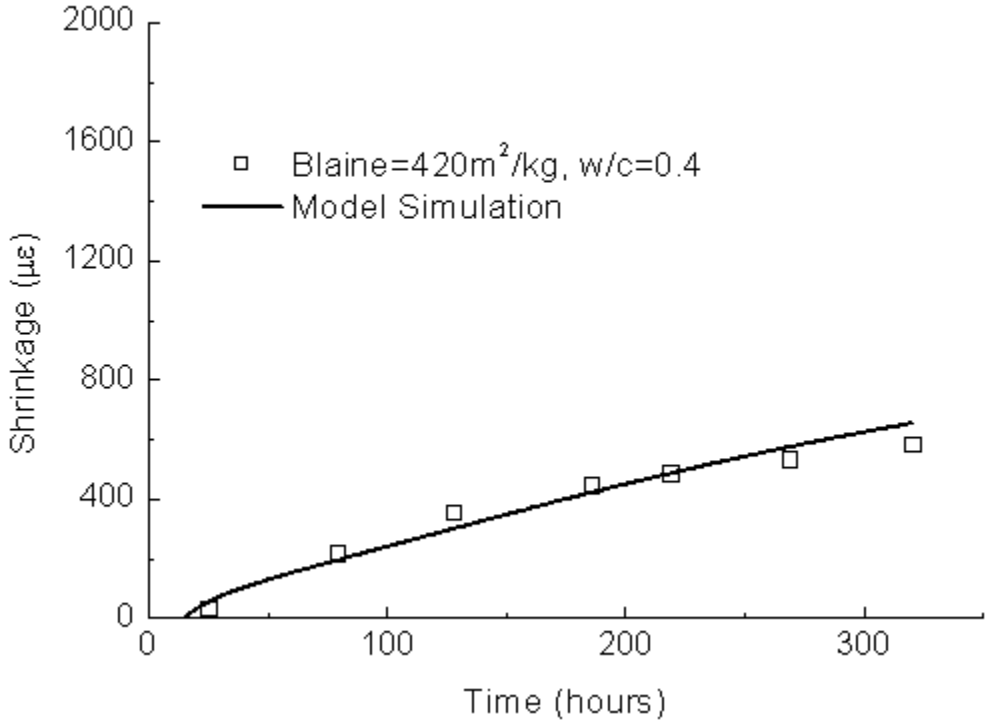
2000
1600
1200
800
400
0
Shrinkage (με)
0
100
200
300
Time (hours)
Blaine=420m²/kg, w/c=0.4
Model Simulation

(b)

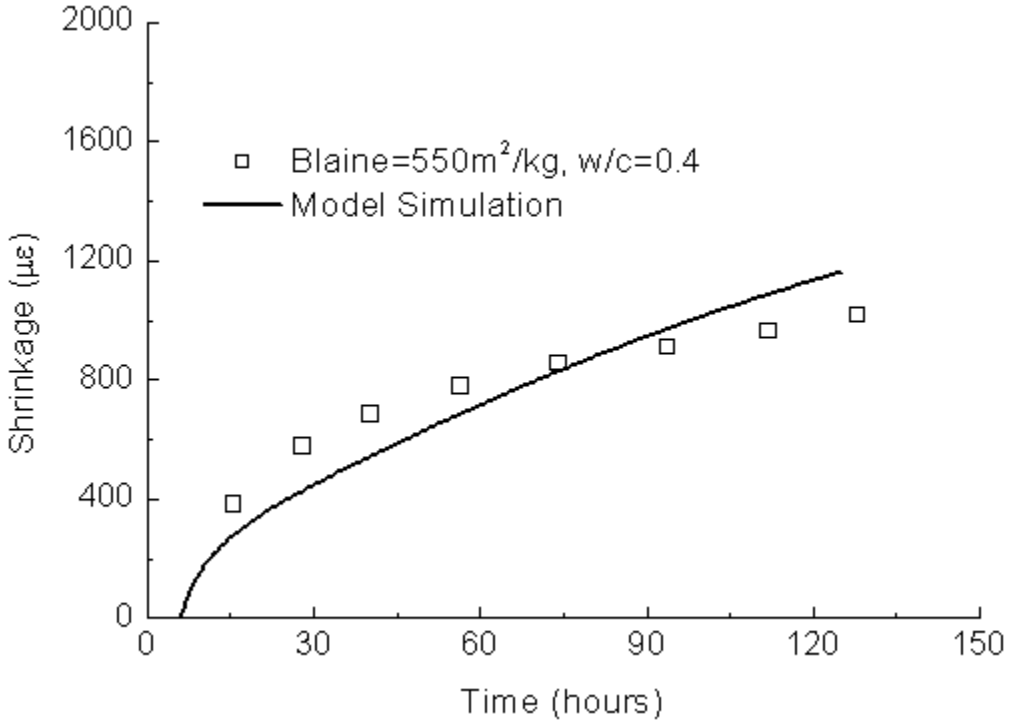

(c)

Fig. 6-6 Simulated and Measured Autogenous Shrinkage of Cement Pastes (Experimental Data from [Koenders (1997)])
(a)–CEM I 32.5R Paste; (b)–CEM I 42.5R Paste; (c)–CEM I 52.5R Paste

CHAPTER 7

SUMMARY AND SUGGESTIONS

7.1 Summary

The present study can be summarized as follows:

1) A mathematical hydration kinetics model has been developed based on the thermodynamics of cement hydration. The mechanism of cement hydration is assumed to be the diffusion of water through layers of hydration products. The proposed model was calibrated using the experimentally determined degree of hydration for a wide range of Portland cements.

2) The effects of chemical composition and fineness of cement as well as water-cement ratio were simulated using the proposed hydration kinetics model. Especially, the influences of elevated curing temperature and high applied pressure were taken into account. The hydration kinetics of different cements at elevated curing temperatures and/or high applied pressures was successfully predicted. The model can be used for a variety of applications, including the prediction of hydration kinetics, adiabatic temperature rise, chemical shrinkage and relative humidity of Portland cement-based materials in different curing environments.

3) A multi-scale and micromechanical constitutive model for the analysis of volume changes of hardening Portland cement paste has been formulated within the frameworks of mechanics of composites and poromechanics. The up-scale approach was used in the formulation considering four different length scales in cement paste,

which are *C–S–H*, hydration products, solid phase of cement paste, and cement paste.

4) The stress redistribution in the solid phase of hardening cement paste was simulated by considering both stress equilibrium and deformation compatibility of the composite materials.

5) The proposed multi-scale and micromechanical models can be used to predict the effective elastic properties of hardening and hardened cement paste with the intrinsic elastic properties of its constituent components.

6) The nonlinearity and creep of the *C–S–H* matrix were considered when simulating the volume changes of Portland cement paste, with the intrinsic time-dependent material properties of *C–S–H* calibrated against the available experimental data.

7) The proposed constitutive model together with the hydration kinetics model can be used to simulate the volume changes of hardening Portland cement paste, given the characteristics and mix proportions of its constituent components.

8) The proposed multi-scale and micromechanical framework that considers the nonlinearity and creep behavior of the constituent components can be used to develop a constitutive model for cement paste at high curing temperatures and high applied pressures provided that relevant experiments are conducted to clarify the mechanisms of volume changes in such curing environment. The proposed framework can also be used to formulate constitutive models for other cement-based materials.

7.2 Suggestions

The following suggestions are proposed for further study:

1) The effects of mineral and chemical admixtures as well as inert fillers can be incorporated in the proposed hydration kinetics model and constitutive model, if the relevant experimental data become available.

2) Once the proposed constitutive model for Portland cement paste has been extended to consider the effects of elevated curing temperature and high applied pressure, it can be applied to cement pastes used in oil wells.

3) The proposed multi-scale and micromechanical framework can be further extended to model the volume changes of mortar and concrete.

REFERENCES

Aboudi, J. (1991), Mechanics of Composite Materials – a Unified Micromechanical Approach, Elsevier Science Publishers B.V., Amsterdam, The Netherlands.

Acker, P. (2001), "Micromechanical Analysis of Creep and Shrinkage Mechanisms," Creep, Shrinkage and Durability Mechanics of Concrete and Other Quasi-Brittle Materials, Cambridge, MA, August 2001, Edited by F.-J. Ulm, Z.P. Bažant and F.H. Wittmann, Elsevier Science Publishers B.V., Amsterdam, The Netherlands, 15-25.

Bangham, D.H. and Fakhoury, N. (1930), "The Swelling of Charcoal. Part I – Preliminary Experiments with Water Vapour, Carbon Dioxide, Ammonia, and Sulphur Dioxide," Proceedings of the Royal Society of London, Series A, Containing Papers of a Mathematical and Physical Character, 130(812), 81-89.

Baroghel-Bouny, V., Mounanga, P., Loukili, A. and Khelidj, A. (2004), "From Chemical and Microstructural Evolution of Cement Pastes to the Development of Autogenous Deformations," Autogenous Deformation of Concrete, Edited by O.M. Jensen, D.P. Bentz and P. Lura, ACI SP-220, USA, 1-21.

Baroghel-Bouny, V., Mounanga, P., Khelidj, A., Loukili, A. and Rafai, N. (2006), "Autogenous Deformations of Cement Pastes Part II. w/c Effects, Micro-Macro Correlations, and Threshold Values," Cement and Concrete Research, 36(1), 123-136.

Basma, A.A., Barakat, S.A. and Al-Oraimi, S. (1999), "Prediction of Cement Degree of Hydration Using Artificial Neural Networks," ACI Materials Journal, 96(2), 167-172.

Bažant, Z.P. and Wittmann, F.H. (1982), Creep and Shrinkage in Concrete Structures, John Wiley & Sons Ltd.

Bažant, Z.P. and Prasannan, S. (1989), "Solidification Theory for Concrete Creep I: Formulation," Journal of Engineering Mechanics, 115(8), 1691-1703.

Beirute, R. and Tragesser, A. (1973), "Expansive and Shrinkage Characteristics of Cements under Actual Well Conditions," Journal of Petroleum Technology, 25, 905-909.

Beltzung, F., Wittmann, F.H. and Holzer, L. (2001), "Influence of Composition of Pore Solution on Drying Shrinkage," Creep, Shrinkage and Durability Mechanics of Concrete and Other Quasi-Brittle Materials, Cambridge, MA, August 2001, Edited by F.-J. Ulm, Z.P. Bažant and F.H. Wittmann, Elsevier Science Publishers B.V., Amsterdam, The Netherlands, 39-48.

Beltzung, F. and Wittmann, F.H. (2005), "Role of Disjoining Pressure in Cement Based Materials," Cement and Concrete Research, 35(12), 2364-2370.

Bentur, A., Berger, R.L., Kung, J.H., Milestone, N.B. and Young, J.F. (1979), "Structural Properties of Calcium Silicate Pastes: II, Effect of the Curing Temperature," Journal of the American Ceramic Society, 62(7-8), 362-366.

Bentz, D.P. and Garboczi, E.J. (1989), "A Digitized Simulation Model for Microstructural Development," Advances in Cementitious Materials, Edited by S. Mindess, American Ceramic Society, Westville, Ohio, USA, 211-226.

Bentz, D.P. and Garboczi, E.J. (1991), "Percolation of Phases in a Three-Dimensional Cement Paste Microstructural Model," Cement and Concrete Research, 21(2-3), 325-344.

Bentz, D.P. (1995), "A Three-Dimensional Cement Hydration and Microstructure Program. I. Hydration Rate, Heat of Hydration, and Chemical Shrinkage," NISTIR 5756, U.S. Department of Commerce, Washington DC.

Bentz, D.P., Garboczi, E.J., Jennings, H.M. and Quenard, D.A. (1995), "Multi-Scale Digital-Image-Based Modelling of Cement-Based Materials," Materials Research Society Symposium – Proceedings, Microstructure of Cement-Based Systems/Bonding and Interfaces in Cementitious Materials, Vol. 370, 33-41.

Bentz, D.P. (1997), "Three-Dimensional Computer Simulation of Portland Cement Hydration and Microstructure Development," Journal of American Ceramic Society, 80(1), 3-21.

Bentz, D.P., Snyder, K.A. and Stutzman, P.E. (1997), "Hydration of Portland Cement: the Effects of Curing Conditions," Proceedings of the 10th International Congress on the Chemistry of Cement, Volume 2, June 1997, Sweden.

Bentz, D.P., Waller, V. and de Larrard, F. (1998), "Prediction of Adiabatic Temperature Rise in Conventional and High-Performance Concretes Using a 3-D Microstructural Model," Cement and Concrete Research, 28(2), 285-297.

Bentz, D.P. and Haecker, C.J. (1999), "An Argument for Using Coarse Cements in High Performance Concretes," Cement and Concrete Research, 29(2), 615-618.

Bentz, D.P. (2006), "Influence of Water-to-Cement Ratio on Hydration Kinetics: Simple Models Based on Spatial Considerations," Cement and Concrete Research, 36(2), 238-244.

Berger, R.L., Bentur, A., Milestone, N.B. and Kung, J.H. (1979), "Structural Properties of Calcium Silicate Pastes: I, Effect of the Hydrating Compound," Journal of the American Ceramic Society, 62(7-8), 358-362.

Bernard, O., Ulm, F.-J. and Lemarchand, E. (2003), "A Multiscale Micromechanics-Hydration Model for the Early-Age Elastic Properties of Cement-Based Materials," Cement and Concrete Research, 33(9), 1293-1309.

Bezjak, A. (1986), “An Extension of the Dispersion Model for the Hydration of Portland Cement,” Cement and Concrete Research, 16(2), 260-264.

Bogue, R.H. (1947), The Chemistry of Portland Cement, Reinhold Publishing Corp., New York, USA.

Boumiz, A., Sorrentino, D., Vernet, C. and Tenoudji, F.C. (1997), “Modelling the Development of the Elastic Moduli as a Function of the Degree of Hydration of Cement Pastes and Mortars,” Proceedings 13 of the 2nd RILEM Workshop on Hydration and Setting: Why Does Cement Set? An Interdisciplinary Approach, Edited by A. Nonat, Dijon, France.

Bresson, B., Meducin, F. and Zanni, H. (2002), “Hydration of Tricalcium Silicates (C_3S) at High Temperature and High Pressure,” Journal of Materials Science, 37(24), 5355-5365.

Byfors, J. (1980), “Plain Concrete at Early Ages,” Report FO 3:80, The Swedish Cement and Concrete Research Institute, CBI: Stockholm, Sweden, 40-43.

Cervera, M., Oliver, J. and Prato, T. (1998), “Thermo-Chemo-Mechanical Model for Concrete. I: Hydration and Aging,” Journal of Engineering Mechanics, ASCE, 125(9), 1018-1027.

Cervera, M., Faria, R., Oliver, J. and Prato, T. (2002), “Numerical Modeling of Concrete Curing, Regarding Hydration and Temperature Phenomena,” Computers and Structures, 80(18-19), 1511-1521.

Chenevert, M.E. and Shrestha, B.K. (1987), “Shrinkage Properties of Cement,” Society of Petroleum Engineers of AIME, (Paper) SPE 16654, Delta, 49-57.

Chenevert, M.E. and Shrestha, B.K. (1991), “Chemical Shrinkage Properties of Oilfield Cements,” SPE Drilling Engineering 6(1), 37-43.

Christensen, R.M. (1979), Mechanics of Composite Materials, John Wiley & Sons, New York, USA.

Christensen, R.M. (1990), “A Critical Evaluation for a Class of Micro-Mechanics Models,” Journal of Mechanics and Physics of Solids, 38(3), 379-340.

Constantinides, G. and Ulm, F.-J. (2004), “The Effect of Two Types of C-S-H on the Elasticity of Cement-Based Materials: Results from Nanoindentation and Micromechanical Modeling,” Cement and Concrete Research, 34(1), 67-80.

Coussy, O. (2004), Poromechanics, John Wiley & Sons, New York, USA.

Danielson, U. (1962), “Heat of Hydration of Cement as Affected by Water-Cement Ratio,” Paper IV-S7, Proceedings of the 4th International Symposium on the Chemistry of Cement, Washington DC, USA, 519-526.

Douglas, K.S. and Hover, K.C. (2004), “Measuring Non-Drying Bulk Shrinkage of Cement Paste and Mortar Using Archimedes’ Principle,” Autogenous Deformation of Concrete, Edited by O.M. Jensen, D.P. Bentz and P. Lura, ACI SP-220, USA, 39-56.

Eguchi, K. and Teranishi, K. (2005), “Prediction Equation of Drying Shrinkage of Concrete Based on Composite Model,” Cement and Concrete Research, 35(3), 483-493.

Escalante-Garcia, J.I. and Sharp, J.H. (1998), “Effect of Temperature on the Hydration of the Main Clinker Phases in Portland Cements: Part I, Neat Cements,” Cement and Concrete Research, 28(9), 1245-1257.

Escalante-Garcia, J.I. (2003), “Nonevaporable Water from Neat OPC and Replacement Materials in Composite Cements Hydrated at Different Temperatures,” Cement and Concrete Research, 33(11), 1883-1888.

Ferraris, C.F. and Wittmann, F.H. (1987), “Shrinkage Mechanism of Hardened Cement Paste,” Cement and Concrete Research, 17(3), 453-464.

Freiesleben Hansen, P. and Pedersen, E.J. (1977), “Maturity Computer for Controlling Curing and Hardening of Concrete,” Nordisk Betong, 1(19), 21-25.

Freiesleben Hansen, P. and Pedersen, E.J. (1985), “Curing of Concrete Structures,” Draft DEB Guide to Durable Concrete Structures, Appendix 1, Comité Euro-International duBéton, Lausanne, Switzerland.

Frigione, G. and Marra, S. (1976), “Relationship Between Particle Size Distribution and Compressive Strength in Portland Cement,” Cement and Concrete Research, 6(1), 113-127.

Goboncan, V.C. and Dillenbeck, R.L. (2003), “Real-Time Cement Expansion/Shrinkage Testing under Downhole Conditions for Enhanced Annular Isolation,” SPE/IADC Drilling Conference, SPE/IADC 79911, Amsterdam, The Netherlands, 1-9.

Haecker, C.J., Garboczi, G.J., Bullarda, J.W., Bohnb, R.B., Sunc, Z., Shahc, S.P. and Voigtc, T. (2005), “Modeling the Linear Elastic Properties of Portland Cement Paste,” Cement and Concrete Research, 35(10), 1948-1960.

Hammer, T.A. (2002), “Is There a Relationship Between Pore Water Pressure and Autogenous Shrinkage Before and During Setting?” Self-Desiccation and Its Importance in Concrete Technology, Edited by B. Persson and G. Fagerlund, Report TVBM-3104, Division of Building Materials, Lund Institute of Technology, Proceedings of the Third International Research Seminar in Lund, 27-38.

Hansen, T.C. (1965), “Influence of Aggregate and Voids on Modulus of Elasticity of Concrete, Cement Mortar, and Cement Paste,” Journal of the American Concrete Institute, 62(2), 193-216.

Hansen, W. (1987), “Drying Shrinkage Mechanisms in Portland Cement Paste,” Journal of the American Ceramic Society, 70(5), 323-328.

Helmuth, R.A. and Turk, D.H. (1966), “Elastic Moduli of Hardened Portland Cement and Tricalcium Silicate Pastes: Effect of Porosity,” Symposium on Structure of Portland Cement Paste and Concrete (Special Report 90), Highway Research Board, Washington DC, USA, 135-144.

Herve, E. and Zaoui, A. (1990), “Modeling the Effective Behavior of Nonlinear Matrix-Inclusion Composites,” European Journal of Mechanics, A/Solids, 9(6), 505-515.

Hill, J., Whittle, B.R., Sharp, J.H. and Hayes, M. (2003), “Effect of Elevated Curing Temperature on Early Hydration and Microstructure of Composites,” Proceedings of the Materials Research Society Symposium, Vol. 757, 699-703.

Horita, T. and Nawa, T. (2003), “The Effect of Water to Cement Ratio on the Autogenous Shrinkage of Cement Paste,” Journal of Structural and Construction Engineering, AIJ, No. 565, 1-7 (in Japanese).

Hua, C., Acker, P. and Ehrlacher, A. (1995), “Analyses and Models of the Autogenous Shrinkage of Hardening Cement Paste I. Modelling at Macroscopic Scale,” Cement and Concrete Research, 25(7), 1457-1468.

Hua, C., Ehrlacher, A. and Acker, P. (1997), “Analyses and Models of the Autogenous Shrinkage of Hardening Cement Paste II. Modelling at Scale of Hydrating Grains,” Cement and Concrete Research, 27(2), 245-258.

Jennings, H.M. and Johnson, S.K. (1986), “Simulation of Microstructure Development During the Hydration of a Cement Compound,” Journal of the American Ceramic Society, 69(11), 790-795.

Jensen, O.M. (1993), “Autogenous Deformation and RH-Change – Self-Desiccation and Self-Desiccation Shrinkage,” PhD Thesis, Building Materials Laboratory, The Technical University of Denmark, TR 285/93.

Jensen, O.M. (1995), “Thermodynamic Limitation of Self-Desiccation,” Cement and Concrete Research, 25(1), 157-164.

Jensen, O.M. and Hansen P.F. (1996), “Autogenous Deformation and Change of the Relative Humidity in Silica Fume-Modified Cement Paste,” ACI Material Journal, 93(6), 539-543.

Jensen, O.M. and Hansen, P.F. (2001), “Autogenous Deformation and RH-Change in Perspective,” Cement and Concrete Research, 31(12), 1859-1865.

Jiang, Z., Wang P. and Sun, Z. (2005), “Autogenous Relative Humidity Change and

Autogenous Shrinkage of High-Performance Cement Pastes," Cement and Concrete Research 35(8), 1539-1545.

Justnes, H., Reyniers, B., van Loo, D. and Sellevold, E.J. (1994), "An Evaluation of Methods for Measuring Chemical Shrinkage of Cementitious Pastes," Nordic Concrete Research, 14, 45-61.

Justnes, H., van Loo, D., Reyniers, B., Skalle, P., Sveen, J. and Sellevold, E.J. (1995), "Chemical Shrinkage of Oil Well Cement Slurries," Advances in Cement Research, 7(26), 85-90.

Justnes, H., van Gemert, A., Verboven, F. and Sellevold, E.J. (1996), "Total and External Chemical Shrinkages of Low w/c Ratio Cement Pastes," Advances in Cement Research, 8(31), 121-126.

Keienburg, R.R. (1976), Particle Size Distribution and Normal Strength of Portland Cement, PhD Thesis, Karlsruhe University, Germany.

Kendal, K., Howard, A.J. and Birchall, J.D. (1983), "The Relation Between Porosity, Microstructure and Strength, and the Approach to Advanced Cement-Based Materials," Philosophical Transactions of the Royal Society of London, Series A, Mathematical and Physical Sciences, 310(1511), 139-153.

Kjellsen, K.O. and Detwiler R.J. (1992), "Reaction Kinetics of Portland Cement Mortars Hydrated at Different Temperatures," Cement and Concrete Research, 22(1), 112-120.

Knudsen, T. (1982), "Modeling Hydration of Portland Cement – The Effect of Particle Size Distribution," Characterization and Performance Prediction of Cement and Concrete, Edited by J.F. Young, United Engineering Trustees, Inc., New Hampshire, USA, 125-150.

Koenders, E.A.B. (1997), Simulation of Volume Changes in Hardening Cement-Based Materials, PhD Thesis, Delft University of Technology, Delft, The Netherlands.

Koenders, E.A.B. and van Breugel, K. (1997), "Numerical Modelling of Autogenous Shrinkage of Hardening Cement Paste," Cement and Concrete Research, 27(10), 1489-1499.

Lerch, W. and Ford, C.L. (1948), "Long-Term Study of Cement Performance in Concrete: Chapter 3. Chemical and Physical Tests of the Cements," ACI Journal, 19(8), 745-795.

Lide, D.R. (1997), CRC Handbook of Chemistry and Physics, 78th Edition, CRC Press, Boca Raton, FL, USA.

Lokhorst, S.J. (1998), Deformational Behaviour of Concrete Influenced by Hydration

Related Changes of the Microstructure, Research Report, Delft University of Technology, Delft, The Netherlands.

Lura, P., Jensen, O.M. and van Breugel, K. (2003), "Autogenous Shrinkage in High-Performance Cement Paste: An Evaluation of Basic Mechanisms," Cement and Concrete Research, 33(2), 223-232.

Mabrouk, R., Ishida, T. and Maekawa, K. (2004), "A Unified Solidification Model of Hardening Concrete Composite for Predicting the Young Age Behavior of Concrete," Cement and Concrete Composites, 26(5), 453-461.

Maekawa, K., Chaube, R. and Kishi, T. (1999), Modelling of Concrete Performance: Hydration, Microstructure Formation and Mass Transport, London: E&FN SPON, UK.

Mills, R.H. (1966), "Factors Influencing Cessation of Hydration in Water Cured Cement Pastes," Special Report No. 90, Proceedings of the Symposium on the Structure of Portland Cement Paste and Concrete, Highway Research Board, Washington DC, USA, 406-424.

Mindess, S., Young, J.F. and Darwin, D. (2002), Concrete, 2nd Edition, Pearson Education, Inc., Upper Saddle River, NJ, USA.

Monteiro, P.J.M. and Chang, C.T. (1995), "The Elastic Moduli of Calcium Hydroxide," Cement and Concrete Research, 25(8), 1605-1609.

Mori, T. and Tanaka, K. (1973), "Average Stress in Matrix and Average Elastic Energy of Materials with Misfitting Inclusions," Acta Metall. 21(5), 571-574.

Mounanga, P., Khelidj, A., Loukili, A. and Baroghel-Bouny, V. (2004), "Predicting $Ca(OH)_2$ Content and Chemical Shrinkage of Hydrating Cement Pastes Using Analytical Approach," Cement and Concrete Research, 34(2), 255-265.

Nakamura, H., Hamada, S., Tanimoto, T. and Miyamoto, A. (1999), "Estimation of Thermal Cracking Resistance for Mass Concrete Structures with Uncertain Material Properties," ACI Structural Journal, 96(4), 509-518.

Navi, P. and Pignat, C. (1996), "Simulation of Cement Hydration and the Connectivity of the Capillary Pore Space," Advanced Cement Based Material, 4(2), 58-67.

Neubauer, C.M., Jennings, H.M. and Garboczi, E.J. (1996), "Three-Phase Model of the Elastic and Shrinkage Properties of Mortar," Advanced Cement Based Materials, 4(1), 6-20.

Paulini, P. (1994), "Through Solution Model for Volume Changes of Cement Hydration," Cement and Concrete Research, 24(3), 488-496.

Perzyna, P. (1966), "Fundamental Problems in Viscoplasticity," Advances in Applied Mechanics, 9, 243-377.

Pommersheim, J.M. and Clifton, J.R. (1979), “Mathematical Modeling of Tricalcium Silicate Hydration,” Cement and Concrete Research, 9(6), 765-770.

Powers, T.C. and Brownyard, T.L. (1947), “Studies of the Physical Properties of Hardened Portland Cement Paste,” Bull. 22, Res. Lab. of Portland Cement Association, Skokie, IL, USA, Reprinted from J. Am. Concr. Inst. (Proc.), vol. 43, 101-132, 249-336, 469-505, 549-602, 669-712, 845-880, 933-992.

Powers, T.C. (1968), “Section I The Thermodynamics of Volume Change and Creep,” Materiaux et Constructions, Materials and Structures, 1(6), 487-507.

Sabins, F.L. and Sutton, D.L. (1991), “Interrelationship Between Critical Cement Properties and Volume Changes During Cement Setting,” SPE Drilling Engineering, 6(2), 88-94.

Schindler, A.K. (2004), “Effect of Temperature on Hydration of Cementitious Materials,” ACI Materials Journal, 101(1), 72-81.

Schindler, A.K. and Folliard, K.J. (2005), “Heat of Hydration Models for Cementitious Materials,” ACI Materials Journal, 102(1), 24-33.

Scovazzo, P. and Todd, P. (2001), “Modeling Disjoining Pressures in Submicrometer Liquid-Filled Cylindrical Geometries,” Journal of Colloid and Interface Science, 238, 230-237.

Shimomura, T. and Maekawa, T. (1997), “Analysis of the Drying Shrinkage Behavior of Concrete Using a Micromechanical Model Based on the Microstructures of Concrete,” Magazine of Concrete Research, 49(181), 303-322.

Soroka, I. (1979), Portland Cement Paste and Concrete, Macmillan, London, UK.

Taplin, J.H. (1969), “A Method for Following Hydration Reaction in Portland Cement Paste,” Australian Journal of Applied Sciences, 10, 329-345.

Taylor, H.F.W. (1997), Cement Chemistry, 2nd edition, Thomas Telford Ltd, London, UK.

Tennis, P.D., Xi, Y. and Jennings, H.M. (1997), “Mathematical Modeling of Cement Paste Microstructure by Mosaic Pattern. Part II. Application,” Journal of Materials Research, 12(7), 1741-1746.

Tennis, P.D. and Jennings, H.M. (2000), “A Model for Two Types of Calcium Silicate Hydrate in the Microstructure of Portland Cement Pastes,” Cement and Concrete Research, 30(6), 855-863.

Ulm, F.-J. and Coussy, O. (1995), “Modeling of Thermochemomechanical Couplings of Concrete at Early Ages,” Journal of Engineering Mechanics, ASCE, 121(7), 785-794.

Ulm, F.-J., Constantinides, G. and Heukamp, F.H. (2004), “Is Concrete a Poromechanics Material? – A Multiscale Investigation of Poroelastic Properties,” Materials and Structures, 37(265), 43-58.

van Breugel, K. (1991), Simulation of Hydration and Formation of Structure in Hardening Cement-Based Materials, PhD Thesis, Delft University of Technology, Delft, The Netherlands.

Velez, K., Maximilien, S., Damidot, D., Fantozzi, G. and Sorrentino, F. (2001a), “Determination by Nanoindentation of Elastic Modulus and Hardness of Pure Constituents of Portland Cement Clinker,” Cement and Concrete Research, 31(4), 555-561.

Velez, K., Maximilien, S., Damidot, D., Sorrentino, F. and Fantozzi, G. (2001b), “Determination by Nanoindentation of the Elastic Modulus and the Hardness of Synthetic Calcium Silicate Hydrates,” Preprint.

Whiting, D. and Kline, E. (1977), “Pore Size Distribution in Epoxy Impregnated Hardened Cement Pastes,” Cement and Concrete Research, 7(1), 53-60.

Xi, Y. and Jennings, H.M. (1997), “Shrinkage of Cement Paste and Concrete Modeled by a Multiscale Effective Homogeneous Theory,” Materials and Structures, 30, 329-339.

Xiong, X. and van Breugel, K. (2001), “Isothermal Calorimetry Study of Blended Cements and Its Application in Numerical Simulations,” HERON, 46(3), 151-159.

Ye, G. (2001), Experimental Study and Numerical Simulation of the Development of the Microstructure and Permeability of Cementitious Materials, PhD Thesis, Delft University of Technology, Delft, The Netherlands.

Zhou, Q. and Beaudoin, J.J. (2003), “Effect of Applied Hydrostatic Stress on the Hydration of Portland Cement and C_3S,” Advances on Cement Research, 15(1), 9-16.

APPENDIX I

COEFFICIENTS A_1, A_2 AND A_3 IN EQUATION (5-7)

According to Christensen (1990), the coefficients A_1, A_2 and A_3 in Eq. (5-7) are given by:

$$\begin{aligned} A_1 = {} & 8\left(\frac{G_{ace}}{G_{hp}}-1\right)(4-5n_{hp})h_1 f_{ace}^{\frac{10}{3}} - 2\left[63\left(\frac{G_{ace}}{G_{hp}}-1\right)h_2 + 2h_1h_3\right] f_{ace}^{\frac{7}{3}} \\ & + 252\left(\frac{G_{ace}}{G_{hp}}-1\right)h_2 f_{ace}^{\frac{5}{3}} - 50\left(\frac{G_{ace}}{G_{hp}}-1\right)(7-12n_{hp}+8n_{hp}^{\,2})h_2 f_{ace} \\ & + 4(7-10n_{hp})h_2h_3 \end{aligned} \tag{I-1}$$

$$\begin{aligned} A_2 = {} & -2\left(\frac{G_{ace}}{G_{hp}}-1\right)(1-5n_{hp})h_1 f_{ace}^{\frac{10}{3}} + 2\left[63\left(\frac{G_{ace}}{G_{hp}}-1\right)h_2 + 2h_1h_3\right] f_{ace}^{\frac{7}{3}} \\ & - 252\left(\frac{G_{ace}}{G_{hp}}-1\right)h_2 f_{ace}^{\frac{5}{3}} + 75\left(\frac{G_{ace}}{G_{hp}}-1\right)(3-n_{hp})h_2 n_{hp} f_{ace} \\ & + \frac{3}{2}(15n_{hp}-7)h_2h_3 \end{aligned} \tag{I-2}$$

$$\begin{aligned} A_3 = {} & 4\left(\frac{G_{ace}}{G_{hp}}-1\right)(5n_{hp}-7)h_1 f_{ace}^{\frac{10}{3}} - 2\left[63\left(\frac{G_{ace}}{G_{hp}}-1\right)h_2 + 2h_1h_3\right] f_{ace}^{\frac{7}{3}} \\ & + 252\left(\frac{G_{ace}}{G_{hp}}-1\right)h_2 f_{ace}^{\frac{5}{3}} + 25\left(\frac{G_{ace}}{G_{hp}}-1\right)(n_{hp}^{\,2}-7)h_2 f_{ace} \\ & - (7+5n_{hp})h_2h_3 \end{aligned} \tag{I-3}$$

with

$$h_1 = \left(\frac{G_{ace}}{G_{hp}}-1\right)(7-10n_{hp})(7+5n_{ace}) + 105(n_{ace}-n_{hp}) \tag{I-4}$$

$$h_2 = \left(\frac{G_{ace}}{G_{hp}} - 1 \right)(7 + 5n_{ace}) + 35(1 - n_{ace}) \quad \text{(I-5)}$$

$$h_3 = \left(\frac{G_{ace}}{G_{hp}} - 1 \right)(8 - 10n_{hp}) + 15(1 - n_{hp}) \quad \text{(I-6)}$$

where G_{ace} and n_{ace} are the shear modulus and Poisson's ratio of the anhydrous cement clinker; G_{hp} and n_{hp} are the effective shear modulus and Poisson's ratio of hydration products; f_{ace} is the volume fraction of the anhydrous cement clinker inclusions in the solid phase of cement paste.